KU LEUVEN

FACULTEIT WETENSCHAPPEN

Probing short-range phenomena in unstable nuclei with A(p,p'NN)A-2 reactions

A feasibility study

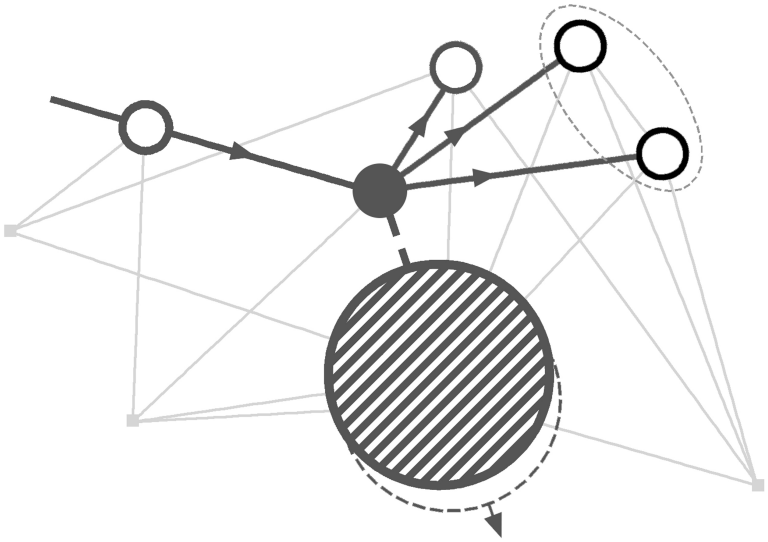

Andreas WAETS

Promotor: Prof. R. Raabe
KU Leuven

Co-promotor: Prof. J. Ryckebusch
UGent

Begeleider: Sam Stevens
UGent

Proefschrift ingediend tot het
behalen van de graad van
Master of Science in de Fysica

Academiejaar 2015-2016

Dankwoord

Deze thesis sluit een heel mooi avontuur aan de universiteit af. Het was een tocht die ik zeker niet alleen gemaakt heb en ik ben dan ook heel blij dat ik dit avontuur met veel mensen heb mogen delen. Daarom bedankt aan iedereen die me hierin heeft bijgestaan, vrienden die zijn gebleven, vrienden die er bij zijn gekomen. Ik heb veel van jullie geleerd en hoop dit ook nog heel lang te mogen doen.

Ik bedank in de eerste plaats Prof. Jan Ryckebusch om mij de kans te geven om een thesis te schrijven over een uitermate interessant onderwerp, en Sam Stevens die mij steeds met woord en daad heeft bijgestaan. Zonder jullie steun en begeleiding was deze thesis ondenkbaar. Bedankt ook Camille voor de nodige feedback en Jannes voor de nodige logistieke ondersteuning.

Bedankt ook aan alle leden van het Instituut voor Kern- en Stralingsfysica van de KU Leuven en Prof. Riccardo Raabe in het bijzonder, het gaf bijzonder veel voldoening om in zo'n boeiende omgeving te mogen studeren. En dat studeren gebeurde uiteraard ook niet alleen: bedankt aan al mijn medestudenten voor de ontelbare herinneringen die ik aan deze tijd overhoud.

Bedankt Nathalie, Elly, Joris en het bureau van de Studentenraad KU Leuven. Ik ben ongelooflijk trots om deel te hebben mogen uitgemaakt van een groep waarin niets onmogelijk is.

Bedankt Arne, Gust, Bert en Iris (en Chico), om mij de afgelopen 3 jaar in jullie gezelschap steeds thuis te laten voelen.

Bedankt mams en paps,
om mij de kans te geven mijn dromen na te jagen.

Andreas

Abstract

Mean-field theories such as the Fermi gas model are able to predict general properties of atomic nuclei. However, they fall short to describe realistic nuclear wave functions due to the assumption the nucleons can be treated as independent particles. In particular the presence of a universal high-momentum tail requires the inclusion of nucleon-nucleon correlations.

The purpose of this thesis is do develop a framework to study these short-range correlations (SRC). This will be done by considering scattering in general and quasi-free knockout reactions in particular which can also be performed in inverse kinematics to study unstable nuclei.

The cross section for the quasi-free $A(p'pNN)A-2$ two-nucleon knockout reaction is calculated from quantum collision theory by using the plane wave impulse approximation (PWIA). The effects of nucleon-nucleon correlations on the wave functions are accounted for by using an effective operator. Initial and final state interactions (IFSI) distorting the incoming and outgoing plane waves are incorporated using the semi-classical eikonal approximation and its relativistic multiple scattering Glauber extension (RMSGA).

Kinematical cuts are applied to probe exclusively the SRC pairs in nuclei by use of the two-nucleon knockout reaction. In addition to this, further kinematical restrictions are considered to efficiently calculate the scattering amplitude. By means of these restrictions and the use of several approximations (including the spectator and zero-range approximation) the $A(p,p'NN)A-2$ cross section is shown to factorize. The free proton-nucleon scattering cross section appears as a separate factor and the factorized expression is shown to be sensitive to the c.m. momentum distribution of the correlated pairs.

A simulation using this factorized expression for reactions in inverse kinematics resulted in the expected kinematical configuration profile for SRC pairs. The kinematical cuts and approximations do limit the available phase space needed for a detailed study of the two-nucleon momentum distributions. Experimental verification of this method is needed to ensure the validity of a quasi-free two-nucleon knockout framework as a tool to study SRC effects in unstable nuclei.

Summary

Mankind has always wondered how the universe works and wanted to understand it. Even a short look at our direct surrounding is enough to make us realize this is a very difficult task. It is extremely ambitious to study, investigate and understand the complexity and vastness of the universe. To make this case a little more manageable we can use a commonly known strategy: instead of considering the problem as a whole, we split it up into tiny pieces. As for the discipline in which this thesis is embedded – nuclear physics – this is in fact to be taken literally. All matter that surrounds us is built from extremely tiny particles called atoms and in nuclear physics, the nuclei of the atoms are studied.

Atoms are composed of a cloud of particles called *electrons* that circles the atomic nucleus. The nucleus itself is composed of two types of particles: *protons* and *neutrons*. Thousands of different nuclei exist, each with a different number of protons and/or neutrons. There are hundreds of nuclei with the right amount of protons and neutrons and are thus stable. All others have too many protons or too many neutrons and are therefore unstable. These unstable nuclei will try to reach stability by emitting radiation – this process is called *radioactivity*. Studying radioactive nuclei is of great importance to a bunch of other domains. They are for example used in medicine for both diagnostics as treatment of patients.

Studying atomic nuclei is an extremely challenging task – especially when these nuclei are also radioactive. Luckily both scientific and technological progress allow us to understand the nuclei better and better. A possible way to extract information is by studying collisions. A proton can be fired at an atomic nucleus and due to the collision protons or neutrons will be knocked out. Measuring these knocked out particles can is a valuable tool to study the nucleus itself. This type of collisional reactions is also called *scattering*.

A particular type of scattering is the subject of this work. We will devote attention to the reaction where a proton is fired upon a nucleus at high speed and knocks out exactly two nucleons. By measuring the energy and the angle under which they are scattered, the positions of the particles inside the nucleus before the collision can be deduced. In this work we investigate pairs of protons and neutrons that are located very closely together and are thus scattered together in a collision. This phenomenon has been studied extensively in stable nuclei but not yet in radioactive nuclei. This thesis forms the theoretical and mathematical basis on which further experimental work can follow.

Samenvatting

De mens heeft zich altijd al afgevraagd hoe het universum in elkaar zit. Het volstaat om zelfs maar een korte blik op onze directe omgeving te werpen om te begrijpen dat dit een enorme uitdaging is. Het is bijzonder ambitieus om de complexiteit en de uitgestrektheid van het heelal te bestuderen, onderzoeken en begrijpen. Om dit vraagstuk wat overzichtelijker te maken kan een alom bekende strategie worden toegepast: in plaats van het geheel te bekijken splitsen we het probleem op in kleine stukjes. In het geval van de kernfysica, het domein waarin deze thesis zich situeert, is dit ook heel letterlijk te nemen. Hierin worden namelijk de kernen van atomen bestudeerd, de minuscule bouwstenen van alle materie waaruit wij en onze omgeving is opgebouwd.

Atomen zijn opgebouwd uit een wolk van deeltjes genaamd *elektronen* die zich rondom een atoomkern bevindt. De atoomkern zelf is dan weer een verzameling van twee soorten andere deeltjes: *protonen* en *neutronen*. Er bestaan duizenden verschillende atoomkernen, elk met een verschillend aantal protonen en/of neutronen. Er zijn honderden kernen met juiste combinaties van protonen neutronen die stabiel zijn. De rest van de kernen heeft ofwel te veel neutronen ofwel te veel protonen en is instabiel. Deze kernen zullen proberen om stabiel te worden door het uitzenden van straling – dit proces heet *radioactiviteit*. Het bestuderen van radioactieve kernen is van belang voor een heel aantal andere domeinen. Ze worden bijvoorbeeld veel gebruikt in de medische wereld, zowel voor beeldvorming als behandeling van kwalen.

Het bestuderen van atoomkernen is allesbehalve een gemakkelijke taak – zeker niet wanneer deze kernen ook nog eens radioactief zijn. Gelukkig zorgt zowel de wetenschappelijke als technische vooruitgang ervoor dat we de ze alsmaar beter kunnen begrijpen. Een manier om informatie te krijgen over de kern is het bestuderen van botsingen. Hierbij schieten we een proton af op een atoomkern en door deze botsing zullen protonen of neutronen uit de kern worden losgeslagen. Het meten van deze losgeslagen deeltjes kan ons dan iets vertellen over hoe de kern in mekaar zit. Dit type van botsingen wordt ook wel *verstrooiing* genoemd.

Zo'n botsingsproces wordt ook onderzocht in dit werk. Specifiek hebben we het over de reactie waarbij een proton met hoge snelheid wordt afgestuurd op een atoomkern en er juist twee protonen of neutronen worden losgemaakt. Door het opmeten van de energie en onder welke hoek ze verstrooid worden kan achterhaald worden welke plaats de deeltjes innamen in de kern voor de botsing. Hier wordt specifiek onderzoek gedaan naar paren van proton en neutronen die zich heel dicht bij elkaar bevinden en dus tijdens een botsing samen verstrooid worden. Dit fenomeen is al uitvoerig bestudeerd in stabiele kernen maar nog niet zo veel in radioactieve kernen. In deze thesis wordt de theoretische en wiskundige basis gelegd waarop toekomstig experimenteel onderzoek kan voortbouwen.

Contents

Chapter 1

Introduction: The Fermi gas model and short-range correlations

Understanding and describing the thousands of stable and unstable nuclei on the nuclear chart represents a major challenge. The number of particles involved, the forces and potentials felt by those particles, the inability to directly "see" the nucleus itself: these are all complications that turn up in the development of both theory and experiment. The long history of research in nuclear physics teaches us that we always rely heavily on an appropriate model to describe the atomic nucleus. The remarkably wide variety in nuclei point to different interesting effects but there is also a powerful set of systematic trends and properties. These general properties are best reflected using a basic *mean field* approach where nucleons move independently from each other in a mean potential due to the other nucleons. Our discussion begins with one of the simplest models to describe a system like the nucleus: the Fermi gas model.

In an independent particle picture, the individual nucleons move independently inside the nucleus without interacting with each other. This is based on the assumption that the mean free path of the nucleons is large compared to the size of the nucleons themselves. Since nucleons are fermions, their motion is governed by the Pauli exclusion principle. A nucleus in its ground state can be described in this simple picture: particles will occupy states obeying the Pauli principle up to a maximal level, depending on the number of particles present in the nucleus. This maximum is characterized by the Fermi energy E_F and its corresponding Fermi momentum k_F (Fig.1.1). Treating the ground-state nucleus like a degenerate Fermi gas at zero temperature is actually the original independent particle model [1]. If two nucleons were to collide resulting in one nucleon occupying a higher energy state, conservation of energy dictates that the other nucleon should occupy a lower energy state. But this is not possible since all levels are completely filled so the nucleons do not scatter off one another. Forces between the nucleons are neglected but they are responsible for the existence of the potential well.

Viewing the nucleus as a gas means we can treat it statistically as in kinetic theory. The individual nucleons obey the Schrödinger equation for a free particle

$$-\frac{\hbar^2}{2m}\nabla^2\psi = E\psi \tag{1.1}$$

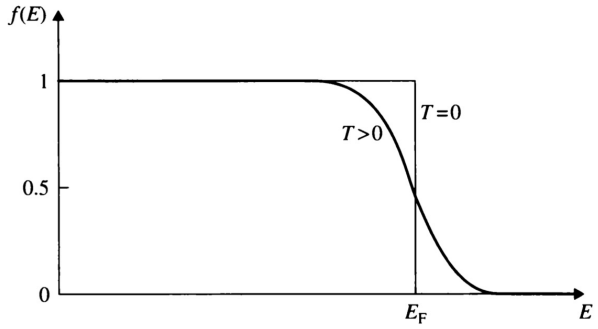

Figure 1.1: The probability $f(E)$ a level is fully occupied as function of the energy E. At $T = 0$, corresponding to a nucleus in the ground state, all levels up to the Fermi level are occupied. The case $T > 0$ can be seen as excitations of nucleons into higher momentum levels.

with m the nucleon mass and E its energy. Boundary conditions restrict the nucleons to a fixed volume V[1]. The number of particles $N(E)dE$ occupying energies between E and $E + dE$ is found to be [2]

$$N(E)dE = \frac{m^{3/2}E^{1/2}V}{\sqrt{2}\pi^2\hbar^3}dE. \tag{1.2}$$

Obeying Fermi-Dirac statistics, two nucleons (spin up and spin down) can exist in the same energy state. Hence the total number of fermions between E and $E + dE$ is $2N(E)dE$. The total number of particles in the energy range from zero up to E_F is given by

$$N = 2\int_0^{E_F} N(E)dE. \tag{1.3}$$

From this we can easily extract an expression for the Fermi energy, assuming a nucleon density ρ inside the nucleus we get

$$E_F = \frac{\hbar^2}{2m}\left(\frac{3\pi^2\rho}{2}\right)^{2/3}. \tag{1.4}$$

Note that we have assumed that protons and neutrons are identical. A more realistic picture is to differentiate between the two and look at the nucleus as composed of two separate gases [3], each with a different density[2] due to the number of protons (Z) and neutrons (N) with $A = Z + N$. The corresponding Fermi momentum

$$p_F = \hbar k_F = \sqrt{2mE_F} \tag{1.5}$$

will be one of the important quantities in the discussion of short-range correlations and how to probe them. Using a well-established average nucleon density $\rho = 0.170$ nucleons/fm^3[4] the Fermi momentum becomes

$$p_F \approx 250\text{MeV/c} \tag{1.6}$$

for a vast majority of nuclei: the value of p_F shows little dependence on the mass number A since the average density ρ is fairly constant for most nuclei.

[1]In this case for the nucleus $V = 4\pi AR_0^3/3$ with $R_0 \cong 1.25$fm.
[2]This will also result in a different shape and depth of the mean field potential felt by the nucleons.

Tests of this nuclear model can be done by performing e.g. electron scattering experiments. Without going in too much detail into scattering, the scattering cross sections are sensitive to the momentum distribution of the nucleons inside the nuclei that are probed with electrons, protons, ... In quasi-elastic scattering as described in [5] a nucleon is ejected from the nucleus by an energetic interaction with the electron and measured. Subsequently extracting the momentum distribution of the nucleons indeed show a similar mean momentum for a large amount of nuclei and by Eq. (1.4), we can conclude a similar mean momentum is indicative of similar nucleon density [1]. This is consistent with the view that nuclei have about the same average density, assuring that our mean-field approach is useful to describe the general behavior of atomic nuclei. A possible refinement of the Fermi gas model is for example the shell model.
However, scattering experiments have revealed clear effects that cannot be attributed to mean field theories. The nuclei under study showed a distinct mismatch in occupancy of energy levels that could not simply be accounted for by single particle excitations beyond the Fermi momentum [6]. At lower nucleon momenta we indeed see the characteristics of a degenerate Fermi gas with a steep downward slope near k_F, but at $k > k_F$ a universal "fat high-momentum tail" is present as also can be seen in Fig. 1.2. An explanation for this is the presence of nucleon-nucleon (NN) correlations, depleting the low-lying energy levels by moving nucleons to higher energies and momenta [6]. These NN correlations are not incorporated in a simple mean field model and will need to be incorporated in a different way.

Theoretical calculations on the effects of NN correlations are able to reproduce the universal character of the high-momentum tails [7]. Next to the observed independence of the mass number A on the distribution, another remarkable property appears: the interaction creates a short-range, correlated pair with a large relative momentum $k_{rel} > k_F$ and a

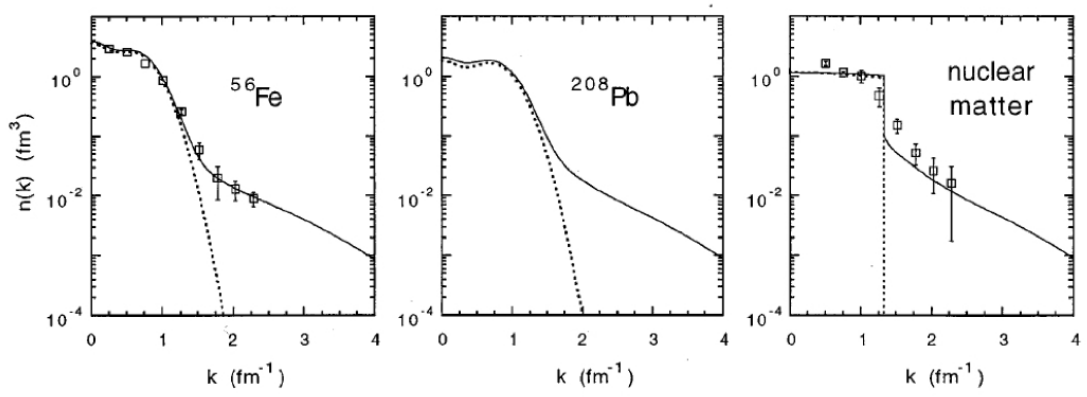

Figure 1.2: Nucleon momentum distributions (solid lines) as shown in Arrington et al. [6] for ^{56}Fe, ^{208}Pb and infinite nuclear matter. The dotted lines show the momentum distribution calculated for a mean field potential, the open squares represent results from scattering experiments indicating "fat high-momentum tails" above the Fermi momentum.

small center-of-mass or total momentum $k_{cm} < k_F$, each with respect to the Fermi momentum k_F [8]. As noted above we can distinguish protons and neutrons instead of seeing the nucleus as simply a system of nucleons. The nucleus is then composed of two Fermi gases: a proton and a neutron gas which don't necessarily have the same Fermi momentum. In the symmetric case $N = Z = A/2$, an equal amount of both fermions is present and we can speak of a *balanced Fermi system*. For these systems a high-momentum tail has been observed, not only in ultra cold atomic gases [8] but symmetric nuclei [9] as well. The goal is to extend this analysis and understanding to (assymetric) *imbalanced Fermi systems* in which there is an unequal amount of protons and neutrons. Note that an imbalanced Fermi system is not the same as an unstable nucleus. As is well known the stable nuclei deviate from the $N = Z$ line on the nuclear chart (Fig. 1.3) but of course also a large number of unstable nuclei exist. The focus of this work will be to find a means to probe the short-range effects in these unstable nuclei. As we can deduce from the chart of the nuclides, in most imbalanced Fermi systems there are more neutrons than protons. When there is no interaction between the particles the Pauli principle states that the majority fermions, in this case the neutrons, get pushed into higher momentum levels on average. Yet including an NN correlation between the fermions shows that there is a higher probability for minority fermions, the protons, to occupy levels above the Fermi momentum. This even implies that in some cases the average momentum of the protons is higher than for the neutrons, an inversion of the momentum sharing in imbalanced nuclei. This effect

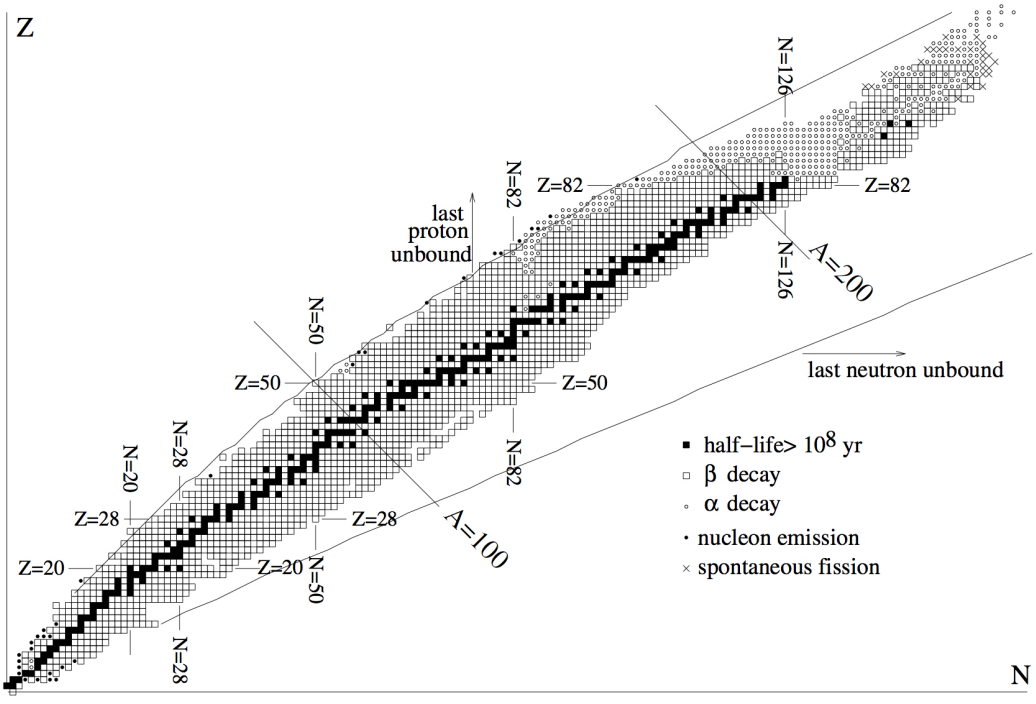

Figure 1.3: The Chart of the Nuclides. Only the small symmetric nuclei ($N = Z$) can be studied as stable balanced Fermi systems. The stable nuclei clearly deviate from the $N = Z$ line for larger mass numbers A and can therefore be classified as imbalanced Fermi systems. However, the majority of imbalanced Fermi systems is unstable and therefore require appropriate means to search for short-range NN correlations.

is due to the short-range interaction populating equal numbers of minority and majority fermions into the high momentum tail, leaving a larger amount of neutrons in lower momentum states. Using a theoretical framework for NN interactions (see Chapter 4) the tendency for a correlated pair to be in a *pn* configuration can be deduced (Fig. 1.4), this can in turn be verified by performing inclusive measurements of two-nucleon knockout reactions [10]. Needless to say, describing the NN correlation requires a complex theoretical framework which a mean field Fermi gas model can not provide since it doesn't include any spin or isospin dependence. We will provide a more complete theoretical description in Chapter 4 which will also allow us to include the correlation dependence in the cross section of the $A(p, p'NN)A-2$ reaction.

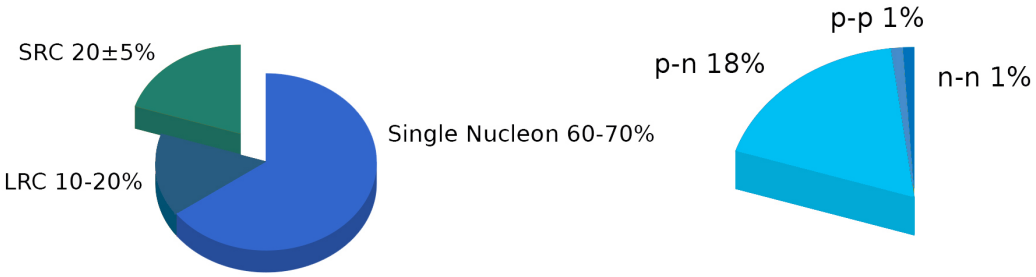

Figure 1.4: A schematic representation of the nucleon structure of ^{12}C from [11] , single-nucleon and long-range correlated (not discussed here) behavior amount for about 80% of the nucleons, 20 % are found in short-ranged correlated pairs. On the right is shown that SRC's result mostly in *pn* pairs.

Chapter 2

(Quasi-free) knockout reactions

In this chapter we will propose a reaction process to study short-range correlations in unstable nuclei. Knowledge of nuclear properties can be obtained mainly in two ways [12]: we can perform an analysis of the electromagnetic radiation that is absorbed or (re-)emitted when transitions between bound states inside the nucleus occur. This is done by performing *spectroscopy*. Spectroscopic measurements have provided a lot of information on exotic nuclei over the past decades. Using well-defined selection rules and the nuclear shell model one can assign energy, spin, isospin, parity, ... to these states and the characteristic radiation gives us back the properties of the nucleus. Another way to gather information is the use of scattering experiments where one particle scatters off the other. Measuring the collision products gives valuable information on the interactions taking place. Following the discovery of the atomic nucleus by Rutherford, many properties of the nuclear force have been deduced by the use of scattering. We quantify the probability for a scattering event to happen by means of a *scattering cross section*, usually denoted by σ.

Spectroscopy provides a means of studying single-particle properties as well as collective motion of nucleons [13]. Here, we will need an efficient way to study in what way exactly two nucleons are correlated. This means we need to select in a specific and quantitative way a small number of degrees of freedom inside the nucleus [14]. The simplest degrees of freedom are of course the properties of the individual nucleons from which the correlated pairs are built. In a scattering experiment the energy of the incoming particle can be tuned to "see" the individual nucleons. As the energy of an incident particle is increased, its de Broglie wavelength [1] is decreased until it becomes more likely to interact with a nucleon-sized object than a nucleus-sized object [15]. When this condition is fulfilled we speak of a *direct* reaction (Fig. 2.1) since it occurs quickly and without forming an intermediate state. A nucleon with a kinetic energy of 500 MeV as projectile has a de Broglie wavelength of about 1.80 fm and can therefore participate in a direct process.

A subdivision of direct reactions which are of great interest to us are the so-called *knockout* reactions. A projectile scatters off a bound nucleon, hereby transferring enough momentum so it is emitted from the nucleus [16]. In some cases multiple nucleons get emitted following this kind of energetic reaction. Measuring the scattered projectile and the ejected nucleon(s) gives information on the bound nucleon's properties. Direct reactions

[1] The de Broglie wavelength is defined as $\lambda = hc/pc$ with p the particle's momentum.

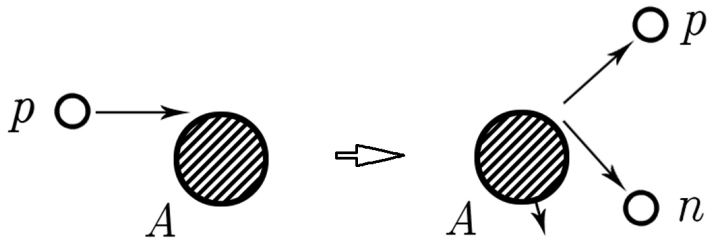

Figure 2.1: An example of a direct reaction. The incoming proton's momentum is high making it's de Broglie wavelength the order of the size of a nucleon. The proton interacts with one nucleon and removes it from the nucleus, this is called a knockout reaction. Direct reactions have the disadvantage of only probing valence nucleons due to strong absorption of the nuclear medium.

do however have the tendency to only probe valence nucleons due to the strong absorption of the nuclear medium. As discussed in the previous chapter, also deeply bound nucleons need to be probed to get a better understanding of how NN correlations work. To overcome this problem we can use *quasi-free* scattering. Here the incoming projectile typically has energies above 100 MeV up to the GeV scale, in this regime absorption in the nuclear medium is significantly reduced and we can assume the incoming projectile only interacts with the probed nucleon. This means we can consider the collision of the projectile and the struck nucleon as "free" and the residual nucleus as a spectator in the reaction [17]. A high energy approach to knockout reactions like this allows us to treat the reaction in a semi-classical fashion which makes life significantly easier, as will become clear in the following chapters. Quasi-free, electron-induced knockout reactions have taught us a great deal about the subnuclear structure. The electron can, not being subject to the strong nuclear force, probe the entire nuclear volume and the interaction itself is theoretically well understood which makes the interpretation of observations more straightforward [18]. We will rely on the knowledge developed by electron scattering for both theoretical and experimental considerations throughout this work.

Quasi-free, single-knockout cross sections from both $(e, e'p)$ and $(p, 2p)$ reactions probe the single-particle properties of nucleons and are therefore known to be powerful spectroscopic tools [14] to test the validity of the shell model. We can define the spectroscopic factor $S(j)$ as the overlap between the wavefunction of the initial and final state of the reaction. In case of single nucleon removal from an A-body nucleus, the overlap can be expanded in single particle wavefunctions [17]

$$\langle \psi_{A-1}(\mathbf{r}) | \psi_A(\mathbf{r}) \rangle = \sum_j c_j \phi_j(\mathbf{r}). \tag{2.1}$$

We can include an explicit shell model wave function in the final state, but since there are no "pure" shell model states, the calculated cross section may describe many different final states. The amplitude of the cross section for any state depends on the fraction of the pure shell model state incorporated in the wave function for that state. The single-

particle cross sections are normalized by the spectroscopic factor reflecting the occupancy of subshells in a particular state [19]. The theoretical cross section yields the cross section for removal from a particular state can be written in factorized form as

$$\sigma_{th} = \sum_j S(j)\sigma_{sp}(j). \tag{2.2}$$

In case of a pure single-particle state the spectroscopic factor is equal to 1, in all other cases the cross section will be reduced by a number between 0 and 1. This theoretical cross section can then be compared with experimental cross sections [20]. As shown in Fig.2.2, these measurements show where the mean-field approach breaks down. Medium-energy $A(e, e'p)X$ reactions on various nuclei have hinted at significant strength of the spectral function beyond single shell excitations [6]. Furthermore, electrons have also been shown to induce two-nucleon knockout as reported in [21] and [22]. Thus for obvious reasons, electron scattering is an extensively used tool to study single particle properties as well as short-range correlations in nuclei. The method itself however has two main drawbacks. First, due to the nature of the electromagnetic force the electron is much more prone to interact with protons than with neutrons. This is obviously an inconvenience if we want to study both protons and neutrons. Second, studying highly unstable or exotic nuclei using electron scattering is impractical. To produce a significant yield, the electrons need to scatter from a stable target, something the short lifetimes of exotic nuclei do not allow. A way to circumvent this problem is the use of *inverse kinematics* where a fast radioac-

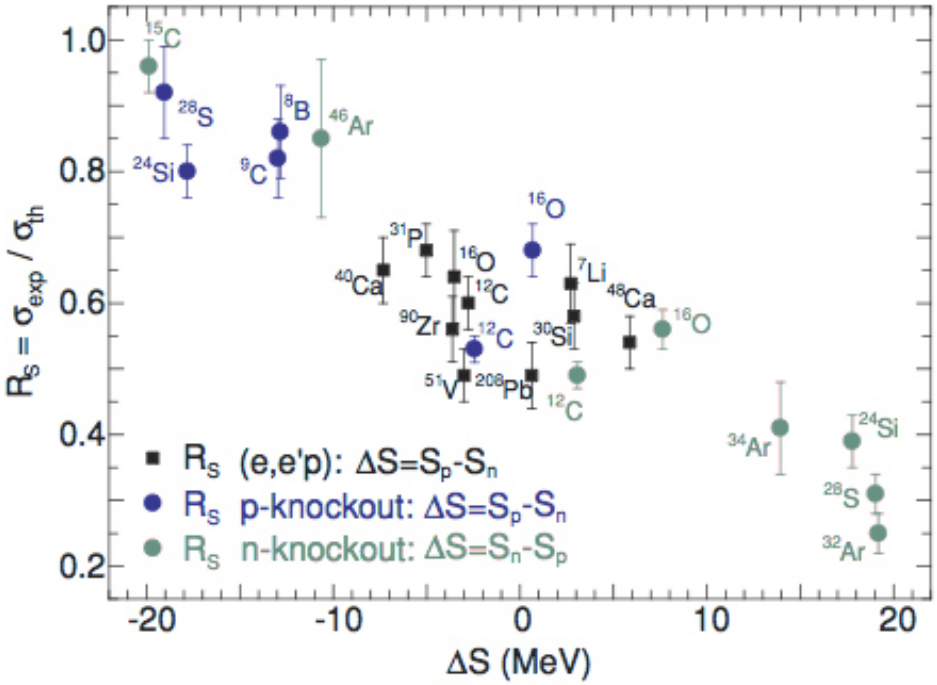

Figure 2.2: Ratios of experimental spectroscopic strength vs. theoretical values (from [17]) as function of the difference ΔS in separation energy of the two nucleon species. The parameter ΔS points to the (im)balance in Fermi energies for protons and neutrons, as discussed in the previous chapter. Single-nucleon knockout experiments clearly hint at beyond mean-field effects in a quantitative way.

tive beam impinges on a stable target made of protons or light nuclei. This method has been successfully used to determine properties of unstable nuclei [23] yielding valuable spectroscopic information far from stability.

A final remark can be made on measuring knockout reaction cross sections in an *inclusive* or an *exclusive* way (shown in Fig. 2.3). An inclusive measurement of decay or collision products means we include a collection of several specific channels in one single analysis. This can be done to determine the number of SRC pairs present in a nucleus, as demonstrated in [24]. In an exclusive analysis we measure enough observables of the reaction products to assure we select only one specific physical process. This method can allow for the determination of the ratio between *pp* and *pn* pairs, described in e.g. [22]. An exclusive measurement, however, does pose constraints on the kinematics of the scattering: the measured momenta and energies should lead to an unambiguous identification of all reaction products. In general, exclusive measurements give more detailed information on the reaction.

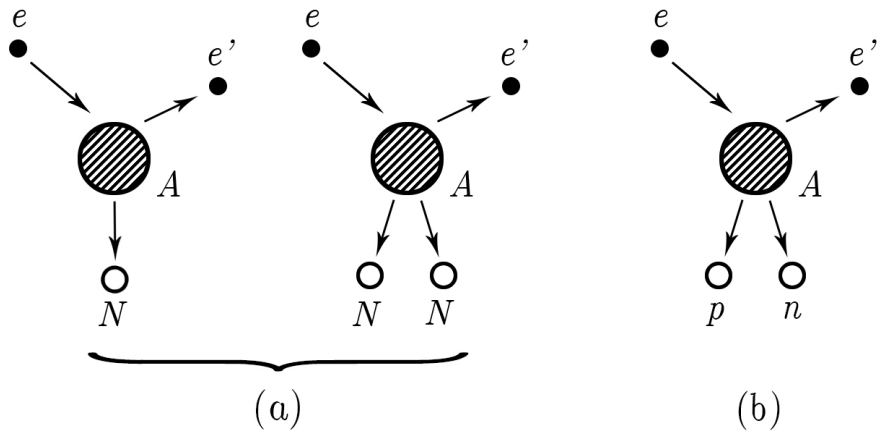

Figure 2.3: The difference between inclusive and exclusive measurements. On the left (a) depicts an inclusive $A(e, e')$ experiment in which both single nucleon and two-nucleon knockout are measured, (b) depicts $A(e, e', pn)$ scattering in which the knocked out nucleons are identified as a proton and a neutron. Exclusive measurements require more elaborate kinematical constraints.

The extensive use in theoretical as well as experimental work assures us we can use quasi-free knockout reactions as a probe to study short-range correlations in unstable nuclei. Since we will continuously refer to this method throughout this work we will summarize the key features why we choose a scattering experiment here:

- We require a way to investigate individual nucleons and therefore choose **direct reactions**. The energy of the projectile should be high enough so it's de Broglie wavelength is of the order of a few fm. This means the projectile will be able to discern nucleon-sized objects. However, due to the absorption of the nuclear medium, these reactions mostly probe valence nucleons.

- We will use **knockout reactions** where the probed nucleon is emitted from the nucleus and measured. The momenta and energy of the final scattering products

give us information on the properties of the struck bound nucleon. This is why knockout reactions are also a powerful spectroscopic tool.

- Research into short-range correlations requires knowledge on deeply bound nucleons. The preference of direct reactions to only probe outer nucleons is overcome by ramping up the energy of the projectile up to the GeV scale where we can consider **quasi-free** knockout reactions. The interaction between the projectile and the bound nucleon is considered to be "free". The nucleons not taking part in the interaction are considered to be spectators, no inelastic collisions between projectile or knocked out nucleons and the nucleus occurs. Hence the reaction is split in a "hard" and a "soft" interaction.

- We will rely on the theoretical and experimental framework of electron-induced knockout reactions but this reaction is not suited to study unstable nuclei. We can study unstable nuclei using **inverse kinematics**, where the role of projectile and target are reversed: A fast radioactive beam impinges on a proton target.

- We can measure scattering cross sections in both an **inclusive** as an **exclusive** manner. Performing both types of measurements can teach us something about the amount and composition of short-range correlated pairs.

Now we have argued quasi-free knockout reactions in inverse kinematics are an appropriate tool to study short-range NN correlations in exotic nuclei, we are ready to look into collision theory that will provide the theoretical tools to calculate the scattering cross section from which we can extract information. In this work the theoretical framework for two-nucleon knockout scattering reactions will be developed by means of $A(p, p'NN)A-2$ reactions. In this reaction a proton hits a nucleus A (or the other way around in inverse kinematics) at relativistic speed and hereby knocks out two nucleons from the nucleus

$$p + A \rightarrow p' + N_1 + N_2 + A - 2. \tag{2.3}$$

The knocked out particles are measured and their momentum distribution will allow us to extract information on short-range phenomena. For the development of this two-nucleon knockout framework we will rely on the theoretical and experimental basis of both single-knockout (p, pN) and two-nucleon knockout $(e, e'NN)$ reactions.

Chapter 3

Collision theory

Having established in the previous chapter that quasi-free knockout reactions are an appropriate method to study NN-correlations and short-range phenomena in particular, we need a way to connect the properties of nuclei to actual observables in the lab. The connection will be made by defining scattering cross sections, which requires a good knowledge of the kinematics of the particles involved but also the quantum mechanical time evolution of the particle states. By means of potential scattering, we can eventually develop a Lorentz-invariant cross section which allows these processes involving particles at relativistic speeds to be evaluated in any reference frame.

3.1 General features

We can start from classical mechanics to describe scattering. Considering a space filled by particles (or *targets*) with a density ρ. The probability P that an incoming particle or *projectile* collides with a target is proportional to the distance traveled L and density ρ

$$P = \rho L \sigma. \tag{3.1}$$

Here σ is the *total scattering cross section*. On a classical level (in absence of other interaction between the particles) the probability of a collision is also proportional to the size of the particles in the target. Since a probability has no dimension, the cross section should have dimension length^2 or area. The probability P can also be written in terms of the ratio between the number of scattered particles and the number of incoming particles N_s/N_i. The analogy with experiment is straightforward: a beam with a number of particles N_i impinges upon a target and a number of scattered particles N_s is measured by a detector. This gives for (3.1):

$$N_s = N_i \rho L \sigma. \tag{3.2}$$

Even more useful than the total cross section is the so-called *differential cross section* $d\sigma/d\Omega$, a quantity that shows the probability of particles to be scattered in a certain direction. The advantage of using differential cross sections is their sensitivity on the interaction between the particles themselves and even their properties, but more on this later. To show how this works we choose a spherical coordinate system with the z-axis fixed along the direction of the incoming particles (Fig. 3.1). We now incorporate time dependence by saying that dN_s is the number of particles per unit time scattered into a

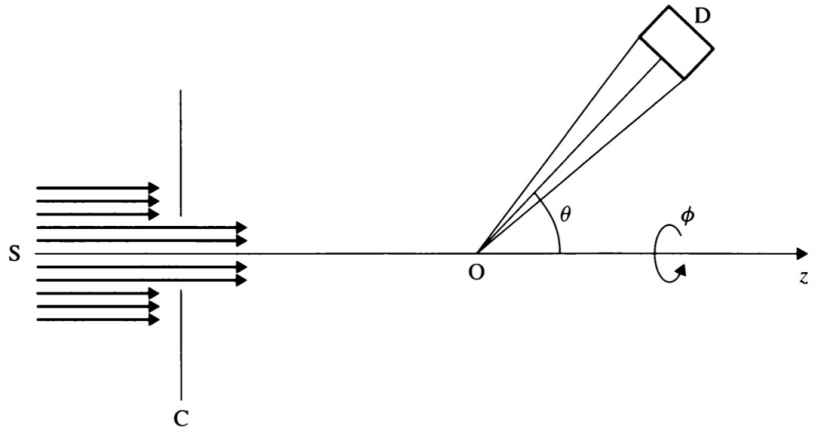

Figure 3.1: The scattering of a beam of particles by a target situated in the origin O. The detector solid angle Ω determines at what angles θ and ϕ the scattered particles are measured.

small solid angle $d\Omega$ with direction (θ, ϕ). The quantity N_i then becomes the number of incident particles per unit time, giving

$$\frac{dN_s}{d\Omega} = N_i \rho L \frac{d\sigma}{d\Omega} \tag{3.3}$$

with $d\Omega = \sin\theta d\theta d\phi$. The total cross section can be calculated by integrating over the entire 4π solid angle

$$\sigma = \int \left(\frac{d\sigma}{d\Omega}\right) d\Omega = \int_0^{2\pi} d\phi \int_0^{\pi} d\theta sin\theta \frac{d\sigma}{d\Omega}. \tag{3.4}$$

Including time dependence we see from Eq.(3.3) that the number of scattered particles is proportional to the flux F. This allows for the differential cross section to be characterized as the number of particles N scattered in a direction (θ, ϕ) per unit time, per unit solid angle, divided by the incident flux [12]:

$$\frac{d\sigma}{d\Omega} = \frac{N}{F} \tag{3.5}$$

We will use this general definition throughout the rest of this work. We can note already the flux F will be an important quantity when working in a relativistic quantum mechanical framework, we will require the wave functions to be properly normalized as will be explained in Sections 3.5.1 and 3.5.2.

3.2 Scattering kinematics

As explained before, the particles participating in the collisions, in our case a nucleus A and a proton p_i, have energies on the GeV scale. This means they will have velocities high enough so that relativistic effects should be taken into account. Furthermore, the cross sections or other measured quantities depend on reference frame we describe them in. It is for example preferable to describe and evaluate collisions in the center-of-momentum

(c.m.) frame since the momenta of the particles are equal and opposite to each other. In our case, the proton target is at rest with a relativistic beam of nuclei impinging on it. It is obvious this arrangement will yield different results when calculating or measuring cross sections and we therefore require a means to transform physical quantities between those frames.

Our particular $A(p, p'NN)A-2$ reaction is of the form

$$1 + 2 \rightarrow 3 + 4 + 5 + 6. \tag{3.6}$$

to keep things general for now. It is however important to note here that particle 2, in our case the nucleus A, is composed of particles 4, 5 and 6 with particle 6 the residual nucleus $A-2$. We can define the Lorentz-invariant *Mandelstam variable* s as [25]

$$s = (p_1^\mu + p_2^\mu)^2 \tag{3.7}$$

with $p_i^\mu = (E_i, \mathbf{p}_i)$ the four momenta of the particles. Defining this variable is a first step to constructing a Lorentz-invariant cross section. This means we can evaluate the cross section in any frame we want: it remains unchanged under the Lorentz transformations that take us from one particular reference frame to another (Fig. 3.2). In our analysis of $A(p, p'NN)A-2$ reactions these are the particular frames we need:

- **The center of momentum frame** (CMF) is the frame where particles 1 and 2, hence the proton and the nucleus collide head on. This is the frame we will rely on the least due to it's limited usefulness in this work.

- **The laboratory frame** (LF) is obviously the most important since here the experimental measurement of the cross section, energies, momenta and angles of the particles is performed. Since the scattering happens in inverse kinematics, in this frame the proton target is at rest and the z-axis is fixed along the direction of the incoming beam of protons for our reaction.

- **The projectile frame** (PF) is the frame where the nucleus is at rest, the z-axis is fixed along the direction of the incident proton which now has the relativistic velocity. This situation would correspond to so-called normal or 'direct' kinematics. For a number of both kinematical and quantum mechanical considerations it is easier to adopt this setting as we will see further on. The transformation between PF and LF is simply a Lorentz transformation along the common z-axis.

- **The nucleon-proton frame** (NPF) is the frame in which the free nucleon proton (Np) cross section is easiest to calculate 6 . The free Np scattering cross section will eventually turn up as a separate factor in the quasi-free $A(p, p'NN)A-2$ cross section. This frame is the same as the c.m. frame of the proton and nucleon.

As stated before, we want to identify the outgoing particles unambiguously to extract as much information as we can. Hence our primary interest goes to measuring the quantities E_j, p_j and θ_j, the energy, momenta and angles of the outgoing particles here labeled by j. If $j > 3$ as in our case, E_j and θ_j are independent. The analysis of two-nucleon knockout has been predominantly studied using electrons on stable nuclei in a target which is at rest. If we want to use information, such as kinematical constraints to select SRC pairs,

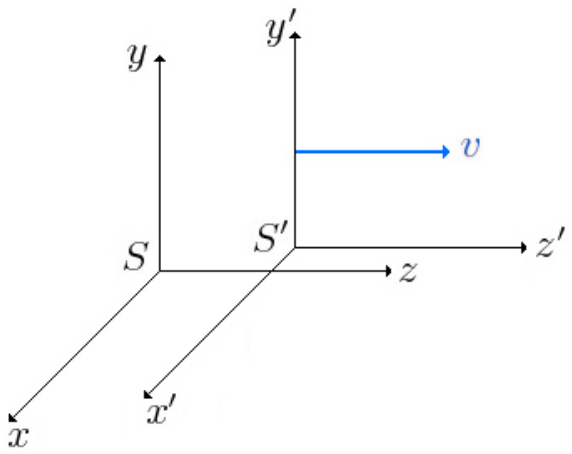

Figure 3.2: The reference frame S' moves at a speed v relative to frame S. This corresponds to the Lorentz boosts that take us from one frame to the other.

that was obtained in these experiments, we need an efficient way to switch between the lab frame and the projectile frame. Luckily, both frames have a common z-axis so the velocity β between the two is completely longitudinal. Hence the transformation will be a Lorentz boost alongs the z-axis, given by

$$\begin{pmatrix} t' \\ z' \end{pmatrix} = \begin{pmatrix} \gamma & -\gamma\beta \\ -\gamma\beta & \gamma \end{pmatrix} \begin{pmatrix} t \\ z \end{pmatrix} \tag{3.8}$$

with $x' = x$ and $y' = y$. Calculating the Minkowski norm of the four-momentum gives a Lorentz invariant quantity

$$p_\mu p^\mu = \frac{E^2}{c^2} + |\mathbf{p}|^2 = -m^2c^2. \tag{3.9}$$

E and $\mathbf{p}$ obey a Lorentz transformation identical to (3.8)

$$\begin{pmatrix} E' \\ p'_z \end{pmatrix} = \begin{pmatrix} \gamma & -\gamma\beta \\ -\gamma\beta & \gamma \end{pmatrix} \begin{pmatrix} E \\ p_z \end{pmatrix} \tag{3.10}$$

with $p'_x = p_x$ and $p'_y = p_y$. In what follows it is useful to write these results in terms of *parallel* and *transverse* momenta w.r.t. the velocity β between the frames

$$p_z \equiv p_\parallel, \qquad p_x \equiv p_{Tx} \qquad \text{and} \qquad p_y \equiv p_{Ty}. \tag{3.11}$$

in this sense we get

$$\begin{pmatrix} E' \\ p'_\parallel \end{pmatrix} = \begin{pmatrix} \gamma & -\gamma\beta \\ -\gamma\beta & \gamma \end{pmatrix} \begin{pmatrix} E \\ p_\parallel \end{pmatrix}, \qquad p'_T = p_T. \tag{3.12}$$

Now if we have quantities in the projectile frame we wish to calculate in the lab frame, the Lorentz transformation reads

$$\begin{pmatrix} E_p \\ p_{\parallel p} \end{pmatrix} = \begin{pmatrix} \gamma_{pl} & -\gamma_{pl}\beta_{pl} \\ -\gamma_{pl}\beta_{pl} & \gamma_{pl} \end{pmatrix} \begin{pmatrix} E_l \\ p_{\parallel l} \end{pmatrix}, \qquad p_{Tp} = p_{Tl}. \tag{3.13}$$

with the projectile frame moving at speed β_{pl} and the corresponding γ factor denoted by γ_{pl}. The inverse transformation reads

$$\begin{pmatrix} E_l \\ p_{\parallel l} \end{pmatrix} = \begin{pmatrix} \gamma_{pl} & -\gamma_{pl}\beta_{pl} \\ -\gamma_{pl}\beta_{pl} & \gamma_{pl} \end{pmatrix} \begin{pmatrix} E_p \\ p_{\parallel p} \end{pmatrix}, \qquad p_{Tl} = p_{Tp} \tag{3.14}$$

with

$$\begin{aligned} p_{\parallel} \equiv p_z &= |\mathbf{p}| \cos\theta, \\ p_T &= |\mathbf{p}| \sin\theta. \end{aligned} \tag{3.15}$$

The energy transformation for the energy of a particle from the lab frame to the projectile frame is

$$\begin{aligned} E_p &= \gamma_{pl}(E_l - \beta_{pl} p_{\parallel l}) \\ &= \gamma_{pl}(E_l - \beta_{pl} |\mathbf{p}_l| \cos\theta_l) \\ &= \gamma_{pl}\left(E_l - \beta_{pl}\sqrt{E_l^2 - m^2}\cos\theta_l\right) \end{aligned} \tag{3.16}$$

using the energy-momentum relation. The angle can be obtained from

$$\tan\theta = \frac{p_T}{p_z} \tag{3.17}$$

so the angle of particle j is

$$\begin{aligned} \tan\theta_{jl} = \frac{p_{Tjl}}{p_{zjl}} &= \frac{p_{Tjp}}{\gamma_{pl}\beta_{pl}E_{jp} + \gamma_{pl}p_{zjp}} \\ &= \frac{|\mathbf{p}_{jp}| \sin\theta_{jp}}{\gamma_{pl}(\beta_{pl}E_{jp} + |\mathbf{p}_{jp}| \cos\theta_{jp})} \end{aligned} \tag{3.18}$$

We will need these last few identities in particular to actually select SRC pairs as final products in collisions. As discussed in Chapter 1, the pairs have low c.o.m. and high relative momenta with respect to the Fermi momentum - assuming the nucleus is at rest. This is obviously not the case in experiments with inverse kinematics where the nuclei are traveling at relativistic speeds. The same goes for the angles of the particles, the beam's high initial velocity will result in particles being measured predominantly in the forward direction. As described in the electron-induced knockout simulations in [26], in order to guarantee the momentum transfer happens primarily with only one nucleon in the SRC pair, the angle between the knocked out nucleon which receives the momentum transfer and the momentum transfer vector should be kept small ($10 - 25^o$). This angle will also be modified by the strong forward motion of the outgoing particles. We will return to this in Chapter 6 where it becomes relevant.

3.3 Scattering dynamics

3.3.1 Potential scattering

Since we deal with particles, our collision theory will need a quantum mechanical description of scattering. We start our discussion from potential scattering: a beam of particles

is scattered from a central potential and to describe the evolution of such a system we can use the Schrödinger equation [12]

$$i\hbar\frac{d}{dt}\psi(\mathbf{r},t) = \left[-\frac{\hbar}{2\mu}\nabla^2 + V(\mathbf{r})\right]\psi(\mathbf{r},t) \tag{3.19}$$

with μ the mass of the colliding particles. We can safely approximate the particles in the incoming beam as plane waves along the z-direction:

$$\psi_i = e^{ikz} \tag{3.20}$$

with k the wave number (the magnitude of the wave vector), this means the momentum is $p = \hbar k$. In general, a wave function of a scattered particle represented by an outgoing spherical wave with amplitude f which depends on the direction (θ, ϕ) [27]

$$\psi_f = f(\theta,\phi)\frac{e^{ikr}}{r}. \tag{3.21}$$

We can regard the sum of the incoming and scattered wave as a boundary condition to solving the Schrödinger equation (4.1) far away from the potential ($V(\mathbf{r}) \cong 0$):

$$\psi_k(\mathbf{r}) \underset{r\to\infty}{\to} e^{ikz} + f(k,\theta,\phi)\frac{e^{ikr}}{r}. \tag{3.22}$$

This is also referred to as the *stationary scattering wave function.* For a stationary state, the probability current density is given by [12]

$$\begin{aligned} j(\mathbf{r}) &= \frac{\hbar}{2\mu i}[\psi^*(\nabla\psi) - (\nabla\psi^*)\psi] \\ &= \frac{\hbar}{\mu i}\mathrm{Re}[\psi^*(\nabla\psi)] \end{aligned} \tag{3.23}$$

with the gradient operator expressed in polar coordinates as [28]

$$\nabla = \frac{\partial}{\partial_r}\hat{\mathbf{r}} + \frac{1}{r}\frac{\partial}{\partial\theta}\hat{\boldsymbol{\theta}} + \frac{1}{r\sin\theta}\frac{\partial}{\partial\phi}\hat{\boldsymbol{\phi}}. \tag{3.24}$$

A plane wave corresponds to a uniform probability flow at speed $v = \frac{\hbar k}{\mu}$. The current in the radial direction is found by neglecting the terms in (3.24) that become very small for $r \to \infty$, so this becomes

$$j_r = \frac{\hbar k}{\mu}\frac{|f(\theta,\phi)|^2}{r^2}. \tag{3.25}$$

This quantity represents a number of particles passing through an area per unit time. The flux of particles passing through an area $dA = r^2 d\Omega$ per unit time is also $N d\Omega$, this gives

$$N d\Omega = \frac{\hbar k}{\mu}\frac{|f(\theta,\phi)|^2}{r^2} r^2 d\Omega. \tag{3.26}$$

The incoming flux is then given by $F d\sigma = \frac{\hbar k}{\mu} d\sigma$ so by (3.5) we can equate the two giving

$$\frac{d\sigma}{d\Omega} = |f(\theta,\phi)|^2. \tag{3.27}$$

The differential cross section is thus equal to the scattering amplitude squared.

3.3.2 Partial waves

In a collision, if two particles have a relative momentum $\mathbf{p} = \hbar\mathbf{k}$ and impact parameter b, their relative angular momentum is $\ell\hbar = pb$, or $\ell = kb$. In case this problem can be dealt with using a central potential $V(\mathbf{r})$, the angular momentum ℓ is a constant of the motion. Solving the Schrödinger equation (4.1) far from the potential ($V(\mathbf{r}) \cong 0$) suffices to find the scattering amplitude and thus the cross section. For a central potential, the system is symmetric around the direction of incidence (z-axis) the amplitude only depends on the angle θ. This allows the scattering wave function to be expanded in a series of Legendre polynomials P_ℓ [12] as

$$\psi_k(r,\theta) = \sum_{\ell}^{\infty} R_\ell(k,r) P_\ell(\cos\theta). \tag{3.28}$$

Correspondingly, the Schrödinger equation (4.1) is split in a radial and an angular part. We call the separate terms in the series *partial waves* and it is a simultaneous eigenfunction of the operators $\mathbf{L}^2$ with eigenvalues $\ell(\ell+1)\hbar^2$ and L_z with eigenvalue 0. We have split the single Schrödinger equation in a series of more manageable equations: for each term in the series, the *partial wave amplitude* f_ℓ is determined by the radial function $R_\ell(k,r)$ corresponding to that particular term. The radial functions satisfy the equation

$$\Big[\frac{d^2}{dr^2} + \frac{2}{r}\frac{d}{dr} - \frac{\ell(\ell+1)}{r^2} - U(r)\Big] R_\ell(k,r) = 0. \tag{3.29}$$

with $k^2 = 2mE/\hbar^2$ and $U(r) = 2mV(r)/\hbar^2$. These separate radial equations can be solved analytically for a number of simple potentials but to analyze real scattering cross sections this is mostly done numerically. Note that for higher impacting energies also the number of partial waves needed to reach convergence increases significantly [29]. We can therefore conclude using partial waves is not the best method to analyse quasi-free reactions where particles have relativistic energies.

3.3.3 The Lippmann-Schwinger equation

At this point it is useful to return to the absolute basics: we will describe the scattering problem by means of a Hamiltonian H which will describe the evolution of the system in time. We will treat the scattering of free states which are governed by a free Hamiltonian H_0 by means of a perturbation potential V. Hence the total Hamiltonian is given by

$$H = H_0 + V. \tag{3.30}$$

In this sense, rewriting the Schrödinger equation (3.19) as

$$\left[i\hbar\frac{d}{dt} - \hat{H}_0\right] \psi(\mathbf{r},t) = V(\mathbf{r})\psi(\mathbf{r},t) \tag{3.31}$$

with $-\frac{\hbar}{2m}\nabla^2 = \hat{H}_0$ is more revealing. When solving this equation to find $\psi(\mathbf{r},t)$, we can consider the right hand side as an inhomogeneous term and representing a source function. The standard procedure procedure to solve this type of equation would be to look for a homogeneous solution and a particular solution which together compose the general solution. However, we will tackle this problem a bit differently by using Green's functions

[30]. As we will see further on this method will allow us to connect the scattering potential V directly to the scattering amplitude $|f(\theta, \phi)|^2$.

Consider the case where we simply have a point source at position $\mathbf{r}'$. The Green's function $G(\mathbf{r}, \mathbf{r}')$ gives the effect of the unit point source in producing a potential at $\mathbf{r}$. This defines the Green's function for the free Hamiltonian H_0 since it would satisfy [31]

$$\left[i\hbar\frac{d}{dt} - \hat{H}_0\right] G(\mathbf{r}, \mathbf{r}') = \delta(\mathbf{r} - \mathbf{r}') \tag{3.32}$$

We can consider the Green's function to take a piece of the source occupying the volume $d\mathbf{r}'$ at position $\mathbf{r}'$ and propagate its effect to the position $\mathbf{r}$. It can actually be regarded as a *propagator* having the additional property it allows waves to travel forward in time. Let us now rewrite the Schrödinger equation again by

$$(\nabla^2 + k^2)\psi(\mathbf{r}) = U(\mathbf{r})\psi(\mathbf{r}). \tag{3.33}$$

with $k^2 = 2mE/\hbar^2$ and $U(r) = 2mV(r)/\hbar^2$ as before. The right hand can again be considered to be a source term. The homogeneous solution $\phi(\mathbf{r})$ can easily be found to be

$$(\nabla^2 + k^2)\phi(\mathbf{r}) = 0 \tag{3.34}$$

and the Green's function now satisfies

$$(\nabla^2 + k^2)G(\mathbf{r}, \mathbf{r}') = \delta(\mathbf{r} - \mathbf{r}') \tag{3.35}$$

In a system governed by a linear differential equation like the Schrödinger equation we can construct $U(\mathbf{r})$ as a sum of point sources. More importantly, the resulting wave function is the sum of all functions $G(\mathbf{r}, \mathbf{r}')$ produced by the point sources at all points $\mathbf{r}'$. So the particular solution of the problem becomes

$$\psi_k(\mathbf{r}) = \int G(\mathbf{r}, \mathbf{r}')U(\mathbf{r}')\psi_k(\mathbf{r}')d\mathbf{r}'. \tag{3.36}$$

At this point however, we face an annoying complication: The Green's function in this equation is not uniquely defined. We can add any solution $\phi(\mathbf{r})$ of the homogeneous equation and it will still obey (3.35) but this will result in a different $\psi(\mathbf{r})$ when plugged into (3.36). What exact form of the Green's function to use will ultimately depend on the boundary conditions we impose on the differential equation. We will choose the general solution, written here as an integral equation

$$\psi(\mathbf{r}) = \phi(\mathbf{r}) + \int G(\mathbf{r}, \mathbf{r}')U(\mathbf{r}')\psi(\mathbf{r}')d\mathbf{r}' \tag{3.37}$$

in such a way it must satisfy the asymptotic boundary conditions of the stationary scattering wave function. Before we work out the exact expression we can visualize what this integral equation means for potential scattering, still regarding the Green's function as a propagator. The interpretation is in fact very simple: ϕ is an incoming wave, it is redirected by U at $\mathbf{r}'$ and propagated by G to $\mathbf{r}$ where we attempt to reconstruct the wave function.

Determining the exact form of the Green's function requires incorporating the boundary conditions for the total stationary scattering wave function. We see when acting with $\nabla^2 + k^2$ on (3.37) and using (3.35) we get (3.33). Now comparing the integral equation (3.37) with the boundary condition for the total wave function (3.22) we see that $\phi(\mathbf{r})$ is nothing but the incident plane wave $e^{i\mathbf{k}\cdot\mathbf{r}} = e^{ikz}$ and the second term should equal the scattered wave. In what follows, we will normalize the plane waves in such a way that

$$\phi_k(\mathbf{r}) = \frac{1}{(2\pi)^{3/2}} e^{i\mathbf{k}\cdot\mathbf{r}} \tag{3.38}$$

and using the bra and ket notation this gives

$$\langle \phi_{k'} | \phi_k \rangle = \langle \mathbf{k}' | \mathbf{k} \rangle = \delta(\mathbf{k}' - \mathbf{k}), \tag{3.39}$$

this normalization will me convenient in what follows. Eq. (3.37) now reads

$$\psi_k(\mathbf{r}) = \frac{1}{(2\pi)^{3/2}} e^{i\mathbf{k}\cdot\mathbf{r}} + \int G(\mathbf{r}, \mathbf{r}') U(\mathbf{r}') \psi_k(\mathbf{r}') d\mathbf{r}' \tag{3.40}$$

To integrate the second term in the integral equation we use the Fourier representation of the delta function

$$\delta(\mathbf{r} - \mathbf{r}') \equiv \frac{1}{(2\pi)^3} \int e^{i\mathbf{k}'\cdot\ (\mathbf{r}-\mathbf{r}')} d\mathbf{k}' \tag{3.41}$$

and rewrite $G(\mathbf{r}, \mathbf{r}')$ as [27]

$$G(\mathbf{r}, \mathbf{r}') = \int e^{i\mathbf{k}'\cdot\ \mathbf{r}} g(\mathbf{k}', \mathbf{r}') d\mathbf{k}'. \tag{3.42}$$

Substituting both in (3.35) gives

$$g(\mathbf{k}', \mathbf{r}') = \frac{e^{i\mathbf{k}'\cdot\mathbf{r}'}}{k^2 - k'^2} \tag{3.43}$$

so we eventually find

$$G(\mathbf{r}, \mathbf{r}') = -\frac{1}{(2\pi)^3} \int \frac{e^{i\mathbf{k}'\cdot(\mathbf{r}-\mathbf{r})}}{k'^2 - k^2} d\mathbf{k}'. \tag{3.44}$$

This expression for the Green's function can be integrated in such a way we get an outgoing spherical wave for $r \to \infty$, as required by the established form of the stationary scattering wave function. To do this, we change to spherical coordinates and subsequently perform the integration in the complex plane. Avoiding the poles at $k' = \pm k'$ by choosing an adequate contour then (complete calculation in Appendix A) results in

$$G(\mathbf{r}, \mathbf{r}') = -\frac{1}{4\pi} \frac{e^{ik|\mathbf{r}-\mathbf{r}'|}}{|\mathbf{r} - \mathbf{r}'|} \tag{3.45}$$

in configuration space. Back in wave vector space, the poles can be avoided by displacing them an infinitesimal amount ϵ giving

$$G(\mathbf{r}, \mathbf{r}') = -\frac{1}{(2\pi)^3} \lim_{\epsilon \to 0+} \int \frac{e^{i\mathbf{k}'\cdot(\mathbf{r}-\mathbf{r}')}}{k'^2 - k^2 - i\epsilon} d\mathbf{k}'. \tag{3.46}$$

We will use this expression in Section 5.2 when we discuss the eikonal approximation. We note that (3.45) indeed satisfies the required form of a spherical outgoing wave $\exp(ikr)/r$ for $r \to \infty$. So we can finally write

$$\psi_k(\mathbf{r}) = \frac{1}{(2\pi)^{3/2}} e^{ikz} - \frac{1}{4\pi} \int \frac{e^{ik|\mathbf{r}-\mathbf{r}'|}}{|\mathbf{r}-\mathbf{r}'|} U(\mathbf{r}')\psi_k(\mathbf{r}')d\mathbf{r}'. \tag{3.47}$$

This integral equation is known as the *Lippman-Schwinger equation* of potential scattering [27] . It incorporates the boundary condition via the Green's function into the Schrödinger equation (3.33). The Lippmann-Schwinger equation is one of the most used identities to describe scattering in quantum mechanics.

We can look into the asymptotic behavior of the wave function more closely by studying the regime in which $r \to \infty$ and r' finite (so $r' \ll r$). Here we have

$$\begin{aligned} |\mathbf{r}-\mathbf{r}'| = \sqrt{r^2 - 2\mathbf{r}\cdot\mathbf{r}' + r'^2} &\underset{r\to\infty}{\to} r\sqrt{1 - \frac{2\mathbf{r}\cdot\mathbf{r}'}{r^2}} \\ &\approx r\left(1 - \frac{\mathbf{r}\cdot\mathbf{r}'}{r^2}\right) = r - \hat{\mathbf{r}}\cdot\mathbf{r}' \end{aligned} \tag{3.48}$$

with $\hat{\mathbf{r}} = \mathbf{r}/r$ the unit vector along the radial direction r. Introducing $\mathbf{k}' = k\hat{\mathbf{r}}$ as the wave vector of the scattered particle with spherical coordinates (k, θ, ϕ) we can write

$$\frac{e^{ik|\mathbf{r}-\mathbf{r}'|}}{|\mathbf{r}-\mathbf{r}'|} \underset{r\to\infty}{\to} \frac{e^{ikr}}{r} e^{-i\mathbf{k}'\cdot\mathbf{r}} \tag{3.49}$$

Using this result, the Lippmann-Schwinger equation (3.47) can once again be rewritten as

$$\psi_k(\mathbf{r}) \underset{r\to\infty}{=} \frac{1}{(2\pi)^{3/2}} e^{ikz} - \frac{1}{4\pi} \frac{e^{ikr}}{r} \int e^{-i\mathbf{k}'\cdot\mathbf{r}'} U(\mathbf{r}')\psi_k(\mathbf{r}')d\mathbf{r}'. \tag{3.50}$$

Now we have established its asymptotic behavior we can compare this last expression to the stationary scattering wave function and arrive at a more elaborate expression of the scattered wave amplitude:

$$\begin{aligned} f(\theta,\phi) &= -\frac{1}{4\pi} \int e^{-i\mathbf{k}'\cdot\mathbf{r}} U(\mathbf{r})\psi_k(\mathbf{r})d\mathbf{r} \\ &= -\frac{1}{4\pi} \langle\phi_{k'}| U |\psi_k\rangle \end{aligned} \tag{3.51}$$

where we have introduced $\phi_{k'} = \exp(i\mathbf{k}'\cdot\mathbf{r})$ as the outgoing plane wave. This is called the *integral representation of the scattering amplitude*. Note that this expression connects the total wave function of the system to the particle we detect at $r \to \infty$ by simply looking at the scattering amplitude. This already gives us a sense of a connection with real experiments where we can only measure particles "far" from the scattering potential. We can now bring back the exact form of the potential $V(\mathbf{r}) = \hbar^2/2mU(\mathbf{r})$ and write the scattering amplitude as

$$f = -\frac{m}{2\pi\hbar^2} \langle\phi_{k'}| V |\psi_k\rangle \tag{3.52}$$

where the *transition matrix element* $T_{k'k}$ is defined by

$$T_{k'k} = \langle\phi_{k'}| V |\psi_k\rangle . \tag{3.53}$$

Plugging this into the expression for the differential cross section (3.27) and denoting the initial and final wave vectors by i and f gives

$$\frac{d\sigma}{d\Omega} = |f|^2 = \frac{m^2}{(2\pi)^2\hbar^4}|T_{fi}|^2 \tag{3.54}$$

To be able to extract useful nuclear information we will need to work out a more elaborate form of this transition matrix T. This will be done in following section.

3.3.4 Born series and the Born approximation

Before digging deeper into the transition matrix, Instead of considering the approximation in the previous chapter we can now look at solving the integral equation (3.37) by means of an expansion [27]. Our starting point will be the incident plane wave as 'zero-order' approximation and writing a sequence of integral functions as

$$\begin{aligned}
\psi_0(\mathbf{r}) &= \phi_k(\mathbf{r}) = e^{i\mathbf{k}\cdot\mathbf{r}} \\
\psi_1(\mathbf{r}) &= \phi_k(\mathbf{r}) + \int G(k,\mathbf{r},\mathbf{r}')U(\mathbf{r}')\psi_0(\mathbf{r}')d\mathbf{r}' \\
&\vdots \\
\psi_n(\mathbf{r}) &= \phi_k(\mathbf{r}) + \int G(k,\mathbf{r},\mathbf{r}')U(\mathbf{r}')\psi_{n-1}(\mathbf{r}')d\mathbf{r}'.
\end{aligned} \tag{3.55}$$

Assuming the sequence converges towards the exact wave function ψ_k we can write the wave function's *Born Series* as

$$\begin{aligned}
\psi_k(\mathbf{r}) = \phi_k(\mathbf{r}) &+ \int G(k,\mathbf{r},\mathbf{r}')U(\mathbf{r}')\phi_k(\mathbf{r}')d\mathbf{r}' \\
&+ \int G(k,\mathbf{r},\mathbf{r}')U(\mathbf{r}')G(k,\mathbf{r}',\mathbf{r}'')U(\mathbf{r}'')\phi_k(\mathbf{r}")d\mathbf{r}'d\mathbf{r}'' \\
&+ \dots \ .
\end{aligned} \tag{3.56}$$

Recalling the picture of Green's functions representing *propagators* we see the expressions on the second and following lines represent multiple 'redirections' of the wave by the potential U (see Fig. 3.3). The particle's momentum is denoted as 'intermediate' when it travels freely between subsequent interaction points, the Green's function G indeed fulfills its role as propagator here. This multiple scattering picture is useful to keep in mind when we discuss the Glauber approximation in Section 5.3 Written in the integral representation from before we get

$$f = -\frac{1}{4\pi}\left\langle \phi_{k'}\right| U + UGU + UGUGU + \dots \left|\phi_k\right\rangle . \tag{3.57}$$

The series is expected to converge quickly if the incident particle's energy is sufficiently fast so it cannot interact with the potential many times or when the potential is sufficiently weak [32]. The first term in this approximation is called the *(first) Born approximation to the scattering amplitude*. We will restrict ourselves to this first term throughout this

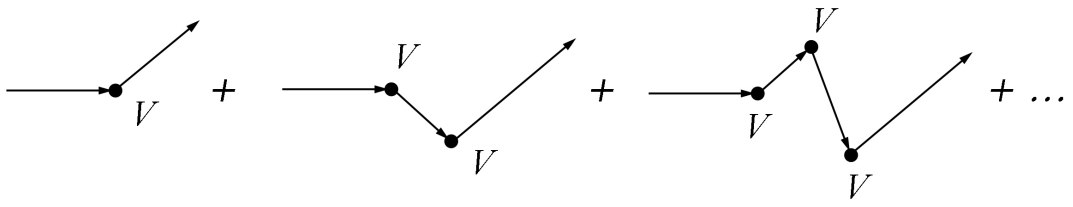

Figure 3.3: Visualization of the Born series as a multiple scattering series.

work. Let us now study this approximation more closely. The amplitude is given by

$$\begin{aligned} f &= -\frac{1}{4\pi}\int e^{i\mathbf{k}'\cdot\mathbf{r}}U(\mathbf{r})e^{i\mathbf{k}\cdot\mathbf{r}}d\mathbf{r} \\ &= -\frac{1}{4\pi}\int e^{i\mathbf{q}\cdot\mathbf{r}}U(\mathbf{r})d\mathbf{r} \end{aligned} \tag{3.58}$$

where we have introduced the wave vector transfer $\mathbf{q} = \mathbf{k} - \mathbf{k}'$ with corresponding momentum transfer equal to $\hbar\Delta$. This last expression shows that the scattering amplitude is proportional to the Fourier transform of the potential corresponding to the wave vector transfer during the collision. Hence the momentum transfer in a collision plays an important role in determining the scattering amplitude. Assuming real potentials we can only have elastic scattering. In this case $|\mathbf{k}| = |\mathbf{k}'| = k$ and the magnitude of the vector $\mathbf{q}$ is given by

$$q = 2k\sin\frac{\theta}{2}. \tag{3.59}$$

3.4 The collision matrix

This section deals with further elaborating the matrix elements we introduced in the previous section. The question here is in what way we can connect a beam of free particles in the remote past (which in between interacts with a target) to the scattered particles which are recorded by the detectors in the far future? At this point we really enter the dynamics of collisions which forces us to choose a certain picture that allows us to study the quantum systems of interest. From the infinite number of pictures we will not choose the familiar Schrödinger or Heisenberg picture but instead the so-called *interaction picture* [25], it is actually an intermediate between the Schrödinger and Heisenberg pictures as we will see below.

3.4.1 The interaction picture

In the interaction picture we split the Hamiltonian in an unperturbed part H_0 and a perturbation V:

$$H_S = H_0 + V \tag{3.60}$$

with the eigenstates of H_0 the free unperturbed solutions ϕ_α such that

$$H_0\phi_\alpha = E_\alpha\phi_\alpha. \tag{3.61}$$

We now want to separate the free motion from the motion of the total system by performing a unitary transformation on the (time-evolving) Schrödinger state vector $\psi_S(t)$:

$$\psi(t) = e^{\frac{i}{\hbar}H_0(t-t_0)}\psi_S(t). \tag{3.62}$$

The time development in the Schrödinger picture is given by

$$i\hbar\frac{\partial}{\partial t}\psi_S(t) = H_S\psi_S(t) \tag{3.63}$$

so this gives for the interaction picture state vector the *Tomonaga-Schwinger* equation [27] :

$$i\hbar\frac{\partial\psi(t)}{\partial t} = V(t)\psi(t) \tag{3.64}$$

with $V(t) = e^{\frac{i}{\hbar}H_0(t-t_0)}Ve^{-\frac{i}{\hbar}H_0(t-t_0)}$. This shows us that the state vector is time dependent as in the Schrödinger picture but this dependence is entirely due to the interaction. The observables are represented by operators whose equations of motion are determined by the unperturbed part of the Hamiltonian H_0 [33]:

$$\frac{dA(t)}{dt} = \frac{1}{i\hbar}[A, H_0] \tag{3.65}$$

with $A(t) = e^{\frac{i}{\hbar}H_0(t-t_0)}A_Se^{-\frac{i}{\hbar}H_0(t-t_0)}$. Hence the operators evolve in time as in the Heisenberg picture but without the interaction. This way we have completely separated the kinematical evolution of observables and the dynamical evolution of state vectors. This separation is particularly convenient for studying collision phenomena.
We can now define an evolution operator in the interaction picture:

$$\psi(t) = U(t, t')\psi(t') \tag{3.66}$$

with group properties $U(t,t) = 1$, $U(t,t') = U(t,t'')U(t'',t')$ and $U^{-1}(t,t') = U(t',t)$. Using the Tomonaga-Schwinger equation (which is valid for all t') we find

$$i\hbar\frac{\partial}{\partial t}U(t,t') = V(t)U(t,t'). \tag{3.67}$$

The fact that U_c is also a unitary operator can simply be shown [27]. Using the same line of thought as with the integral representation of potential scattering we can also write the previous expression as an integral equation:

$$U(t,t') = I - i\int_{t'}^{t} V(t_1)U(t_1,t')dt_1 \tag{3.68}$$

with $U(t,t) = I$ as initial condition. Just like the development of the Born series, we can try to solve this equation by iteration. Starting from the zero order approximation $U^{(0)}(t,t') = I$, the first order approximation becomes

$$U^{(1)}(t,t') = I - i\int_{t'}^{t} V(t_1)dt_1, \tag{3.69}$$

similarly to second order in V

$$U^{(2)}(t,t') = I - i\int_{t'}^{t} V(t_1)dt_1 + (-i)^2 \int_{t'}^{t} dt_1 \int_{t'}^{t_1} dt_2 V(t_1)V(t_2). \tag{3.70}$$

Now we assume the series indeed converges to the evolution operator U so we can write

$$U(t,t') = \sum_{n=0}^{\infty} U_n(t,t') \tag{3.71}$$

with $U^{(0)}(t,t') = I$ and for $n \geq 1$

$$U_n(t,t') = (-i)^n \int_{t'}^{t} dt_1 \int_{t'}^{t1} dt_2 \ldots \int_{t'}^{t_{n-1}} dt_n V(t_1)V(t_2)\ldots V(t_n). \tag{3.72}$$

This is *Dyson's perturbation expansion for the evolution operator*. Since in general the operators $V(t_i)$ do not commute we need to impose the ordering $t' \leq t_n \leq \ldots \leq t_1 \leq t$ for $t' < t$. This is done by introducing the chronological ordering operator P such that

$$P[A(t_1)B(t_2)] = \begin{cases} A(t_1)B(t_2) & \text{if} \quad t_1 > t_2 \\ B(t_2)A(t_1) & \text{if} \quad t_2 > t_1 \end{cases}. \tag{3.73}$$

Integrating for the evolution operator using the operator P gives the expression

$$U_n(t,t') = I + \sum_{n=1}^{\infty} \frac{(-i)^n}{n!} \int_{t'}^{t} dt_1 \int_{t'}^{t} dt_2 \ldots \int_{t'}^{t} dt_n P[V(t_1)V(t_2)\ldots V(t_n)]. \tag{3.74}$$

Applying the operator P and writing the expression in the correct time ordering is often called the *reduction to normal form*.

3.4.2 The Plane Wave Impulse Approximation

Now we have established the interaction picture and its time evolution operator we can start looking into real collisions. In experiments we will need to consider different *channels* or *arrangement channels* [16]. Straightforward examples are elastic and inelastic scattering: given two particles in an initial channel, if the channels are *open*[1] both an elastic and an inelastic collision can occur, hence they each correspond to a different final channel. Another example are one- and two-nucleon knockout, if enough energy is available for a knockout reaction, there is a possibility a second nucleon gets emitted due to the break up of a correlated pair. That being said, we can consider the two-nucleon knockout reaction under study here:

$$p + A \to p' + N_1 + N_2 + A - 2. \tag{3.75}$$

As discussed, in the interaction picture we require a splitting of the Hamiltonian H in an unperturbed part H_0 and a perturbation V. This is a bit problematic in our case since the total Hamiltonian of the system is given by

$$\begin{aligned} H &= H_i + V_{pN_1} + V_{pN_2} + V_{pA-2} \\ &= H_f + V_{pN_1} + V_{pN_2} + V_{N_1A-2} + V_{N_2A-2} + V_{pA-2}. \end{aligned} \tag{3.76}$$

[1] An *open* channel means thre is enough energy available so the reaction can actually happen.

Here H_f and H_i denote the "free" Hamiltonians and contain the kinetic energies of the particles: in the initial channel for a proton and the nucleus, in the final channel for the scattered proton, two knocked-out nucleons and the residual nucleus. This form is obviously too difficult for our analysis here. However, the quasi-free scattering framework helps us out here: we can split the interaction in a "hard" and a "soft" part. Due to the small de Broglie wavelength of the projectile, the interaction happens with only one of the nucleons and not with the nucleus as a whole. This is the so-called *impulse approximation*. We expect the structure of the transition operator to be essentially the same as in free space, the use of plane waves in the matrix element is therefore allowed. Hence we adopt the *plane wave impulse approximation* (PWIA) here, an approximation which will be necessary to eventually factorize the cross section. To justify it, we assume that the interaction between projectile and nucleon is sufficiently short-ranged so that the distorted waves do not change significantly over the range which contributes significantly to the matrix element [34]. The distortion due to initial and final state interactions (IFSI) between the nucleons in the free scattering and the A-2 residual nucleons will be developed in Chapter 5. This also means the Hamiltonian above reduces to

$$H_0 + V = H_i + V_{pN_1} = H_f + V_{pN_1}. \tag{3.77}$$

and for this theoretical calculation we will assume only this channel exists. If a decomposition like this exists, in general also an evolution operator $U(t, t')$ for this particular arrangement channel exists. For what follows it is useful to define the eigenstates of the full and free Hamiltonians separately (using bra and ket notation now)

$$H\left|\psi\right\rangle = E\left|\psi\right\rangle, \qquad \text{and} \qquad H_0\left|\phi\right\rangle = E_0\left|\phi\right\rangle, \tag{3.78}$$

hence ϕ denotes the free state in the asymptotic region.

3.4.3 The S- and T-matrix

In this section we investigate the behavior of the evolution operators at infinite times. After all, these asymptotic regimes are the ones that are interesting since in experiment we can look at the initial states as being prepared in the remote past in a certain arrangement channel ($t' \to -\infty$) and the final states recorded by our detector in the far future ($t \to +\infty$) (in the same or another channel). Therefore it is essential to examine the limit[2] of

[2]Here we use the limiting procedure by Gell-Mann and Goldberger. This is defined by

$$\lim_{t\to-\infty} F(t) = \lim_{\epsilon\to 0^+} \int_{-\infty}^{0} e^{\epsilon t'} F(t')dt'$$

and

$$\lim_{t\to+\infty} F(t) = \lim_{\epsilon\to 0^+} \int_{0}^{+\infty} e^{-\epsilon t'} F(t')dt'.$$

Performing integration by parts on these equations we see that if $F(t)$ has proper limits at $t = \pm\infty$, taking the limit $t = \pm\infty$ and finally letting $\epsilon \to 0^+$ we have

$$\lim_{t\to-\infty} F(t) = F(-\infty) \quad \text{and} \quad \lim_{t\to+\infty} F(t) = F(+\infty).$$

If $F(t)$ oscillates at large $|t|$ the oscillations will be damped by the exponential factors.

the evolution operator for infinite arguments. We define the four operators

$$\begin{aligned} U_c(t,-\infty) &\equiv \lim_{\epsilon\to 0^+} \quad \epsilon\int_{-\infty}^{0} e^{\epsilon t'} U_c(t,t')dt' \\ U_c(t,+\infty) &\equiv \lim_{\epsilon\to 0^+} \quad \epsilon\int_{0}^{+\infty} e^{-\epsilon t'} U_c(t,t')dt' \\ U_c(-\infty,t) &\equiv \lim_{\epsilon\to 0^+} \quad \epsilon\int_{-\infty}^{0} e^{\epsilon t'} U_c(t',t)dt' \\ U_c(+\infty,t) &\equiv \lim_{\epsilon\to 0^+} \quad \epsilon\int_{0}^{+\infty} e^{-\epsilon t'} U_c(t',t)dt'. \end{aligned} \tag{3.79}$$

These operators satisfy the same integral equation as (3.68). We also have the properties

$$U_c^\dagger(t,\pm\infty) = U_c(\pm\infty,t) \quad \text{and} \quad U_c^\dagger(\pm\infty,t) = U_c(t,\pm\infty). \tag{3.80}$$

Subsequently we define the *Møller* operators [27] as

$$\Omega^{(\pm)} \equiv U(0,\mp\infty) \quad \text{and} \quad \Omega^{(\pm)\dagger} \equiv U(\mp\infty,0), \tag{3.81}$$

we see these operators convert an eigenstate ϕ of the free part governed by H_0 to an eigenstate ψ of the full Hamiltonian at $t=0$

$$|\psi^{(\pm)}\rangle = \Omega^{(\pm)}\,|\psi\rangle \qquad \text{and} \qquad \langle\psi^{(\pm)}| = \langle\phi^{(\pm}|\,\Omega^{(\pm)\dagger}. \tag{3.82}$$

The Møller operators are unitary only if the full Hamiltonian H and the free Hamiltonian H_0 have no bound states. This however stands in contrast with the unitarity of the evolution operators for finite times [27].

We can find a less abstract way of connecting the eigenstates of the free Hamiltonian with those of the full Hamiltonian. For this we can reach back to our discussion on potential scattering, we defined the scattering state (using bra and ket notation) in (3.37) as

$$|\psi\rangle = |\phi\rangle + |\psi_{sc}\rangle \tag{3.83}$$

We also know that the scattering wave function satisfies

$$(E_s - H_0)\,|\psi_{sc}\rangle = V\,|\psi\rangle\,. \tag{3.84}$$

with E_s the energy of the free state. Operating on each side with $(E_s - H_0)^{-1}$ and using (3.83) leads to

$$(E_s - H_0 - V)\,|\psi_{sc}\rangle = V\,|\psi\rangle\,. \tag{3.85}$$

Multiplying from the left with $G(E_s)$ we get

$$|\psi_{sc}\rangle = G(E_s)V\,|\psi\rangle \tag{3.86}$$

with the Green's function now corresponding to the full Hamiltonian $H = H_0 + V$. Now we use the same procedure to avoid the poles as we used in (3.46) to write down a general form of the Green's function [35]

$$G(E_s) = \lim_{\epsilon\to 0^+} \frac{1}{E_s - H + i\epsilon} \tag{3.87}$$

Using(3.83) again we can eventually write

$$|\psi\rangle = |\phi\rangle + \lim_{\epsilon\to 0^+} \frac{1}{E_s - H + i\epsilon} V |\phi\rangle \tag{3.88}$$

We can use this result to write for the initial and final channels in our Hamiltonian

$$\begin{aligned} |\psi_i^{(\pm)}\rangle &= |\phi_i\rangle + \lim_{\epsilon\to 0^+} \frac{1}{E_i - H \pm i\epsilon} V_i |\phi_i\rangle \\ |\psi_f^{(\pm)}\rangle &= |\phi_f\rangle + \lim_{\epsilon\to 0^+} \frac{1}{E_f - H \pm i\epsilon} V_f |\phi_f\rangle . \end{aligned} \tag{3.89}$$

and so we have connected the eigenstates ψ of the full Hamiltonian with ϕ the eigenstates of the free Hamiltonian, just like the Møller operators do in (3.82)

Now we are ready to define the so-called *S-matrix*, the central object of collision theory, which relates the state vectors in the remote past ($t' \to -\infty$) and the far future ($t \to \infty$). We define the collision operator S as the composition of two Møller operators [27]

$$S \equiv U(+\infty, 0)U(0, -\infty) = \Omega^{(-)\dagger}\Omega^{(+)}. \tag{3.90}$$

We assume tis operator acts on the free eigenstates $|\phi_i\rangle$ and $|\phi_f\rangle$. Denoting two particular eigenstates as i and f we can obtain the S-matrix element

$$\begin{aligned} \langle f| S |i\rangle &= \langle \phi_f| S |\phi_i\rangle \\ &= \langle \phi_f| \Omega^{(-)\dagger}\Omega^{(+)} |\phi_i\rangle \\ &= \langle \psi_f^{(-)}|\psi_i^{(+)}\rangle . \end{aligned} \tag{3.91}$$

The S-matrix element $\langle f| S |i\rangle$ represents the (time independent) probability amplitude of finding the system described by the interaction picture state $\psi_i^{(+)}$ into the state $\psi_f^{(-)}$. In other words the $\psi_i^{(+)}$ states originates from the asymptotic free state ϕ_i while the $\psi_f^{(-)}$ transforms into ϕ_f. A more explicit expression for can be achieved starting from (3.91)

$$\langle f| S |i\rangle = \langle \psi_f^{(-)}|\psi_i^{(+)}\rangle = \langle \psi_f^{(+)}|\psi_i^{(+)}\rangle + \langle \psi_f^{(-)} - \psi_f^{(+)}|\psi_i^{(+)}\rangle . \tag{3.92}$$

Using the fact that solutions coming from different arrangement channels are orthogonal [27] and (3.89) to get

$$\begin{aligned} \langle f|S|i\rangle &= \delta_{fi} + \lim_{\epsilon\to 0^+} \langle \phi_f| V_f \left(\frac{1}{E_f - H + i\epsilon} - \frac{1}{E_f - H - i\epsilon} \right) |\psi_i^{(+)}\rangle \\ &= \delta_{fi} + \lim_{\epsilon\to 0^+} \left(\frac{1}{E_f - E_i + i\epsilon} - \frac{1}{E_f - E_i - i\epsilon} \right) \langle \phi_f| V_f |\psi_i^{(+)}\rangle \end{aligned} \tag{3.93}$$

By recognizing the representation of the Dirac delta as limit of Lorentzian distributions

$$\lim_{\epsilon\to 0^+} \frac{\epsilon}{(E_f - E_i)^2 + \epsilon^2} = \pi\delta(E_f - E_i) \tag{3.94}$$

we can write

$$\langle f| S |i\rangle \equiv S_{fi} = \delta_{fi} + 2\pi i\delta(E_f - E_i) \langle \phi_f| V_f |\psi_i^{(+)}\rangle . \tag{3.95}$$

In a similar way we get

$$\langle f|\, S\, |i\rangle = \delta_{fi} + 2\pi i\delta(E_f - E_i)\, \langle \psi_f^{(-)}|\, V_i\, |\phi_i\rangle\,. \tag{3.96}$$

Now we can define the transition operator $\hat{T}$ as [27]

$$\hat{T}_{fi}(E) = V_i + V_f \frac{1}{E - H + i\epsilon} V_i, \tag{3.97}$$

which means

$$\langle f|\, \hat{T}\, |i\rangle = T_{fi} = \langle \phi_f|\, V_f\, |\psi_i^{(+)}\rangle = \langle \psi_f^{(-)}|\, V_i\, |\phi_i\rangle\,. \tag{3.98}$$

as long as we remain *on-shell* ($E_i = E_f$), this is assured by the delta function in (3.96). The *T-matrix element* is defined as T_{fi} in will describe the scattering process itself since it contains the scattering potential which in our case is $V_i = V_f = V_{pN_1}$. The entire dynamical content is contained in this expression. This gives

$$S_{fi} = \delta_{fi} + i2\pi\delta(E_f - E_i)T_{fi}. \tag{3.99}$$

We can readily demand momentum conservation as well by inserting another delta function $\delta(\mathbf{P}_f - \mathbf{P}_i)$, this will allow us to imply four-momentum conservation in our reactions

$$S_{fi} = \delta_{fi} + i(2\pi)^4\delta^{(4)}(P_f - P_i)T_{fi} \tag{3.100}$$

where an additional factor $(2\pi)^3$ is included, this is required by the normalization of the initial and final four-momenta, P_i and P_f.

3.5 The Lorentz-invariant cross section

We are almost ready to calculate transition probabilities and cross sections from our knowledge of the S- and T-matrices. But before we do this we should return to our discussion of the kinematics: since we deal with particles at relativistic velocities we require our cross section to be Lorentz-invariant. For this reason we first make sure the states are properly normalized to assure the transition probability and subsequently the cross section are properly defined in a relativistic framework. From this point on we assume $\hbar = c = 1$ unless where they are explicitly stated. They can be added again when numerically evaluating the cross section.

3.5.1 The Lorentz-invariant phase space

As we have just stated, the states that appear in the cross section need to be properly normalized so we can define it as a Lorentz-invariant quantity. The normalization which we wish to choose has its direct implications on the density of final states and thus also on the phase space of the reaction. We will call this the Lorentz-invariant phase space (LIPS). Let us consider a test wave function ψ_0

We could choose

$$\int |\psi_0|^2 dV = \int_V \psi_0^*\psi_0\; d^3\mathbf{x} = 1 \tag{3.101}$$

as normalisation. Using the above normalisation will not result in proper Lorentz invariant expressions. A Lorentz boost along an arbitrary axis will modify the normalisation volume to

$$V = \frac{V_0}{\gamma}. \tag{3.102}$$

Hence the wave function ψ is clearly not Lorentz invariant. The choice of normalisation should assure the wave function behaves correctly under Lorentz transformation. Hence it should be proportional to

$$\gamma = \frac{E}{m}. \tag{3.103}$$

with m the rest mass of the particle. Since the proportionality to the energy E will be decisive, we choose the normalisation of the particle wavefunctions ψ equal to E/m [36] and therefore

$$\psi_0 = \sqrt{\frac{E}{m}}\psi \tag{3.104}$$

resulting in

$$\langle \mathbf{p}|\mathbf{p}'\rangle = \frac{E}{m} V \delta_{\mathbf{p},\mathbf{p}'}. \tag{3.105}$$

In the continuum limit, having $d^3x d^3p = h^3$ this normalization becomes

$$\sum_{\mathbf{p}} \rightarrow \frac{V}{(2\pi)^3}\int d^3p, \qquad\qquad \langle \mathbf{p}|\mathbf{p}'\rangle = \frac{E}{m}(2\pi)^3\delta(\mathbf{p}-\mathbf{p}'). \tag{3.106}$$

The corresponding Lorentz-invariant phase space which we will use becomes

$$d_{LIPS}(\mathbf{p}) = \frac{m}{E}\frac{d^3\mathbf{p}}{(2\pi)^3}. \tag{3.107}$$

To check this is indeed Lorentz invariant, we consider a Lorentz boost along the z-axis, the quantities in the moving frame are denoted by primes:

$$p'_z = \gamma(p_z - \beta E) \qquad \text{and} \qquad E' = \gamma(E - \beta p_z) \tag{3.108}$$

with $\beta = v/c$ and v the speed of the frame. The integration element $d^3\mathbf{p}$ transforms to $d^3\mathbf{p}'$ as

$$d^3\mathbf{p}' = dp_x dp_y \frac{dp'_z}{dp_z} dp_z = d^3\mathbf{p}\frac{dp'_z}{dp_z} \tag{3.109}$$

Differentiating p'_z to p_z gives

$$\frac{dp'_z}{dp_z} = \gamma\left(1 - \beta\frac{dE}{dp_z}\right). \tag{3.110}$$

Now we differentiate E to p_z and we use the energy-momentum relation $E^2 = \mathbf{p}^2 + m^2$. This results in

$$\frac{dE}{dp_z} = \frac{d}{dp_z}\sqrt{\mathbf{p}^2 + m^2} = \frac{p_z}{E}. \tag{3.111}$$

Substituting this result into the previous equation gives

$$\frac{dp'_z}{dp_z} = \frac{\gamma(E - \beta p_z)}{E} = \frac{E'}{E} \tag{3.112}$$

This final statement also means that

$$\frac{m}{E}\frac{d\mathbf{p}}{(2\pi)^3} = \frac{m}{E'}\frac{d\mathbf{p}'}{(2\pi)^3} \tag{3.113}$$

from which we can conclude the phase space is Lorentz invariant and appropriate to use in our calculations. The used normalization will also be important in the determination of the incoming flux as explained below.

3.5.2 The transition probability and cross section

The quantity of interest to look at as an intermediate step to constructing the cross section if the transition probability per unit space-time volume Γ_{fi} given by [37]

$$\Gamma_{fi} = \lim_{V,T\to\infty} \frac{|\langle f|S|i\rangle|^2_{VT}}{VT} \tag{3.114}$$

with the modulus of the matrix element squared (to obtain a probability) evaluated for a finite space-time volume VT [25]. In squaring this expression also the square of the delta function appears. We know that

$$\delta(P_f - P_i) = \frac{1}{(2\pi)^4}\int e^{i(P_f-P_i)\cdot x}d^4x \tag{3.115}$$

and evaluating one integral with $P_f = P_i$ over a large finite volume V and finite time interval T results in a factor $VT/(2\pi)^4$. This allows the limit in (3.114) to be written as

$$\lim_{V,T\to\infty}\frac{1}{VT}\left|\int_{VT} e^{i(P_f-P_i)\cdot x}d^4x\right|^2 = (2\pi)^4\delta^4(P_f - P_i). \tag{3.116}$$

The transition probability per unit space-time volume becomes

$$\Gamma = (2\pi)^4\delta^{(4)}(P_f - P_i)\,|\langle f|T|i\rangle|^2 \tag{3.117}$$

with $\langle f|T|i\rangle = T_{fi}$ the transition matrix element. Γ will however depend on the experiment itself. We include here the average over initial spins and summation over final spins and also the available phase space of the final particles. In case we have a system where only two initial particles are present, the ratio of the transition probability per unit volume and the flux density of the initial state is the cross section [25]

$$d\sigma = \frac{d\overline{\Gamma}}{F}d\Phi \tag{3.118}$$

with $d\Phi$ the phase space and F the flux factor which we also encountered already in Section 3.1. Stated in general, this factor is equal to the probability to find particle 1 per unit volume times the probability to find particle 2 per unit volume multiplied by their relative velocity, correctly providing a measure for the incident flux as required by (3.5). Since we have normalized the states according to (3.106), the flux factor F becomes

$$F = \frac{E_1}{m_1}\frac{E_2}{m_2}\beta_{12} \tag{3.119}$$

with E_1, m_1 the energy and mass of particle 1, E_2, m_2 the energy and mass of particle 2 and β_{12} their relative velocity before collision. Note that this expression is also Lorentz invariant. In a frame where the particles move in a collinear fashion before the interaction (which will be the case in nearly all experiments) we can indeed associate a Lorentz-invariant expression with it. Writing out the expression for the relative velocity gives

$$\begin{aligned} E_1E_2\beta_{12} &= E_1E_2\left|\frac{\mathbf{p}_1}{E_1} - \frac{\mathbf{p}_2}{E_2}\right| \\ &= \left[E_1^2E_2^2\left(\frac{\mathbf{p}_1^2}{E_1^2} + \frac{\mathbf{p}_2^2}{E_2^2} - 2\frac{\mathbf{p}_1\cdot\mathbf{p}_2}{E_1E_2}\right)\right]^{\frac{1}{2}} \\ &= [\mathbf{p}_1^2E_2^2 + \mathbf{p}_2^2E_1^2 - 2E_1E_2\mathbf{p}_1\cdot\mathbf{p}_2]^{\frac{1}{2}}. \end{aligned} \tag{3.120}$$

We now use the properties of the four-momentum and plug in the relation

$$(p_1p_1)^2 = (E_1E_2 - \mathbf{p}_1\cdot\mathbf{p}_2)^2. \tag{3.121}$$

This identity allows a number of terms to cancel out, leaving only

$$E_1E_2\beta_{12} = [(p_1p_2)^2 - m_1^2m_2^2 + \mathbf{p}_1^2\mathbf{p}_2^2 - (\mathbf{p}_1\cdot\mathbf{p}_2)^2]^{\frac{1}{2}}. \tag{3.122}$$

Now we can use the fact that the proton and nucleus move collinearly before the collision by calculating the cross product of the velocities

$$|\mathbf{v}_1\times\mathbf{v}_2|^2 = v_1^2v_2^2 - (\mathbf{v}_1\mathbf{v}_2)^2 = 0 \tag{3.123}$$

which implies $v_1^2v_2^2 = (\mathbf{v}_1\mathbf{v}_2)^2$ and so the last terms also cancel, leaving only

$$E_1E_2\beta_{12} = [(p_1p_2)^2 - m_1^2m_2^2]^{\frac{1}{2}}. \tag{3.124}$$

and

$$E_1E_2\beta_{12} = \sqrt{(p_1p_2)^2 - m_1^2m_2^2} = \frac{1}{2}\sqrt{\lambda(s, m_1^2, m_2^2)} \tag{3.125}$$

where we have used the Mandelstam variable s and defined the triangular λ function

$$\begin{aligned} \lambda(x,y,z) &= (x-y-z)^2 - 4yz \\ &= x^2 + y^2 + z^2 - 2yx - 2zx - 2yz. \end{aligned} \tag{3.126}$$

This expression holds in any Lorentz frame where the particles move collinearly. So finally, for our $A(p,p'NN)A-2$ two-nucleon knockout reaction (using four-momenta)

$$\begin{aligned} &k^\mu_{p_i}(E_{p_i},\mathbf{p}_i) + k^\mu_A(E_A,\mathbf{p}_A) \rightarrow \\ &\quad k^\mu_{p_f}(E_{p_f},\mathbf{p}_f) + k^\mu_{N_1}(E_{N_1},\mathbf{p}_{N_1}) + k^\mu_{N_2}(E_{N_2},\mathbf{p}_{N_2}) + k^\mu_{A-2}(E_{A-2},\mathbf{p}_{A-2}) \end{aligned} \tag{3.127}$$

the Lorentz-invariant cross section becomes

$$\begin{aligned} d\sigma = \overline{\sum_i}\sum_f |\mathcal{M}_{fi}|^2 \frac{2m_{p_i}m_A(2\pi)^4}{\sqrt{\lambda(s,m_{p_i}^2,m_A^2)}}\delta^{(4)}(k_{p_i} + k_A - k_{p_f} - k_{N_1} - k_{N_2} - k_{A-2}) \\ \times \frac{m_{p_f}}{E_f}\frac{d^3\mathbf{p}_f}{(2\pi)^3}\frac{m_{N_1}}{E_{N_1}}\frac{d^3\mathbf{p}_{N_1}}{(2\pi)^3}\frac{m_{N_2}}{E_{N_2}}\frac{d^3\mathbf{p}_{N_2}}{(2\pi)^3}\frac{m_{A-2}}{E_{A-2}}\frac{d^3\mathbf{p}_{A-2}}{(2\pi)^3}. \end{aligned} \tag{3.128}$$

with $\mathcal{M}_{fi}$ the Lorentz-invariant matrix element which will be made explicit in Chapter 6. Now before we continue with writing this expression in a more manageable shape, we need two additional ingredients: our cross section has to include some form of correlation between the probed nucleon states to yield a realistic picture of the nucleus and we must also deal with the initial and final state interactions which we have neglected for now. These topics will be dealt with in the next two chapters.

Chapter 4

Nucleon-nucleon correlations

As discussed before, mean-field methods are able to provide detailed information on a wide variety of nuclei. When it comes to more complex, dense structures inside the nucleus these calculations fall short. In an independent-particle model the nucleons move in an average potential and a lot of nucleon correlations (long- and short range) are neglected [11]. To fully grasp what processes shape the atomic nucleus we need to look beyond this mean-field approach and take correlations between nucleons into account. There is strong reason to believe these correlations can explain the high momentum tail in the distributions above the Fermi momentum [6]. The strengths of the different terms in the NN potential can be determined by scattering experiments and in this way, a phenomenological potential can be derived [3]. In this chapter we will incorporate these phenomena in the scattering cross section: this will be done by including an appropriate correlation operator, as developed in [11]. The behavior of the NN potential will also have a significant effect on the kinematics of the knocked-out particles in our scattering reaction, this will be discussed in 4.4.

4.1 Features of short-range correlations

Nucleon-nucleon correlations can be classified in two categories. The long-range correlations (LRC) are well understood and caused by a one-pion-exchange potential [38]. They account for some reduction of spectroscopic strength, depleting the levels below the Fermi momentum and occupying the states above partially but not enough to explain observations. Short-range correlations are needed to provide a realistic description of the nucleus.

The nucleus can be considered as a quantum mechanical, non-relativistic, A-body system. Its states ψ_A^n are described by A-body wave functions which are a solution to the Schrödinger equation

$$\hat{H}(\mathbf{x}_1, \mathbf{x}_2, \ldots, \mathbf{x}_A)\psi_A^n(\mathbf{x}_1, \mathbf{x}_2, \ldots, \mathbf{x}_A) = E_A^n \psi_A^n(\mathbf{x}_1, \mathbf{x}_2, \ldots, \mathbf{x}_A) \tag{4.1}$$

with $\mathbf{x}_i = (\mathbf{r}_i, \boldsymbol{\sigma}_i, \boldsymbol{\tau}_i)$ representing the generalized coordinate including spatial, spin and isospin degrees of freedom, the Hamiltonian operator $\hat{H}$ in its most general form [39] equal

to

$$\hat{H}(\mathbf{x}_1, \mathbf{x}_2, \ldots, \mathbf{x}_A) = -\frac{\hbar^2}{2m_N}\sum_{i}^{A}\nabla_i^2 + \sum_{i<j}^{A}\hat{v}_2(\mathbf{x}_i, \mathbf{x}_j) \tag{4.2}$$

$$+ \sum_{i<j<k=1}^{A}\hat{v}_3(\mathbf{x}_i, \mathbf{x}_j, \mathbf{x}_k) + \ldots \tag{4.3}$$

and m_N the nucleon mass. The two body $\hat{v}_2$, three body $\hat{v}_3$, ... A-body $\hat{v}_A$ describe the nucleus in an approximative way, each term added provides a more realistic picture of the nucleus. Solving this equation for realistic potentials represents a considerable challenge. The many-body forces are unknown and even if we cut off the expansion at the two-body potentials, the problem remains difficult since a realistic NN potential has a complicated structure due to its spin, isospin and tensor dependence.

It has become a common practice to implement a model for SRC effects in simulations of scattering experiments. We will need a number of basic features extracted from experiments and theoretical calculations from which we can build a realistic NN potential that can also account for these short-range correlations. The most obvious one is the very strong repulsive behavior at short distances (~ 0.5 fm). For this reason usually a "hard core" where $V(r) \to \infty$ for a certain radius r (Fig. 4.1). From electron scattering and other experiments the established value for the proton radius is $\sim 0.8 - 0.9$ fm [40]. However in most calculations a repulsive core at ~ 0.5 fm is chosen [3]. This central, repulsive contribution to short-range correlations is expected to dominate for relative momenta $k >$ 800 MeV/c [6].

Second, for momenta $300 < k < 600$ MeV/c the tensor interaction dominates. It has an attractive nature and preferably selects iso-singlet[1] states as SRC nucleon pairs. This means the correlated pairs will be dominated by np (deuteron) configurations as has also been experimentally verified [22]. We could therefore expect the two-nucleon momentum distribution $n_2(k)$ to be nearly identical to the deuteron momentum distribution $n_D(k)$ above the Fermi momentum k_F. Furthermore it is suggested that this distribution can be scaled to arbitrary nuclei of mass A [41] by

$$n_A(k) = a_2(A, Z)n_D(k) \quad \text{with} \quad k > k_F. \tag{4.4}$$

The ratio $a_2(A, Z)$ can be seen as the relative strength in high momentum tails which is related to the abundance of SRC pairs in comparison to the deuteron. Hence the distribution will be susceptible to the number of possible SRC pairs in a nucleus A. The tensor force also induces a correlation between the spins of the two nucleons as well as a strong spatial correlation. This impacts on the kinematics of SRC measurements which we will discuss in Sec. 4.4.

Spin-isospin correlations are also often put forward as another significant contribution. It indeed contains valuable information on SRC's reflected in measured momentum distributions but the effect of the central and tensor correlations on SRC's is much stronger. A realistic nuclear two-body operator will need to take all of these elements into account.

[1]By definition, a singlet denotes a state in which the total spin adds up to zero.

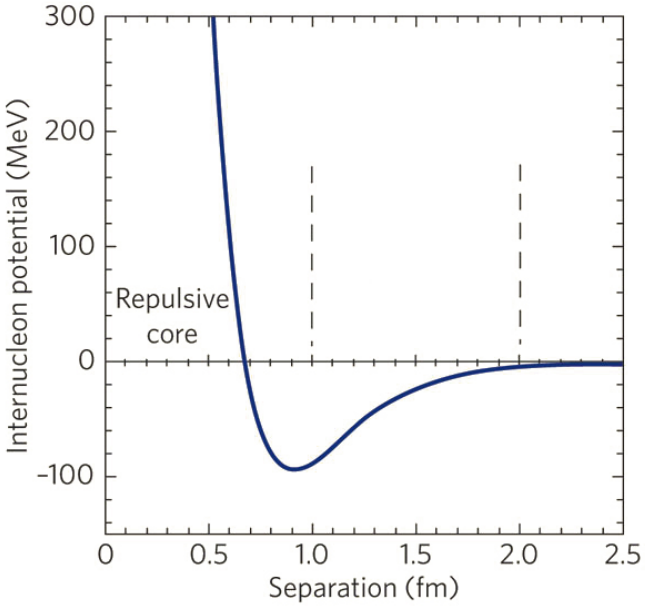

Figure 4.1: The nucleon-nucleon potential as function of the relative distance between two nucleons. The most prominent features are the central repulsive core and the intermediate-range attractive tensor interaction.

4.2 The correlation operator

Now we have identified the main features of short-range correlations we can start incorporating them into our calculations. Starting from an independent particle model, we can write the uncorrelated ground state of a nucleus as an A-body Slater determinant [42]

$$|\Phi_A\rangle = \Phi(\mathbf{x}_1, \mathbf{x}_2, \ldots, \mathbf{x}_A) = \frac{1}{\sqrt{A!}} \det[\phi_{\alpha_i}(\mathbf{x}_j)] \tag{4.5}$$

with ϕ_{α_i} the single particle wave functions and as before $\mathbf{x}_i = (\mathbf{r}_i, \boldsymbol{\sigma}_i, \boldsymbol{\tau}_i)$. We define as in [11] $\alpha_i \equiv n_i l_i j_i m_{j_i} t_i$ the single particle quantum numbers. Stepping away from the IPM and going to a more realistic nuclear wave function, we introduce a correlation operator $\hat{\mathcal{G}}$. To keep everything manageable, we will choose to shift the complexity of including the correlations from the wave functions to the operators. This will allow us to continue working with uncorrelated wave functions in our transition matrix element as well, simplifying things considerably. As stated in [39], the Jastrow ansatz is a first attempt to incorporate the central, spin, isospin and tensor correlations into the original wavefunction

$$\hat{\mathcal{G}} = \hat{\mathcal{S}} \prod_{i<j=1}^{A} \hat{f}(\mathbf{r}_{ij}, \boldsymbol{\sigma}_i, \boldsymbol{\sigma}_j, \boldsymbol{\tau}_i, \boldsymbol{\tau}_j) \tag{4.6}$$

with $\mathbf{r}_{ij} = |\mathbf{r}_i - \mathbf{r}_j|$ the relative coordinate between two nucleons and $\hat{\mathcal{S}}$ the symmetrization operator. The function $\hat{f}$ can be cast in operator form [43] by

$$\hat{f}(\mathbf{r}_{ij}, \boldsymbol{\sigma}_i, \boldsymbol{\sigma}_j, \boldsymbol{\tau}_i, \boldsymbol{\tau}_j) = \sum_{p=1}^{n} \hat{f}^p(r_{ij}) = \sum_{p=1}^{n} f^p(r_{ij}) \mathcal{O}_{ij}^p. \tag{4.7}$$

In a realistic nucleon-nucleon potential like e.g. the Argonne v_{18} [44] this operator consists of $n = 18$ terms. However, we will only need the terms that deliver the SRC given in the previous section: As often described and implemented [45] these correspond to the central ($p = 1$), spin-isospin ($p = 4$) and tensor correlations ($p = 6$)

$$\begin{aligned} \mathcal{O}_{ij}^{p=1} &= 1 && \text{(central)} \\ \mathcal{O}_{ij}^{p=4} &= (\boldsymbol{\sigma}_i \cdot \boldsymbol{\sigma}_j)(\boldsymbol{\tau}_i \cdot \boldsymbol{\tau}_j) && \text{(spin-isospin)} \\ \mathcal{O}_{ij}^{p=4} &= \hat{S}_{ij}(\boldsymbol{\tau}_i \cdot \boldsymbol{\tau}_j) && \text{(tensor)} \end{aligned} \tag{4.8}$$

with $\hat{S}_{ij} = \frac{3}{r_{ij}^2}(\boldsymbol{\sigma}_i \cdot \mathbf{r}_{ij})(\boldsymbol{\sigma}_j \cdot \mathbf{r}_{ij}) - \boldsymbol{\sigma}_i \cdot \boldsymbol{\sigma}_j$ the tensor operator which exclusively affects nucleon pairs in a relative S=1 state. The short-hand notations for the corresponding correlation operators are

$$\begin{aligned} \hat{g}_{ij} &\equiv 1 - f^{p=1}(r_{ij}) = 1 - g(r_{ij}) \\ \hat{s}_{ij} &\equiv f^{p=4}(r_{ij})(\boldsymbol{\sigma}_i \cdot \boldsymbol{\sigma}_j)(\boldsymbol{\tau}_i \cdot \boldsymbol{\tau}_j) = s(r_{ij})(\boldsymbol{\sigma}_i \cdot \boldsymbol{\sigma}_j)(\boldsymbol{\tau}_i \cdot \boldsymbol{\tau}_j) \\ \hat{t}_{ij} &\equiv f^{p=6}(r_{ij})\hat{S}_{ij}(\boldsymbol{\tau}_i \cdot \boldsymbol{\tau}_j) = t(r_{ij})\hat{S}_{ij}(\boldsymbol{\sigma}_i \cdot \boldsymbol{\sigma}_j)(\boldsymbol{\tau}_i \cdot \boldsymbol{\tau}_j). \end{aligned} \tag{4.9}$$

The correlation operator can then be written as

$$\hat{\mathcal{G}} = \hat{\mathcal{S}} \left(\prod_{i<j=1}^{A} [1 - \hat{g}_{ij} + \hat{s}_{ij} + \hat{t}_{ij}] \right). \tag{4.10}$$

The transition matrix element in our cross section should in principle be evaluated between correlated states since it are those states we want to probe. In a rudimentary form it would look like

$$\langle \Psi_A | \hat{\mathcal{O}} | \Psi_A \rangle \tag{4.11}$$

with Ψ_A representing the correlated A-body wave functions. However, shifting the complexity to the operators allows us to construct an effective operator which acts between uncorrelated, independent particle states which will turn out to be a lot easier when we calculate the actual cross section. So instead, an effective operator that will account for the desired correlations is used, giving

$$\frac{1}{\mathcal{N}} \langle \Phi_A | \hat{\mathcal{O}}^{\text{eff}} | \Phi_A \rangle \tag{4.12}$$

with the uncorrelated states Φ_A and the normalization factor $\mathcal{N} = \langle \Phi_A | \hat{\mathcal{G}}^\dagger \hat{\mathcal{G}} | \Phi_A \rangle$.

4.3 The central correlation function

The operator (4.10) can be used in many-body theories and calculations to determine the correlation functions we can use in our cross section. It is important to note that the properties of short-range correlations imply that this is a very local phenomenon, this also explains why there is little mass dependence to be seen in the momentum distributions [46]. The correlation functions are therefore strongly confined to the bulk of the nucleus and depend on internucleon distances [47]. However this does not mean also the correlations functions are universal. The many-body framework from which they are calculated

depends on particular choices of Hamiltonian, single particle basis states, approximation schemes, ... To account for short-range correlations in simulations or experiments the central $g(r_{12})$ and tensor $t(r_{12})$ functions are included since they contribute the most. However, in many cases only central correlations are accounted for [11], we will do the same in this analysis of two-nucleon knockout reactions. In particular the Fourier transform of the central correlation function turns up as a factor in the development of the factorized two-nucleon knockout cross section in Chapter 6. Also the Fourier transform of the tensor correlation would turn up here if it would be included.

The central correlation function $g(r_{12})$ can be calculated by using a G-matrix. This can be carried out in a Brueckner-Hartree-Fock (BHF) approximation in terms of the $\mathcal{G}$-matrix with the bare NN-potential V_{NN} as a variational parameter [48]. The results can be fitted to NN scattering data to eventually yield a realistic central correlation function $g(r_{12})$. In this case a soft-core Reid potential is used, it differs from our hard-core example since this potential only goes to infinity for $r \to 0$ [49] instead of at a fixed value around $r_c = 0.5$ fm. This central correlation function was calculated by Dickhoff and Gearheart and we will use its parametrization as described in [11]. It has a hard core that repels the nucleons for short distances and the function becomes zero for values of $r \geq \frac{2.5}{\sqrt{2}}$ fm where there is no longer an effect of short-range correlations. The function indeed shows the correct long range dependence (Fig. 4.2): due to the shape of the operator (4.10) the factor in our matrix element will be $1 - g(r_{ij}) = 1$ for large r, the particles move independently. This function has been used successfully in exclusive $^{12}C(e, e'pp)$ [50] and $^{16}O(e, e'pp)$ [51] reactions and will also be used in the simulations of Chapter 6.

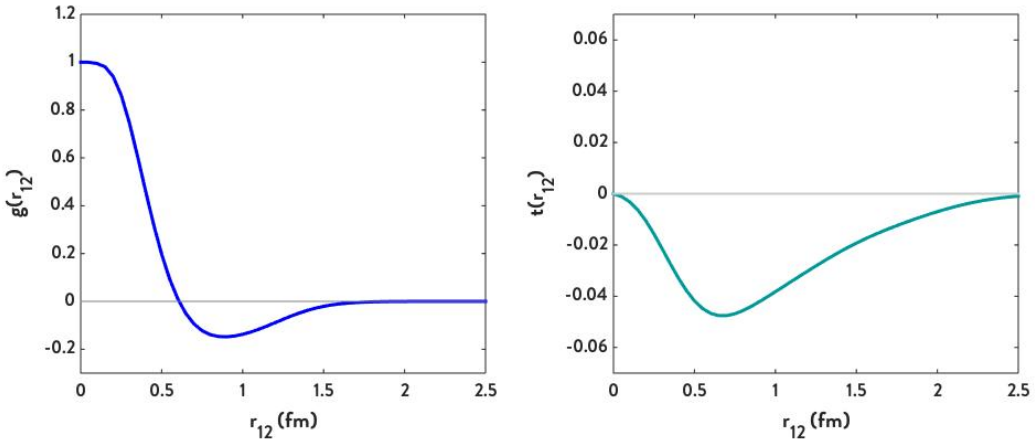

Figure 4.2: The central (left) and tensor (right) correlations functions as parametrized in [11] as function of the internucleon distance r. The tensor correlation function, calculated using a realistic Argonne v_{18} potential is shown only as illustration, it will not be used here when calculating the two-nucleon knockout cross section.

4.4 SRC pair kinematics

The features of short-range correlated pairs discussed above also have their implications on the way they can eventually be detected after a knockout reaction. In literature, SRC

pairs are referred to most of the time as two nucleons with a large relative momentum but small total or center-of-mass momentum, e.g. in [6] and [52]. We can understand this from the strong repulsive nature of the NN potential for short distances. Probing specifically these SRC pairs by quasi-free knockout reactions means taking a 'snapshot' of the momentum configuration and due to the strong repulsion the momenta of the two nucleons in the pair, $\mathbf{k}_1$ and $\mathbf{k}_2$, will be almost completely balanced by each other. This configuration results indeed in a high relative momentum $\mathbf{k}_{12}$ and a low c.o.m. momentum momentum $\mathbf{K}_{12}$ compared to the Fermi momentum k_F, these are defined as

$$\mathbf{k}_{12} \equiv \frac{\mathbf{k}_1 - \mathbf{k}_2}{2} \qquad \text{and} \qquad \mathbf{K}_{12} \equiv \mathbf{k}_1 + \mathbf{k}_2. \tag{4.13}$$

We will come back to these definitions in Chapter 6. For the remainder of this chapter we will assume these quantities are defined w.r.t. the rest frame of the nucleus. We assume that the two-nucleon SRC pair has a small but nonzero total momentum balancing the momenta of the residual $A-2$ nucleus

$$\mathbf{k}_2 \cong -\mathbf{k}_1 \qquad \text{and} \qquad \mathbf{k}_1 + \mathbf{k}_2 + \mathbf{K}_{A-2} = 0. \tag{4.14}$$

Then, by definition (4.13)

$$\mathbf{K}_{A-2} = \sum_{i=3}^{A} \mathbf{k}_i = -\mathbf{K}_{12}. \tag{4.15}$$

This situation corresponds to a *few-nucleon configuration* [53] and is depicted in Fig. 4.3. In a knockout reaction, the SRC nucleons are emitted from the nucleus by the hard interaction with an energetic projectile, in our case a proton with momentum $\mathbf{p}_i$. We will assume the Plane Wave Impulse Approximation is valid for this reaction, this will imply the proton transfers momentum to only one of the nucleons and the measured momenta will not be distorted by interaction of the initial and the final reaction products. The struck nucleon acquires an additional momentum $\mathbf{q}$ from a projectile with initial momentum $\mathbf{p}_i$ and is emitted from the nucleus, the projectile retains a final momentum $\mathbf{p}_f$. This interaction breaks the SRC pair which causes the correlated nucleon to also be emitted due to the high relative momentum of the pair before the reaction. The final momenta of the nucleons after emission are

$$\begin{aligned} \mathbf{p}_1 &= \mathbf{k}_1 + \mathbf{q}, \\ \mathbf{p}_2 &= \mathbf{k}_2 \end{aligned} \tag{4.16}$$

with $\mathbf{q} = \mathbf{p}_i - \mathbf{p}_f$ the transferred momentum. The residual $A-2$ nucleus will get a recoil momentum $\mathbf{P}_r = \mathbf{P}_{A-2} = -\mathbf{K}_{12}$. Hence measuring the momentum of the residual momentum is also a probe for the c.o.m. momentum of the correlated pair. As discussed in Chapter 1, the short-range interactions populate states above the Fermi momentum resulting in a universal 'high-momentum tail'. Since it are exactly these states we wish to probe, we can already apply a certain kinematical cut that assures us we probe only SRC pairs [52]:

$$\mathbf{p}_1 = \mathbf{k}_1 + \mathbf{q} \gg k_F, \qquad \mathbf{p}_2 = \mathbf{k}_2 > k_F. \tag{4.17}$$

A final remark to be made concerns the fact that the momenta of the bound nucleons balance each other almost completely. If the distortion of momenta by initial and final

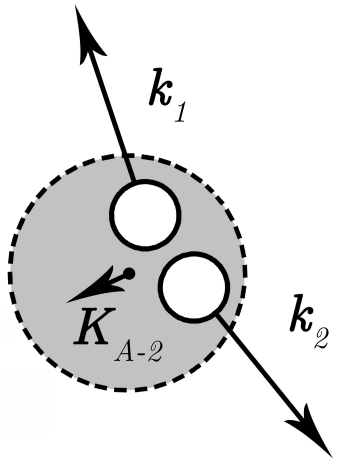

Figure 4.3: Due to the repulsive nature of the NN potential for short distances, the momenta of SRC pairs will almost be balanced by each other as in $\mathbf{k}_2 \cong -\mathbf{k}_1$. Therefore the pairs will have a large relative and small c.o.m. momentum. In the *few-nucleon configuration* [53] the c.o.m. momentum will be balanced by the momentum of the residual $A-2$ nucleus: $\mathbf{K}_{A-2} = -\mathbf{K}_{12}$ due to momentum conservation. The quantities are all expressed in the rest frame of the nucleus (projectile frame).

state interactions remains limited we can assume the PWIA. In this case the "back-to-back" profile can be reconstructed when the particles momenta and directions are measured as in [54] and [22] . We can define the opening angle γ as

$$\cos\gamma = \frac{\mathbf{k}_1 \cdot \mathbf{k}_2}{|\mathbf{k}_1||\mathbf{k}_2|} \tag{4.18}$$

As shown in Fig. 4.4, experiments show a clear tendency towards $\cos\gamma = -1$, pointing at an angle of 180° or a "back-to-back" configuration (Fig. 4.4). We do however need to be careful when initial and final state interactions should be taken into account as will be discussed in Chapter 5.

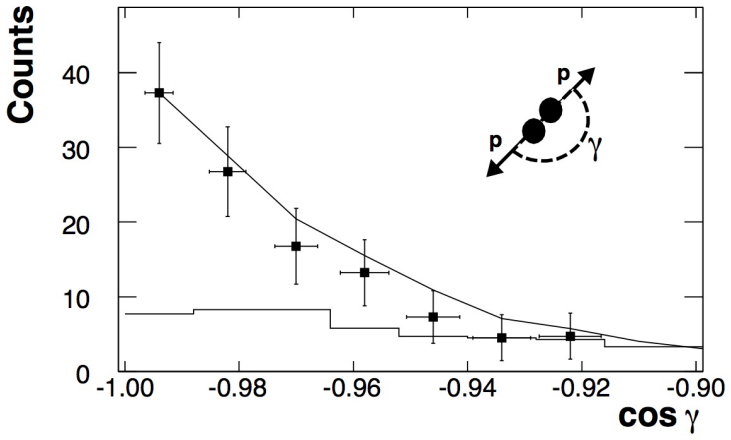

Figure 4.4: Distribution of counts as function of $\cos\gamma$ with γ the opening angle between the momenta of the bound nucleons (from [22]). The SRC pairs show a clear tendency towards a "Back-to-back" configuration for which $\gamma = 180°$.

Chapter 5

Initial and Final state interactions

In Chapter 2 we introduced quasi-free scattering as a possible tool to study short-range correlations. The big advantage of this method is that we can divide our scattering problem in a "hard" and "soft" part. In this chapter we will predominantly focus on the latter. Models of quasi-free (or quasi-elastic) nucleon-knockout reactions rely on the Impulse Approximation: the high-momentum projectile, in our case a proton, probes individual nucleons inside the nucleus A and the energetic interaction causes the bound nucleon(s) to be knocked out. The other nucleons are considered to be 'spectators', the momentum is fully absorbed by the struck nucleon and hence the term 'quasi-free' reaction. In this sense it is tempting to consider the particles in the hard interaction as plane waves. This also allows for a straightforward reconstruction of the initially bound nucleon's momentum by measuring the reaction products. But in reality the "hard" interaction is obscured by the "soft" interactions [55]. The single hard interaction however remains the dominant mechanism contributing to the knockout reaction [34]. In particular, the incoming proton must travel through the nuclear medium before hitting a nucleon experiencing initial-state interactions and also the scattered and knocked out particles are subject to final-state interactions (Fig. 5.1).

5.1 The distorted wave approximation

As in many topics on nuclear reactions and scattering, we can approach these distortion effects from optics. The analogy here is straightforward: the particles that behave like plane waves are distorted when they pass through a certain medium - in this case the nucleus. To account for this distortion a complex optical potential can be used [15], the plane waves ϕ in the PWIA matrix element 3.4.2 are replaced with distorted waves χ. These distorted waves χ are usually found by solving Schrödinger's equation with an appropriate optical nuclear potential which has been obtained by fitting measurements of the corresponding elastic scattering cross-sections [16]. The transition matrix element in the Distorted Wave Impulse Approximation (DWIA) becomes

$$T_{k',k} = \langle \chi_{k'} | V | \chi_k \rangle \tag{5.1}$$

in analogy with (3.53) and the potential V causing the hard interaction. In practice, each distorted wave is expanded in a sum of partial waves which are subsequently integrated to calculate the matrix element. This approach also has a significant drawback: in our quasi-free experiments the particles have relativistic energies on the GeV scale, this makes the

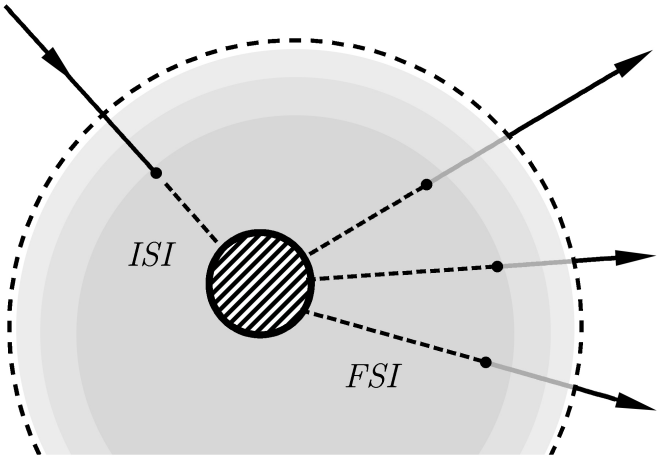

Figure 5.1: Schematic depiction of initial- (ISI) and final-state (FSI) interactions. An incoming projectile interacts with the nuclear medium before the hard collision, the same happens to the outward particles after the collision. These "soft" interactions (dashed lines) obscure the "hard" collision.

number of partial waves needed to reach convergence very high. A relativistic distorted approximation (RDWIA) has been developed to account for energies up to 1 GeV and applied [56] but the parametrization of the optical potentials are usually not available for kinetic nucleon energies above 1 GeV. Also a matter of major concern is the question on how to constrain optical potentials for unstable nuclei. This makes the DWIA not the most economical way to account for IFSI [57] and we will therefore turn to semi-classical theories like the eikonal approximation.

5.2 The eikonal approximation

Having established that the (R)DWIA is not the best way to account for the IFSI in the quasi-free experiments we have in mind, we will need to focus on other methods. An alternative is the *eikonal approximation* which also finds its origins in optics. As in Chapter 2, we look at the de Broglie wavelength λ_{DB} of the particles

$$\lambda_{DB} = \frac{hc}{pc} \tag{5.2}$$

In knockout reactions, particles have kinetic energies typically in the high MeV or even GeV scale. The de Broglie wavelength of the particles become roughly a few femtometer (Fig. 5.2), this short wavelength is a necessary condition if we want to use semi-classical methods like the eikonal approximation [58]. The relative simplicity of both the method itself and the required physical input make the eikonal approximation a valuable tool in studying nuclear reactions [19].

We start the development of the eikonal[1] approximation by considering the scattering of a spinless particle of mass m by a potential $V(\mathbf{r})$ with a characteristic range a and

[1]The word *eikonal* comes from the Greek $\epsilon\iota\kappa o\nu$, which means "image".

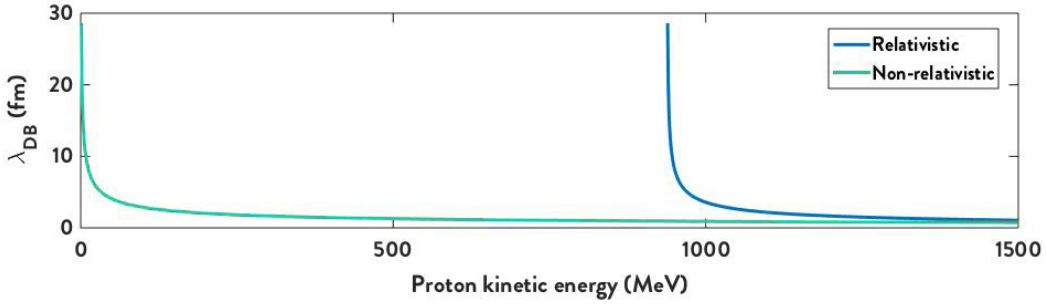

Figure 5.2: The de Broglie wavelength λ_{DB} of a proton as function of its kinetic energy in both the relativistic (blue) and non-relativistic (orange) case. For relativistic protons, energies above 1 GeV are needed to validate the semi-classical eikonal approximation.

V_0 the typical strength of the potential [59]. Then $U(\mathbf{r}) = 2mV(\mathbf{r})/\hbar^2$ is the reduced potential with corresponding strength U_0. The stationary scattering wave function $\psi_k(\mathbf{r})$, exhibiting the correct asymptotic behaviour (incoming plane wave, outgoing spherical wave) satisfies the Lippman-Schwinger equation 3.37

$$\psi_k(\mathbf{r}) = e^{i\mathbf{k}\cdot\mathbf{r}} + \int G_0(\mathbf{r},\mathbf{r}')U(\mathbf{r}')\psi_k(\mathbf{r}')d\mathbf{r}' \tag{5.3}$$

with k the wave number of the incident plane wave, and the Green's function in configuration space written as

$$G_0(\mathbf{r},\mathbf{r}') = -(2\pi)^{-3}\lim_{\epsilon\to 0^+}\int d\mathbf{k}'\frac{e^{i\mathbf{k}'\cdot(\mathbf{r}-\mathbf{r}')}}{k'^2-k^2-i\epsilon}. \tag{5.4}$$

Eqs. (5.3) and (5.4) readily give the correct asymptotic behaviour

$$\psi_k(\mathbf{r}) = \frac{1}{(2\pi)^{3/2}}\left(e^{i\mathbf{k}\cdot\mathbf{r}} + f(\theta,\phi)\frac{e^{ikr}}{r}\right) \tag{5.5}$$

for $\mathbf{r}\to\infty$. In our high-energy approximation, the potential varies slowly with respect to the scale of the incident wavelength. In other words, we assume that if the rapid oscillation of the incident wave is removed, the remainder of the wave function does not oscillate much [60]. This allows us to factor out the free incident plane wave from the stationary scattering wave function and write

$$\psi_k(\mathbf{r}) = \frac{1}{(2\pi)^{3/2}}e^{i\mathbf{k}\cdot\mathbf{r}}\phi(\mathbf{r}). \tag{5.6}$$

Inserting this equation and (5.4) into the (5.3) gives [2]

$$\phi(\mathbf{r}) = 1 - \frac{1}{(2\pi)^3}\int d\mathbf{R}\int d\mathbf{k}'\frac{e^{i(\mathbf{k}'-\mathbf{k})\cdot\mathbf{R}}}{k'^2-k^2-i\epsilon}U(\mathbf{r}-\mathbf{R})\phi(\mathbf{r}-\mathbf{R}) \tag{5.7}$$

where we have set $\mathbf{R} = \mathbf{r}-\mathbf{r}'$. To easily derive an approximate form for $\phi(\mathbf{r})$ we introduce a new variable $\mathbf{p} = \mathbf{k}'-\mathbf{k}$ which modifies the form of the Green's function to a kind of Fourier transform of $U\phi$ and get

$$\phi(\mathbf{r}) = 1 - \frac{1}{(2\pi)^3}\int d\mathbf{R}\int d\mathbf{p}\frac{e^{i\mathbf{p}\cdot\mathbf{R}}}{2\mathbf{k}\cdot\mathbf{p}+p^2-i\epsilon}U(\mathbf{r}-\mathbf{R})\phi(\mathbf{r}-\mathbf{R}) \tag{5.8}$$

[2]From now on we imply taking the limit $\epsilon\to 0^+$ in all steps.

The reason why we redefined $\phi(\mathbf{r})$ and consequently the Lippman-Schwinger equation is now clear: the product $U\phi$ appearing in the momentum space integral varies slowly on the scale of the incident wavelength [27] . Hence, the largest contributions to the integral come from small p/k values, giving us the opportunity to expand the denominator of the Green's function in (5.8) in terms of p/k. We fix the z-axis along the incident wave vector which gives

$$\frac{1}{2\mathbf{k}\cdot\mathbf{p}+p^2-i\epsilon} = \frac{1}{2kp_z+p^2-i\epsilon} \tag{5.9}$$

$$= \frac{1}{2kp_z-i\epsilon} - \frac{1}{(2kp_z-i\epsilon)^2}p^2 + \dots \ . \tag{5.10}$$

Choosing this specific direction will prove to be very important to our approximation as we will show further on. Taking only the first (linear) term in the expansion into account we can now write for the Green's function

$$G_0^{(1)}(\mathbf{R}) = -\frac{e^{(i\mathbf{k}\cdot\mathbf{R})}}{(2\pi)^3}\int d\mathbf{p}\frac{e^{i\mathbf{p}\cdot\mathbf{R}}}{2kp_z-i\epsilon}. \tag{5.11}$$

To justify this particular step we use our short-wavelength condition $ka \gg 1$ with a the range of the potential. By

$$k = \frac{p}{\hbar}, \qquad \text{and} \qquad \lambda_{DB} = \frac{h}{p} \tag{5.12}$$

we can infer that due to the small de Broglie wavelength, the wave number k will be large and since the potential range a is typically of the order of femtometers [55]. This means the condition $ka \gg 1$ is fulfilled and as a result $G_0^{(2)}(\mathbf{R})$ is a lot smaller than $G_0^{(1)}(\mathbf{R})$. Furthermore the second term in the expansion will result in an expression of order U_0/k^2. In light of this we also demand $U_0/k^2 \ll 1$ or equivalently $|V_0|/E \ll 1$ with E the energy of the particle. This requirement is also fulfilled since a typical potential strength V_0 is of order 50 MeV [15] so we can safely continue.

We examine the $\mathbf{p}$ integral in the above expression by switching to Cartesian coordinates

$$\int d\mathbf{p}\frac{e^{i\mathbf{p}\cdot\mathbf{R}}}{2kp_z-i\epsilon} = \int_{-\infty}^{+\infty} dp_x\ e^{ip_xX}\int_{-\infty}^{+\infty} dp_y\ e^{ip_yY}\int_{-\infty}^{+\infty} dp_z\frac{e^{ip_zZ}}{2kp_z-i\epsilon} \tag{5.13}$$

$$= (2\pi)^2\delta(X)\delta(Y)\int_{-\infty}^{+\infty} dp_z\frac{e^{ip_zZ}}{2kp_z-i\epsilon} \tag{5.14}$$

where we used the integral representation of the Dirac delta function. The integral over p_z can be performed easily in the complex plane (see Appendix A) . Closing the contour in both hemispheres renders the following expression

$$G_0^{(1)}(\mathbf{R}) = \begin{cases} -\frac{ie^{ikZ}}{2k}\delta(X)\delta(Y) & \text{if } Z>0, \\ 0 & \text{if } Z<0. \end{cases} \tag{5.15}$$

We can now return to our original variables and introduce the step function to express the two values of the Green's function in a more elegant way

$$G_0(\mathbf{r},\mathbf{r}') = -\frac{ie^{ik(z-z')}}{2k}\delta(x-x')\delta(y-y')\Theta(z-z') \tag{5.16}$$

where we have dropped the redundant superscript (1). This expression forms a cornerstone in formulating the eikonal approximation: as we can clearly see, the delta functions fix the propagator to the z-axis and the step function ensures there is only purely forward motion. Using this linearized propagator simplifies the expression (5.8) when we evaluate the integrals

$$\phi(x,y,z) = 1 - \frac{i}{2k}\int_{-\infty}^{z} U(x,y,z')\phi(x,y,z')dz' \tag{5.17}$$

where we have switched to the variable $z' = z - Z$. Recalling the series expansion of the exponential function we can write

$$\phi(x,y,z) = e^{-\frac{i}{2k}\int_{-\infty}^{z} U(x,y,z')dz'}. \tag{5.18}$$

We can notice that ϕ varies negligibly over distances of order k^{-1} since U_0/k^2 is small. Thus for distances which are large compared to k^{-1} the product $U\phi$ also varies slowly. Hence the important values of p in (5.8) are small compared to k, justifying the expansion in powers of p/k. Now we can return to our ansatz (5.6) and obtain the *eikonal wave function*

$$\psi_{eik}(\mathbf{r}) = \frac{1}{(2\pi)^{3/2}} e^{i\left(\mathbf{k}\cdot\mathbf{r} - \frac{1}{2k}\int_{-\infty}^{z} U(x,y,z')dz'\right)}, \tag{5.19}$$

or in terms of the potential $V(\mathbf{r}) = \hbar^2 U(\mathbf{r})/2m$

$$\psi_{eik}(\mathbf{r}) = \frac{1}{(2\pi)^{3/2}} e^{i\left(\mathbf{k}\cdot\mathbf{r} - \frac{1}{\hbar v}\int_{-\infty}^{z} V(x,y,z')dz'\right)} \tag{5.20}$$

with $v = \hbar k/m$ the magnitude of the incident velocity. The eikonal approximation simply results in a phase shift of the incident plane wave.

We do need to admit the eikonal wave function does not exhibit the correct asymptotic behavior (5.5) for $\mathbf{r} \to \infty$. However, since we will use the integral representation to calculate the scattering amplitude we only need to know the scattering wave function where the potential is non-vanishing, thus only here the modulating function ϕ modifies the incident plane wave.

Now the eikonal wave function can be used to calculate scattering amplitudes. The eikonal scattering amplitude is given by

$$f_E = -\frac{1}{4\pi}\langle \phi_{k'} | U | \psi_{eik} \rangle \tag{5.21}$$

$$= -\frac{1}{4\pi}\int d\mathbf{r}\; e^{-i\mathbf{k}'\cdot\mathbf{r}} U(\mathbf{r}) e^{i\left(\mathbf{k}\cdot\mathbf{r} - \frac{1}{2k}\int_{-\infty}^{z} U(x,y,z')dz'\right)} \tag{5.22}$$

with $\phi_{k'} = e^{-i\mathbf{k}'\cdot\mathbf{r}}$ the outgoing plane wave. Denoting with $\mathbf{q} = \mathbf{k} - \mathbf{k}'$ the wave vector transfer we can write

$$f_{eik} = -\frac{1}{4\pi}\int d\mathbf{r}\; e^{i\mathbf{q}\cdot\mathbf{r}} U(\mathbf{r}) e^{-\frac{i}{2k}\int_{-\infty}^{z} U(x,y,z')dz'} \tag{5.23}$$

We can intuitively understand why the (linearized) z' integration results in a loss of accuracy: since the approximation is semi-classical we should be evaluating this expression

along the actual curved classical trajectory. It is possibly better to perform the integration along a direction $\hat{\mathbf{n}}$, parallel to the bisector of the scattering angle θ and perpendicular to the vector $\mathbf{q}$. To simplify we adopt a cylindrical coordinate system [35] with $\mathbf{r} = \{b, z, \varphi\}$ and decompose the vector $\mathbf{r}$ as

$$\mathbf{r} = \mathbf{b} + z\hat{\mathbf{n}}. \tag{5.24}$$

Now $\mathbf{b}$ is an 'impact parameter' vector corresponding to the projection of $\mathbf{r}$ on the xy-plane, it is perpendicular to $\hat{\mathbf{n}}$ and subtends an azimuthal angle φ within the range $(0, 2\pi)$. Accordingly the volume element is

$$d\mathbf{r} = bdbdzd\varphi \tag{5.25}$$

The z component of $\mathbf{r}$ lies along $\hat{\mathbf{n}}$. When dealing with impact parameters it is only logical we integrate in terms of surface elements $d^2\mathbf{b} = bdbd\varphi$. This way we can write (5.23) as

$$f_{eik} = -\frac{1}{4\pi}\int d^2\mathbf{b}\int_{-\infty}^{+\infty} dz\; e^{i\mathbf{q}\cdot\mathbf{b}}U(\mathbf{b},z)e^{-\frac{i}{2k}\int_{-\infty}^{z}U(\mathbf{b},z')dz'} \tag{5.26}$$

since $\mathbf{q}\cdot\mathbf{r} = \mathbf{q}\cdot\mathbf{b}$. The integration over the z variable is now pretty straightforward: we change variables to

$$z \to w = -\frac{i}{2k}\int_{-\infty}^{z} U(\mathbf{b},z')dz' \quad \text{with} \quad dz = \frac{2k}{iU(\mathbf{b},z)}dw. \tag{5.27}$$

The integral now takes the form

$$f_{eik} = -\frac{ik}{2\pi}\int d^2\mathbf{b}e^{i\mathbf{q}\cdot\mathbf{b}}\int_{0}^{i\chi(k,\mathbf{b})} dw\; e^{w} \tag{5.28}$$

where we introduced the *eikonal phase shift function*

$$\chi(k,\mathbf{b}) = -\frac{1}{2k}\int_{-\infty}^{+\infty} U(\mathbf{b},z)dz. \tag{5.29}$$

Performing the w integral yields the eikonal scattering amplitude

$$f_{eik} = \frac{ik}{2\pi}\int d^2\mathbf{b}\; e^{i\mathbf{q}\cdot\mathbf{b}}[1 - e^{i\chi(k,\mathbf{b})}]. \tag{5.30}$$

A final remark can be made on the angular validity of the eikonal approximation. Suppose we perform the z' integration along the original direction $\hat{\mathbf{k}}_i$. For small scattering angles the vector $\mathbf{q}$ will be almost perpendicular to $\mathbf{k}_i$ so we can construct our cylindrical coordinate system with

$$\mathbf{r} = \mathbf{b} + z\hat{\mathbf{k}}_i. \tag{5.31}$$

We can expand the quantity $\mathbf{q}\cdot\mathbf{r}$ for small angles to

$$\mathbf{q}\cdot\mathbf{r} = \mathbf{q}\cdot(\mathbf{b} + z\hat{\mathbf{k}}_i) = \mathbf{q}\cdot\mathbf{b} + kz(1-\cos\theta) \simeq \mathbf{q}\cdot\mathbf{b} \tag{5.32}$$

where we have neglected the terms of order $\theta^2 kz \lesssim \theta^2 ka$. Consequently a qualitative angular validity criterion is given by $\theta \ll (ka)^{-1/2}$ using this coordinate system. It is not

unreasonable to expect that the choice of coordinate system as in (5.24) will lead to an improved angular domain of validity [59].

The big advantage of the eikonal approximation is the ability to expand this theory to multiple scattering. Instead of considering the distortion due to a general nuclear optical potential, the distortion by scattering with multiple particles is used. This will form the basis of the Glauber approximation discussed in the next section.

5.3 The Glauber approximation

As we already stated before, when the wavelength of the incident particle is short compared to the interaction region we can use a semiclassical approach. An approximation like this is justified since the average trajectory differs little from the classical one. This also allows us to use classically well know phenomena such as diffraction patterns in optics to deduce structure information from nuclei.

A first naive interpretation can be made by considering diffraction from a black disk, where *black* means that any incident particle is completely absorbed. We can discern characteristic features like a large, forward diffraction peak and the appearance of minima and maxima in the diffraction pattern. The first minimum lies approximately at an angle $\theta_{min} \approx \lambda/2R_0$ with R_0 the radius of the disk. The equivalent in nuclear scattering physics of this optical analysis is known as *Fraunhofer diffraction*. This approximation can be derived from the eikonal approximation when the effects of the Coulomb field can be neglected [16].

We can improve the amount of information we can collect by making an adjustment: instead of considering the nucleus as a black disk we assume it to be *gray* [61]. As we can recall from our discussion of the eikonal approximation, in the cylindrical coordinate system

$$\mathbf{r} = \mathbf{b} + z\hat{\mathbf{n}}, \tag{5.33}$$

the shadow of a grey scatterer will not be uniformly black but instead its transmission will be a function of $\mathbf{b}$ (Fig. 5.3). In the black disk approximation the total wave function behind the scatterer is zero. For a gray scatterer it is assumed that the total wave function behind the scatterer in the shadow plane is modified by a multiplicative factor [61]

$$\psi_s(\mathbf{b}) = -e^{i\mathbf{k}\cdot\mathbf{b}} e^{i\chi(k,\mathbf{b})} \tag{5.34}$$

with $\mathbf{k}$ the incident wave vector chosen along the z-axis. This means the factor $\exp(i\mathbf{k}\cdot\mathbf{b})$ is equal to 1 but we will keep it here since it will prove to be convenient. We can understand this more clearly when looking at the optical analog: when a light wave passes through a medium with refraction index of refraction n and thickness d its electric vector is modified by a factor $\exp(i\chi)$ with $\chi = k(1-n)d$. If the index of refraction is complex, the imaginary part describes absorption of the wave. Recalling our formulation for the total stationary scattering wave function 5.5

$$\begin{aligned} \psi_k(\mathbf{r}) &\sim e^{i\mathbf{k}\cdot\mathbf{r}} + f(\theta,\phi)\frac{e^{ikr}}{r} \\ &= e^{i\mathbf{k}\cdot\mathbf{r}} + \psi_s(\mathbf{r}) \end{aligned} \tag{5.35}$$

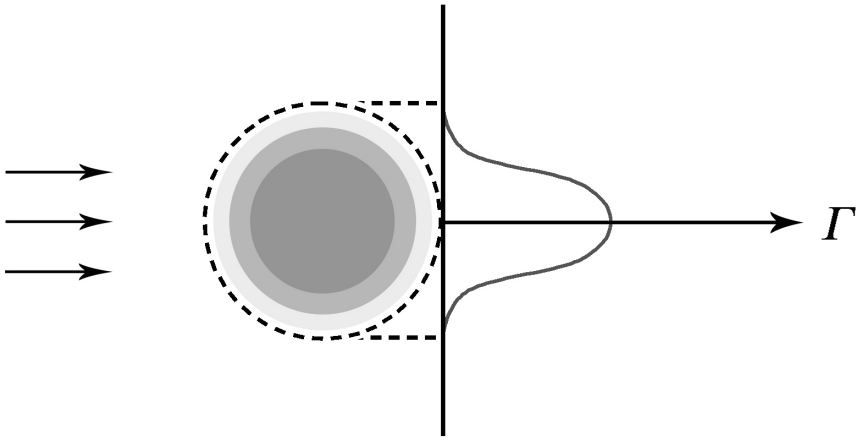

Figure 5.3: In analogy with optical scattering, the nucleus can be depicted realistically as a grey scatterer instead of a black disk. The shadow cast by an incoming beam on an imaginary plane has a profile Λ and will be a function of the impact parameter $\mathbf{b}$.

with $\exp(i\mathbf{k}\cdot\mathbf{r}) = \exp(ikz)$ and ψ_s the scattered wave function. Converting to the cylindrical coordinate system and evaluating in the shadow plane ($z = 0$) we get

$$\psi_k(\mathbf{r}) = \psi_k(\mathbf{b}, z = 0) = 1 + \psi_s(\mathbf{b}). \tag{5.36}$$

This should be equal to (5.34) so we get for ψ_s

$$\begin{aligned}\psi_s(\mathbf{b}, z = 0) &= e^{i\mathbf{k}\cdot\mathbf{b}} - e^{i\mathbf{k}\cdot\mathbf{b}} e^{i\chi(k,\mathbf{b})} \\ &= e^{i\mathbf{k}\cdot\mathbf{b}}[1 - e^{i\chi(k,\mathbf{b})}]\end{aligned} \tag{5.37}$$

The expression in between brackets is called the *profile function* $\Gamma(\mathbf{b})$. For small scattering angles we can prove analogously to (5.30) that the scattering amplitude is equal to

$$f(\mathbf{q}) = \frac{ik}{2\pi}\int d^2\mathbf{b} e^{i\mathbf{q}\cdot\mathbf{b}}\Gamma(\mathbf{b}) \tag{5.38}$$

with as inverse

$$\Gamma(\mathbf{b}) = \frac{1}{2\pi ik}\int d^2\mathbf{q} e^{-i\mathbf{q}\cdot\mathbf{b}} f(\mathbf{q}) \tag{5.39}$$

and still $\mathbf{q} = \mathbf{k} - \mathbf{k}'$. Hence the scattering amplitude is the Fourier transform of the profile function. Note that equation (5.38) is equivalent to Eq. (5.30), the eikonal scattering amplitude. The extension to relativistic energies can simply be made by calculating this amplitude for relativistic wavefunctions [62]. This in turn allows us to develop a relativistic Glauber approximation.

It is important to note that in principle the profile function of a scatterer can readily be determined from an experiment in which the eikonal approximation is validated. The potential $U(\mathbf{b}, z)$ doesn't need to be known, the eikonal phase shift function $\chi(k, \mathbf{b})$ (5.29) can be extracted by analyzing elastic scattering data. We deal with individual nucleons in our case, so the profile function can be fitted to free NN scattering cross sections. To

sketch how we can achieve this let us assume the NN scattering amplitude at high energy, small angles and neglecting Coulomb effects can be written as a Gaussian [63]

$$f(\mathbf{q}) = \frac{k'\sigma}{4\pi}(\epsilon + i)e^{-\frac{\beta^2\mathbf{q}^2}{2}} \tag{5.40}$$

with σ the total cross section. The elastic scattering amplitude is directly related to the elastic cross section by [64]

$$\frac{d\sigma_{el}}{dq} = \frac{1}{k'^2}|f(\mathbf{q})|^2 = \frac{\sigma^2}{16\pi^2}(1+\epsilon^2)e^{-\beta^2 q^2} \tag{5.41}$$

corresponding to the standard high energy parametrization[3] of the elastic differential cross section [62]. From fitting this cross section to experimental NN cross sections (Fig. 6.2) we can extract the fit parameters ϵ and β which both are momentum dependent. These can in turn be used to invert (5.40) so the NN profile function becomes [65]

$$\Gamma_{NN}(\mathbf{b}) = \frac{\sigma_{NN}}{4\pi\beta_{NN}^2}(1 - i\epsilon_{NN})e^{-\frac{\mathbf{b}^2}{2\beta_{NN}^2}} \tag{5.42}$$

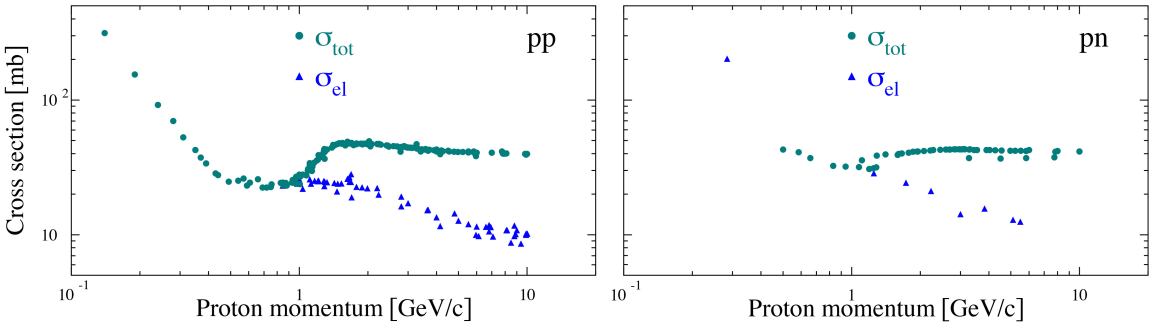

Figure 5.4: Elastic *pp* and *pn* cross section data from [66]. The fit parameters ϵ and β in (5.42) can be used to determine the NN profile functions Γ_{NN} which we will use in a multiple scattering Glauber framework to analyze the IFSI. Image taken from [64].

Up to now we have only considered diffraction scattering from a single object. A second adjustment consists of taking into account the coherent scattering of a projectile from a target composed of several subunits, like a nucleus made up of several nucleons. We reach back once more to optical diffraction where a wave passes through n absorbers, each of them characterized by a certain phase χ_i. The initial electric vector is then modified by a factor $\exp(i\chi_1)\exp(i\chi_2)\ldots\exp(i\chi_i) = \exp(i[\chi_1 + \chi_2 + \ldots + \chi_n])$. The phases of the different absorbers add. This forms the criterion for the *Glauber approximation*: we assume the phases from individual scatterers in a compound system, such as a nucleus, also add. In a nucleus, the individual nucleons are located at a certain distance s_i from the z-axis perpendicular to the shadow plane (Fig. 5.5). Hence the distance that determines the profile function for each nucleon is no longer b but $b - s_i$. The phase factor for the ith nucleon is then given by

$$e^{i\chi_i} = 1 - \Gamma_i(\mathbf{b} - \mathbf{s}_i). \tag{5.43}$$

[3]In this sense, note we can write this expression in terms of the Mandelstam variable $t = (k^\mu - k'^\mu)^2$, defined in Chapter 3. In literature, the elastic cross section is mostly expressed this way.

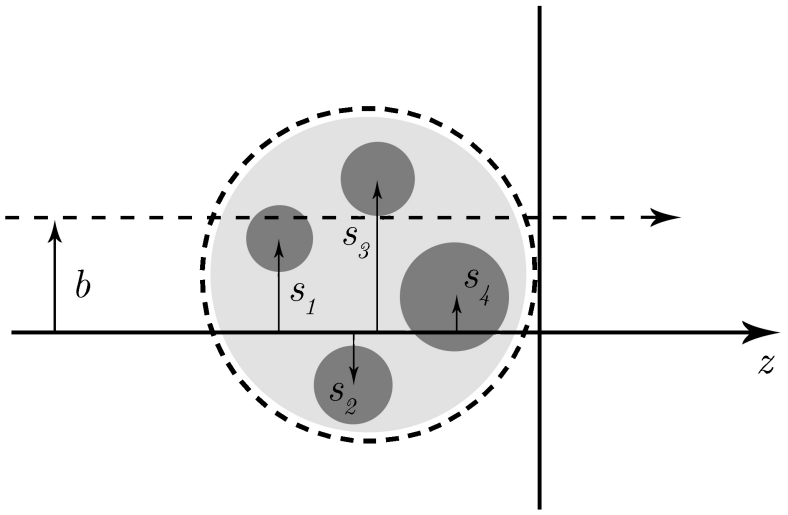

Figure 5.5: The nucleus is arranged as a system of different scatterers, the nucleons. The distance that determines the profile functions on the shadow plane of these individual scatterers is now $b - s_i$ with s_i denoting the distance of each nucleon from the z-axis.

The Glauber approximation tells us we can add the individual phases so the total phase factor becomes

$$e^{i\chi} = e^{i\chi_1} e^{i\chi_2} \dots e^{i\chi_A} \tag{5.44}$$

$$= \prod_{i=1}^{A} [1 - \Gamma_i(\mathbf{b} - \mathbf{s}_i)], \tag{5.45}$$

so the complete profile function for the composite scatterer becomes

$$\Gamma(\mathbf{b}) = 1 - \prod_{i=1}^{A} [1 - \Gamma_i(\mathbf{b} - \mathbf{s}_i)]. \tag{5.46}$$

Applying these statements to real situations is now straightforward. In particular for our $A(p, p'NN)A-2$ reaction the individual profile function Γ_i can be replaced by the NN profile functions Γ_{NN}. Four particles, the initial and final proton and the two knocked-out nucleons, travel through the nuclear medium before and after the hard interaction and are attenuated by the spectator $A-2$ nucleons. Hence their respective wave functions should be multiplied by the appropriate Glauber operator which incorporates the multiple

scattering picture according to [11]:

$$\begin{aligned}
\hat{S}_{p_i}(\mathbf{r}_1, \mathbf{r}_2; \mathbf{r}_3, \ldots, \mathbf{r}_A) &= \prod_{j=3}^{A} [1 - \Gamma_{pN}(p_i, \mathbf{b} - \mathbf{b}_j)\theta(z - z_j)], \\
\hat{S}_{p_f}(\mathbf{r}_1, \mathbf{r}_2; \mathbf{r}_3, \ldots, \mathbf{r}_A) &= \prod_{j=3}^{A} [1 - \Gamma_{pN}(p_f, \mathbf{b}' - \mathbf{b}'_j)\theta(z'_j - z')], \\
\hat{S}_{N_1}(\mathbf{r}_1, \mathbf{r}_2; \mathbf{r}_3, \ldots, \mathbf{r}_A) &= \prod_{j=3}^{A} [1 - \Gamma_{NN}(p_{N_1}, \mathbf{b}'' - \mathbf{b}''_j)\theta(z''_j - z'')], \\
\hat{S}_{N_2}(\mathbf{r}_1, \mathbf{r}_2; \mathbf{r}_3, \ldots, \mathbf{r}_A) &= \prod_{j=3}^{A} [1 - \Gamma_{NN}(p_{N_2}, \mathbf{b}''' - \mathbf{b}''''_j)\theta(z'''_j - z''')].
\end{aligned} \tag{5.47}$$

with the distances s_i replaced by b_j here.The step functions are added to the Glauber operators to ensure that the incoming proton only interacts with nucleons in its forward propagating path before the collision, likewise the outgoing nucleons only interact with nucleons on their outward path after collision. The coordinates $(\mathbf{r}_3, \ldots \mathbf{r}_A)$ denote the positions of the frozen spectator nucleons, the interactions itself can take place at coordinates $(\mathbf{r}_1, \mathbf{r}_2)$ but we will come back to this later.

The Glauber operators are genuine A-body operators, this makes the numerical evaluation of the compound effect of initial and final state interactions very difficult. The big advantage however is that all parameters necessary for this relativistic multiple scattering Glauber approximation (RMSGA from now on) can be extracted from experiment, something which is not the case for distorted wave approximations like the RDWIA. The Glauber theory and its relativistic extension have been shown to be very successful in high energy electron and proton scattering processes, as reported in [67] and [68].

5.4 Nuclear Transparency

As established in Chapter 1, we want to perform experiments that are sensitive to specific features of short-range correlated pairs in nuclei. We are particularly interested in measuring the momentum distribution of the nucleons that will reveal those features. To give a hint at what comes up in the next chapter: it turns out that the cross section for quasi-free two-nucleon knockout reactions we will develop in the next chapter is indeed sensitive to the c.m. momentum distribution of the SRC pairs. The reason why quasi-free knockout reactions are an ideal probe is the fact that due to the Plane Wave Impulse Approximation (PWIA), we can reconstruct the individual momenta of the bound nucleons by measuring the reaction products. Knowing the kinematics of the particles before and after the reaction suffices since the projectile only has a hard interaction with a single nucleon inside the nucleus. However, as we have just established, the measured momenta of the final products will inevitably be distorted because of the "soft" interaction with the spectator nucleons inside the nucleus. The aggregated effect of the distortion enters

as a factor $\hat{S}_{\text{IFSI}}$ in the momentum distribution of the knocked out nucleons as

$$F^{NN,D}_{\alpha_1,\alpha_2}(\mathbf{K}_{12}) = \sum_{\alpha_1,\alpha_2} \left| \int d\mathbf{R}_{12} e^{i\mathbf{K}_{12}\cdot\mathbf{R}_{12}} \psi_{\alpha_1}(\mathbf{R}_{12})\psi_{\alpha_2}(\mathbf{R}_{12})\hat{S}_{\text{IFSI}}(\mathbf{R}_{12}) \right|^2 \tag{5.48}$$

with $\mathbf{K}_{12}$ and $\mathbf{R}_{12}$ respectively the c.o.m. momentum and coordinate of the nucleon pair. In this expression D denotes the fact that the distribution is distorted and α_i the quantum numbers of the individual nucleons. In full, we can write the factor $\hat{S}_{\text{IFSI}}$ as [69]

$$\begin{aligned} \hat{S}_{\text{IFSI}}(\mathbf{R}_{12}) = \int d\mathbf{r}_3 \cdots \int d\mathbf{r}_A \ |\phi_{\alpha_3}(\mathbf{r}_3)|^2 \cdots |\phi_{\alpha_A}(\mathbf{r}_A)|^2 \hat{S}_{p_i}(\mathbf{R}_{12};\mathbf{r}_3,\ldots,\mathbf{r}_A) \\ \times \hat{S}_{p_f}(\mathbf{R}_{12};\mathbf{r}_3,\ldots,\mathbf{r}_A)\hat{S}_{N_1}(\mathbf{R}_{12};\mathbf{r}_3,\ldots,\mathbf{r}_A)\hat{S}_{N_2}(\mathbf{R}_{12};\mathbf{r}_3,\ldots,\mathbf{r}_A) \end{aligned} \tag{5.49}$$

according to the RMSGA operators in (5.47). Note that here we have already explicitly made use of the zero-range approximation in the sense that we assume the wave functions of the knocked-out pair have been brought into the continuum at the same point, in this case their c.m. coordinate. This is reasonable for short-range pairs [70], we will come back to this essential approximation in the next chapter. We can now define the *nuclear transparency* according to [26] as

$$T^{NN}_A \approx \frac{\int d\mathbf{K}_{12}\ F^{NN,D}_{\alpha_1,\alpha_2}(\mathbf{K}_{12})}{\int d\mathbf{K}_{12}\ F^{NN}_{\alpha_1,\alpha_2}(\mathbf{K}_{12})} \tag{5.50}$$

where the expression in the denominator is the momentum distribution in the PWIA and is attained by setting the distortion factor $\hat{S}_{\text{IFSI}}$ to one in (5.48). The transparency allows us to express the effect of IFSI on the free momentum distribution F^{NN} in terms of the mass number A. Note the parallel to the scaling of the deuteron momentum distribution we discussed in Chapter 4. An important caveat is that the integration over $\mathbf{K}_{12}$ does imply the transparency is phase-space dependent.

We can gain a better understanding into the characteristics of nuclear transparencies by looking at a toy model described in [26]. In this model, the nucleus is a homogeneous sphere with constant density ρ. Hence without attenuation, the cross section for scattering from this nucleus is proportional to the integrated density

$$\int d\mathbf{r}\rho(\mathbf{r}) = A. \tag{5.51}$$

We can describe the effect of distortion or attenuation by considering a classical survival probability $P(\mathbf{r})$ for a nucleon with momentum $\mathbf{p}$ brought into a continuum state at coordinate $\mathbf{r}$:

$$P(\mathbf{r}) = e^{-\sigma \int_z^{+\infty} dz' \rho(\mathbf{r}')} \tag{5.52}$$

with the z' axis fixed along $\mathbf{p}$. We restrict our discussion to outgoing nucleons here, the extension to include incoming particles as well is straightforward. The scattering cross section σ of the nucleon with the nuclear medium is a measure of the effect of the attenuation calculated in the RMSGA. For a homogeneous sphere with radius R, the survival probability becomes

$$P(\mathbf{r}) = e^{[-\sigma\rho\sqrt{R^2 - r^2\sin^2\xi} - r\cos\xi]} \tag{5.53}$$

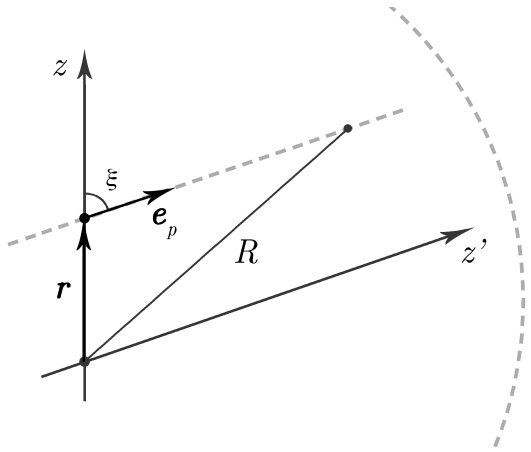

Figure 5.6: Coordinates used to define the classical survival probability.

with ξ the angle between $\mathbf{r}$ and $\mathbf{e}_p = \frac{\mathbf{p}}{p}$ (Fig. 5.6).

Integrating over all possible outgoing nucleon momentum directions, the single-nucleon transparency becomes

$$T_A^N = \frac{\int d\Omega_p \int d\mathbf{r} \rho(\mathbf{r}) P(\mathbf{r})}{\int d\Omega_p \int d\mathbf{r} \rho(\mathbf{r})}. \tag{5.54}$$

In a naive way we could extend this analysis to two-nucleon knockout. Assuming the two nucleons are uncorrelated, we could simply include the survival probabilities of the pair which gives

$$T_A^{NN} = T_A^N \times T_A^N. \tag{5.55}$$

This can intuitively be understood as a naive picture. We can understand why by comparing the uncorrelated and correlated cross sections. For uncorrelated knockout, the cross section without attenuation is proportional to

$$\sigma^N \propto \int d\Omega_{p_1} \int d\Omega_{p_2} \int d\mathbf{r}_1 \rho(\mathbf{r}_1) \int d\mathbf{r}_2 \rho(\mathbf{r}_2) = A^2. \tag{5.56}$$

A first adjustment can be done by making the zero-range approximation. This approximation will be critical to the factorization of the cross section as we will see in Chapter 6 and requires the initial nucleons to be found at the same spatial coordinate. This implies for the cross section

$$\sigma^{NN} \propto \int d\Omega_{p_1} \int d\Omega_{p_2} \int d\mathbf{r}_1 \rho(\mathbf{r}_1) \int d\mathbf{r}_2 \rho(\mathbf{r}_2) \delta(\mathbf{r}_1 - \mathbf{r}_2) \tag{5.57}$$

$$= (4\pi)^2 \int d\mathbf{r} \rho(\mathbf{r})^2 = (4\pi)^2 \rho A \tag{5.58}$$

which already poses a significant difference to the uncorrelated case [26]. We will now add another important feature: the back-to-back nature of SRC-pairs, discussed in Section 4.1 and attributed to the strong short-range repulsive nature of the NN potential. This resulted in a $\mathbf{k}_2 \approx -\mathbf{k}_1$ or $\gamma \approx 180°$ configuration with γ the opening angle between the two initial momenta. Introducing this angular constraint

$$\delta(\phi_1 - \phi_2 + \pi) \delta(\theta_1 + \theta_2 - \pi) \tag{5.59}$$

the transparency becomes

$$T_A^{NN} \propto \frac{2\pi\rho}{A} \int_0^R dr\ r^2 \int_{-1}^1 d\cos\theta_1 e^{[-\sigma\rho(\sqrt{R^2-r^2(1-\cos^2\theta_1)}-r\cos\theta_1)]} \times \int_{-1}^1 d\cos\theta_2 e^{[-\sigma\rho(\sqrt{R^2-r^2(1-\cos^2\theta_2)}-r\cos\theta_2)]}\delta(\theta_1+\theta_2-\pi). \tag{5.60}$$

Using the substitution $(r, \cos\theta_1) \to (r, l = \sqrt{R^2 - r^2(1-\cos^2\theta_1)})$ and further manipulations this becomes

$$T_A^{NN} \propto \frac{2\pi\rho}{A} \int_0^R dl\ l\ \sqrt{R^2-l^2} \ln\left(\frac{R+l}{R-l}\right) e^{-2\rho\sigma l}. \tag{5.61}$$

This toy model was used to set bounds on simulated power law dependencies [26]. The aggregated effect of FSI were found to considerably reduce the plane wave cross sections but showed little effect on the c.m. distribution. The mass dependence of the transparency $T_A^{NN} \propto A^\lambda$ is shown to be robust for probing back-to-back nucleon pairs

$$T_A^{pp} \propto A^{-0.49\pm0.06} \qquad \text{and} \qquad T_A^{pn} \propto A^{-0.42\pm0.05} \tag{5.62}$$

both well within the bounds imposed by the toy model $\lambda \in [-0.37, -0.78]$. This result indeed shows that one could expect a softer mass dependence for SRCs than one would expect from naively doubling the single-nucleon transparencies $T_A^p \propto A^{-0.33}$ found by experiment [57]. The wide applicability of these transparency power laws is yet to be put to the test so we stress that, although more cumbersome, calculating the RMSGA effects for a specific experiment is still recommended. It is important to note that the effects of IFSI are dependent on the kinematics selected. We conclude with noting that also charge exchange effects can be included in the IFSI framework. This process entails an outgoing proton (neutron) that rescatters into a neutron (proton) [26], an effect that should be taken into account but we will not include it here.

Chapter 6

Factorization of the A(p,p'NN)A-2 cross section

In this chapter we will reformulate and calculate the cross section for the two-nucleon knockout reaction $A(p,p'NN)A-2$, written using four-momenta as

$$\begin{aligned} &k^{\mu}_{p_i}(E_{p_i},\mathbf{p}_i)+k^{\mu}_{A}(E_A,\mathbf{p}_A)\rightarrow \\ &\quad k^{\mu}_{p_f}(E_{p_f},\mathbf{p}_f)+k^{\mu}_{N_1}(E_{N_1},\mathbf{p}_{N_1})+k^{\mu}_{N_2}(E_{N_2},\mathbf{p}_{N_2})+k^{\mu}_{A-2}(E_{A-2},\mathbf{p}_{A-2}). \end{aligned} \tag{6.1}$$

As we have established in Chapter 3 the Lorentz-invariant cross section becomes

$$\begin{aligned} d\sigma = \overline{\sum_i}\sum_f |\mathcal{M}_{fi}|^2 \frac{m_{p_i}m_A(2\pi)^4}{E_{p_i}E_A\beta_{p_iA}}\delta^{(4)}(k_{p_i}+k_A-k_{p_f}-k_{N_1}-k_{N_2}-k_{A-2}) \\ \times \frac{m_{p_f}}{E_{p_f}}\frac{d^3\mathbf{p}_f}{(2\pi)^3}\frac{m_{N_1}}{E_{N_1}}\frac{d^3\mathbf{p}_{N_1}}{(2\pi)^3}\frac{m_{N_2}}{E_{N_2}}\frac{d^3\mathbf{p}_{N_2}}{(2\pi)^3}\frac{m_{A-2}}{E_{A-2}}\frac{d^3\mathbf{p}_{A-2}}{(2\pi)^3}. \end{aligned} \tag{6.2}$$

In this chapter, all ingredients we have developed so far will be used to rewrite the above expression. The goal of this chapter is to come up with an expression that is *factorized*. This means the "free" nucleon-proton scattering cross section appears as a factor in the expression for the cross section [34]. We can then use free nucleon-proton scattering data to simulate the cross section for particular reactions. Also the distorted c.o.m. distribution of the correlated pair, which is called the factorization function [70], appears as a separate factor. This factorization scheme is extremely helpful in the calculations of cross sections due to the considerable simplification of the problem. Factorization of the cross section has been achieved and tested experimentally for the $(e,e'p)$ [71], (p,pN) [34] and $(e,e'NN)$ [72] knockout reactions but not yet for $(p,p'NN)$ reactions. The most important calculations will be done by working out the matrix element $\mathcal{M}_{fi}$.

6.1 Calculating the matrix element $\mathcal{M}_{fi}$

In order for us to calculate the matrix element we will need a number of things. First the wave functions of the particles that are taking part in the interaction need to be defined. After this, the interaction potential V_{pN_1} we defined in the PWIA (Chapter 3) needs to be replaced by an appropriate operator. Calculating the matrix element will also include a critical step towards factorization of the cross section: the zero-range approximation.

6.1.1 Defining the wave functions

Concerning the wave functions in the matrix element we assume the incoming and outgoing particles are plane waves according to the PWIA. The distortion due to the interaction with the nuclear medium will be added later in the calculation. Perhaps a more drastic adjustment is made by considering the wave functions as non-relativistic. This is necessary due to the way the effects of correlation operators was included in Section 4.2: the complexity has been shifted towards an effective operator which allows us to use mean-field IPM states. The nucleus will be approximated as a many-body system of nucleons in a spherically symmetric mean-field harmonic oscillator (HO) potential. These HO states are not Lorentz invariant and in the matrix element describing the interaction we will therefore assume the free states are also non-relativistic since this is far easier to work with. The normalization factors that make the wave functions Lorentz invariant are simply pulled out of the transition matrix as

$$\mathcal{M}_{fi} = \sqrt{\frac{E_{p_f} E_{N_1} E_{N_2} E_{A-2}}{m_{p_f} m_{N_1} m_{N_2} m_{A-2}}} T_{fi} \sqrt{\frac{E_{p_i} E_A}{m_{p_i} m_A}} \tag{6.3}$$

with the transition matrix element T_{fi} and the energies of the incoming and outgoing particles as given in (6.1). For simplicity we omit these factors in the coming calculations but we will add them in the final expression for the cross section.

With all of this in mind we can write the wave functions for the free particles as

$$\begin{aligned}
\langle \mathbf{r}|\mathbf{p}_i\rangle &= \frac{1}{(2\pi)^{3/2}} e^{i\mathbf{p}_i\cdot\mathbf{r}} \chi_{m_{s,i}} \tau_{m_{t,i}} && \text{(incoming proton)} \\
\langle \mathbf{r}|\mathbf{p}_f\rangle &= \frac{1}{(2\pi)^{3/2}} e^{i\mathbf{p}_f\cdot\mathbf{r}} \chi_{m_{s,f}} \tau_{m_{t,f}} && \text{(outgoing proton)} \\
\langle \mathbf{r}|\mathbf{p}_{N_1}\rangle &= \frac{1}{(2\pi)^{3/2}} e^{i\mathbf{p}_{N_1}\cdot\mathbf{r}} \chi_{m_{s,1}} \tau_{m_{t,1}} && \text{(outgoing nucleon 1)} \\
\langle \mathbf{r}|\mathbf{p}_{N_2}\rangle &= \frac{1}{(2\pi)^{3/2}} e^{i\mathbf{p}_{N_2}\cdot\mathbf{r}} \chi_{m_{s,2}} \tau_{m_{t,2}} && \text{(outgoing nucleon 2)}
\end{aligned} \tag{6.4}$$

where the normalization condition

$$\langle \mathbf{p}|\mathbf{p}'\rangle = \delta(\mathbf{p}-\mathbf{p}'). \tag{6.5}$$

is implied. The spinors in spin and isospin space have been denoted by respectively χ and τ. The wave functions for the initial nucleus A and final (or residual) nucleus $A-2$ are also needed. These states will be represented by Slater determinants of single-particle wave functions ϕ_{α_i} [42], these are states in a symmetric[1] 3D harmonic oscillator basis. The effect of the mass number A of the nucleus on the energy (in MeV) of these states can be parametrized as $\hbar\omega = 45A^{1/3} - 25A^{2/3}$ [70]. This gives

$$\begin{aligned}
\langle \mathbf{r}_1 \dots \mathbf{r}_A|\alpha_1 \dots \alpha_A\rangle &= \frac{1}{\sqrt{A!}} \sum_{\mathcal{P}} (-1)^{\mathcal{P}} \phi_{\mathcal{P}(\alpha_1)}(\mathbf{r}_1) \cdots \phi_{\mathcal{P}(\alpha_A)}(\mathbf{r}_A) && \text{(nucleus } A\text{)} \\
\langle \mathbf{r}_3 \dots \mathbf{r}_A|\alpha_3 \dots \alpha_A\rangle &= \frac{1}{\sqrt{A!}} \sum_{\mathcal{P}} (-1)^{\mathcal{P}} \phi_{\mathcal{P}(\alpha_3)}(\mathbf{r}_3) \cdots \phi_{\mathcal{P}(\alpha_A)}(\mathbf{r}_A) && \text{(nucleus } A-2\text{)}
\end{aligned} \tag{6.6}$$

[1]Here we implicitly assume the nucleus is a spherically symmetric system. This means our analysis is strictly speaking only valid for 0^+ ground state nuclei, a crude approximation but making calculations in a non-spherical system brings a lot of difficulties with it.

The bound nucleon wave functions will be approximated by using this same single-particle HO basis, the bound nucleon states can be expanded in terms of spherical harmonics as

$$\begin{aligned} \langle \mathbf{r}|\alpha_1\rangle &= \psi_{\alpha_1}(\mathbf{r})\tau_{m_{t,\alpha_1}} = R_{E_{\alpha_1},l_{\alpha_1}}(r)\mathcal{Y}_{l_{\alpha_1}j_{\alpha_1}m_{\alpha_1}}(\theta,\phi)\tau_{m_{t,\alpha_1}} \qquad \text{(bound nucleon 1)} \\ \langle \mathbf{r}|\alpha_2\rangle &= \psi_{\alpha_2}(\mathbf{r})\tau_{m_{t,\alpha_2}} = R_{E_{\alpha_2},l_{\alpha_2}}(r)\mathcal{Y}_{l_{\alpha_2}j_{\alpha_2}m_{\alpha_2}}(\theta,\phi)\tau_{m_{t,\alpha_2}} \qquad \text{(bound nucleon 2)} \end{aligned} \tag{6.7}$$

where the quantum numbers of bound nucleons are represented short-hand as $|\alpha_i\rangle = |E_{\alpha_i} l_{\alpha_i} j_{\alpha_i} m_{\alpha_i} \tau m_{t,\alpha_i}\rangle$ and the spin-spherical harmonics $\mathcal{Y}_{ljm}(\theta,\phi)$ are given by [73]

$$\mathcal{Y}_{l_{\alpha_i}j_{\alpha_i}m_{\alpha_i}}(\theta,\phi) = \sum_{m'_s,m'_l} \left\langle l_{\alpha_i}\ m'_l\ \frac{1}{2}\ m'_s \,\middle|\, j_{\alpha_1}\ m_{\alpha_1} \right\rangle Y_{l_{\alpha_i},m'_l}(\theta,\phi)\chi_{m'_s}. \tag{6.8}$$

We also assign momenta $\mathbf{k}_1$ and $\mathbf{k}_2$ to the initially bound nucleons.

6.1.2 Approximating the operator

As discussed in Section 3.4.2 when we assumed the Plane Wave Impulse Approximation, the interaction potential that governs the dynamics of the scattering process will be V_{pN1}. Hence only two particles actually take part in the "hard" interaction. However for a two-nucleon knockout process, we should assume a three-body operator $\hat{\mathcal{O}}^{[3]}$ as a start (Fig. 6.1). This three-body operator has a very general definition, we assume the actual nature of the interaction to be completely unknown. Instead of calculating the matrix element using this form of operator, we will make a number of specific approximations that simplify calculations considerably. The initial state is clearly composed of the incoming proton and a nucleus A and the final state of the scattered proton, the knocked-out nucleons and the residual $A-2$ nucleus. However, to begin we assume the operator acts between two general many-body wave functions composed of $A+1$ single-particle states φ_i

$$\mathcal{M}_{fi} = \langle (A+1)^f | \sum_{i<j<k=0}^{A} \hat{\mathcal{O}}(\mathbf{r}_i, \mathbf{r}_j, \mathbf{r}_k) | (A+1)^i \rangle \,. \tag{6.9}$$

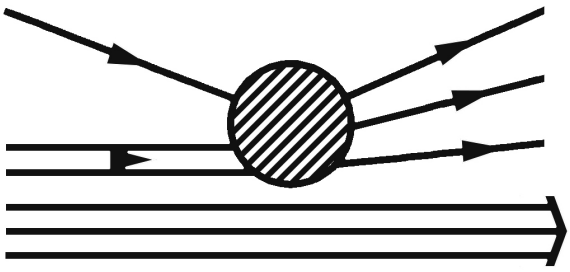

Figure 6.1: As a start, we assume a three-body operator acting on the three initial and final states that take part in the interaction, here depicted schematically. The $A-2$ residual nucleons do not take part in the interaction and are considered to be *fixed spectators*. The nature of the interaction itself we will assume to be unknown.

Since we deal with fermions, these $(A+1)$-body wave functions need to be fully antisymmetrized, this is taken care of by the antisymmetrization operator $\hat{\mathcal{A}}$ [42] which was also used in the Slater determinants of (6.6)

$$\hat{\mathcal{A}} = \frac{1}{\sqrt{N!}} \sum_{\mathcal{P}} (-1)^{\mathcal{P}} \hat{\mathcal{P}} \tag{6.10}$$

and $\hat{\mathcal{P}}$ the permutation operator. So, if the initial and final wave functions are fully antisymmetrized this becomes [74]

$$\begin{aligned} \mathcal{M} &= \frac{(A+1)A(A-1)}{6} \langle A+1 | \hat{\mathcal{O}}(\mathbf{r}_0, \mathbf{r}_1, \mathbf{r}_2) | A+1 \rangle \\ &= \frac{(A+1)A(A-1)}{6} \int d\mathbf{r}_0 \ldots \int d\mathbf{r}_A \; \hat{\mathcal{A}} \left[\varphi^\dagger_{0f}(\mathbf{r}_0) \ldots \varphi^\dagger_{Af}(\mathbf{r}_A) \right] \\ &\quad \times \hat{\mathcal{O}}(\mathbf{r}_0, \mathbf{r}_1, \mathbf{r}_2) \; \hat{\mathcal{A}} \left[\varphi_{0i}(\mathbf{r}_0) \ldots \varphi_{Ai}(\mathbf{r}_A) \right] \end{aligned} \tag{6.11}$$

where we have located the interaction with the initial proton at coordinate $\mathbf{r}_0$. Writing out the antisymmetrization operator $\hat{\mathcal{A}}$ explicitly gives

$$\begin{aligned} \mathcal{M} = \frac{(A+1)A(A-1)}{6(A+1)!} &\int d\mathbf{r}_0 \ldots \int d\mathbf{r}_A \sum_{\mathcal{P}_f} (-1)^{\mathcal{P}_f} \left[\varphi^\dagger_{0f}(\mathbf{r}_0) \ldots \varphi^\dagger_{Af}(\mathbf{r}_A) \right] \\ &\times \hat{\mathcal{O}}(\mathbf{r}_0, \mathbf{r}_1, \mathbf{r}_2) \sum_{\mathcal{P}_i} (-1)^{\mathcal{P}_i} \left[\varphi_{0i}(\mathbf{r}_0) \ldots \varphi_{Ai}(\mathbf{r}_A) \right]. \end{aligned} \tag{6.12}$$

Since the single particle wave functions are mutually orthogonal this expression becomes zero unless

$$\begin{cases} \mathcal{P}_{i(3)} = \mathcal{P}_{f(3)}, \\ \mathcal{P}_{i(4)} = \mathcal{P}_{f(4)}, \\ \quad \vdots \\ \mathcal{P}_{i(A)} = \mathcal{P}_{f(A)} \end{cases} \tag{6.13}$$

This "fixation" is also called the *Frozen Spectator Approximation* which states that the residual $A-2$ nucleons will retain a fixed location and will not be affected by the interaction. The spectator approximation is only valid if the recoil momentum of the $A-2$ nucleus remains small [70]. Remember, in Chapter 4 we have characterized the SRC pairs as residing in a few-nucleon configuration which means the pair has a large relative and low c.m. momentum. In the rest frame of the nucleus (the projectile frame), the recoil momentum was identified as equal and opposite to the c.m. momentum of the pair so when probing SRC pairs specifically, this condition should be fulfilled. However, the kinematics should always be appropriately tuned to make sure this condition is met.

There are $(A-2)!$ remaining possibilities to permute the wavefunctions. We can now introduce the *Levi-Civita* symbol [30] to denote the correct antisymmetrization of the remaining three wavefunctions to be considered in the matrix element:

$$\epsilon_{ijk} = \begin{cases} 0 & \text{if} \quad i=j, \; j=k, \; \text{or} \; k=i, \\ -1 & \text{if} \quad (i,j,k) = (3,2,1), \; (1,3,2) \; \text{or} \; (2,1,3), \\ +1 & \text{if} \quad (i,j,k) = (1,2,3), \; (3,1,2) \; \text{or} \; (2,3,1). \end{cases} . \tag{6.14}$$

Using this, the matrix element becomes

$$\begin{aligned}\mathcal{M} = \frac{1}{6}\int d\mathbf{r}_0 \int d\mathbf{r}_1 \int d\mathbf{r}_2 \sum_{h,j,k=0}^{2} \epsilon_{hjk} \sum_{l,m,n=0}^{2} \epsilon_{lmn} \\ \times \varphi^{\dagger}_{hf}(\mathbf{r}_0)\varphi^{\dagger}_{jf}(\mathbf{r}_1)\varphi^{\dagger}_{kf}(\mathbf{r}_2)\hat{\mathcal{O}}(\mathbf{r}_0,\mathbf{r}_1,\mathbf{r}_2)\varphi_{li}(\mathbf{r}_0)\varphi_{mi}(\mathbf{r}_1)\varphi_{ni}(\mathbf{r}_2) \\ \times \prod_{i=3}^{A}\int d\mathbf{r}_i |\varphi_{\alpha_3}(\mathbf{r}_3)|^2 \dots \ |\varphi_{\alpha_A}(\mathbf{r}_A)|^2 \end{aligned} \tag{6.15}$$

In this expression we can include the Glauber factors (5.47) we introduced in Chapter 5 to account for the initial and final state interactions. The incoming and outgoing wave functions will therefore pick up a phase

$$\begin{aligned}\varphi_i(\mathbf{r}_j) \to \varphi_i(\mathbf{r}_j)\mathcal{S}_i(\mathbf{r}_j;\mathbf{r}_3\dots\mathbf{r}_A), \\ \varphi_f(\mathbf{r}_j) \to \varphi_f(\mathbf{r}_j)\mathcal{S}_f(\mathbf{r}_j;\mathbf{r}_3\dots\mathbf{r}_A)\end{aligned} \tag{6.16}$$

. We define the factor describing the IFSI according to (5.49)

$$\begin{aligned}S_{\mathrm{IFSI}}(\mathbf{r}_0,\mathbf{r}_1,\mathbf{r}_2) = \left(\prod_{i=3}^{A}\int d\mathbf{r}_i \ |\varphi_{\alpha_i}(\mathbf{r}_i)|^2\right) \mathcal{S}_i(\mathbf{r}_0;\mathbf{r}_3,\dots,\mathbf{r}_i)\mathcal{S}_f(\mathbf{r}_0;\mathbf{r}_3,\dots,\mathbf{r}_i) \\ \times \mathcal{S}_f(\mathbf{r}_1;\mathbf{r}_3,\dots,\mathbf{r}_i)\mathcal{S}_f(\mathbf{r}_2;\mathbf{r}_3,\dots,\mathbf{r}_i)\end{aligned} \tag{6.17}$$

As noted in the discussion on nuclear transparencies, we could also omit the IFSI factors here for the time being and multiply the momentum distribution (that will eventually appear in the final expression of the cross section) by the appropriate transparency corresponding to a nucleus of mass A at the end of the calculation. However, we will keep working with the IFSI factors included since it is important to know in what way they could affect the calculation.

To move on we need to make a particular kinematical choice: we fix the kinematics in such a way we are certain that the scattered proton which was used as a projectile will not be detected as one of the two knocked out nucleons. As discussed in Chapter 4, kinematical cuts can make sure we only probe SRC pairs, here we impose additional conditions on the kinematics of the reaction. This can be done together with the demand that the momentum transfer happens primarily with one of the two nucleons. A reaction of this kind will result in a scattered proton which has transferred an amount of momentum q to a "leading" nucleon which will be detected with a high momentum and a nucleon that is knocked out simply due to the breakup of the correlated pair. Measuring the momenta of the outgoing particles in an exclusive way (Chapter 2) in experiments allows us to impose these conditions. Only then the hierarchy in momentum between the three outgoing nucleon momenta can be observed and the knocked out nucleons can be discerned from the scattered nucleon correctly. In [26], the kinematical cuts are applied for simulations by requiring the angle $\theta_{\mathbf{p}_1,\mathbf{q}}$ between the emitted leading nucleon $\mathbf{p}_1$ and the momentum transfer $\mathbf{q}$ is small and also the fraction $\|\mathbf{p}_1\|/\|\mathbf{q}\|$ (with $\mathbf{p}_1 = \mathbf{k}_1 + \mathbf{q}$) is restricted. It is important to note here these cuts correspond to kinematics where the nucleus is at rest in the lab frame. A Lorentz transformation from the projectile frame to the lab frame is needed if we would want to apply these cuts in inverse kinematics. A

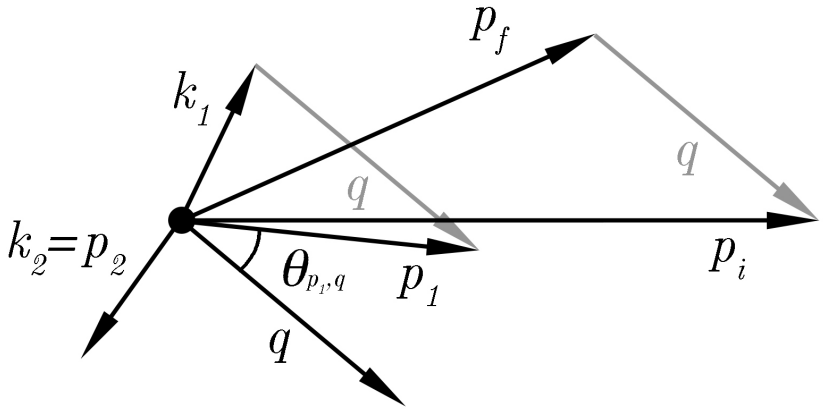

Figure 6.2: The kinematical conditions that are required to probe SRC pairs in the projectile frame. Assuming a *few nucleon configuration* as in Chapter 4, the momenta of the bound nucleons are related by $\mathbf{k}_1 \approx -\mathbf{k}_2$. In addition to the kinematic restrictions to exclusively probe SRC pairs, to calculate the matrix element we assume the momentum transfer $\mathbf{q} = \mathbf{p}_i - \mathbf{p}_f$ occurs only with $\mathbf{k}_1$, hence the momentum of scattered nucleon 1 is $\mathbf{p}_1 = \mathbf{k}_1 + \mathbf{q}$. This requirement can be implied by placing restrictions on the ratio $\|\mathbf{p}\|_1/\|\mathbf{q}\|$ and the angle $\theta_{p_1,q}$, also restricting the phase space that can be probed by the reaction.

significant drawback of this highly selective kinematics is the fact that the phase space gets small and a detailed study of the c.m. distribution is limited. Covering a larger phase space in experiment will result in more difficult calculations [26].

By selecting the appropriate kinematics, we can first reduce the summation in (6.15) to

$$\sum_{h,j,k=0}^{2} \sum_{l,m,n=0}^{2} \epsilon_{hjk}\epsilon_{lmn} = \sum_{j,k,m,n=0}^{2} \epsilon_{0jk}\epsilon_{0mn} + \sum_{h,k,l,n=0}^{2} \epsilon_{h0k}\epsilon_{l0n} + \sum_{h,j,l,m=0}^{2} \epsilon_{hj0}\epsilon_{lm0}. \tag{6.18}$$

Second, we can simplify this by demanding the actual interaction to take place in a single point: a point interaction. To account for the correlations between the two bound nucleons we can now insert the correlation function $g(\mathbf{r}_i, \mathbf{r}_j)$ as established in Chapter 4. The approximated operators at each of the points are

$$\begin{aligned}
\hat{\mathcal{O}}^{[3]}(\mathbf{r}_0, \mathbf{r}_1, \mathbf{r}_2) &\cong \hat{\mathcal{O}}_{pN}(\mathbf{r}_0)[\delta(\mathbf{r}_0 - \mathbf{r}_1) + \delta(\mathbf{r}_0 - \mathbf{r}_2)]g(\mathbf{r}_1, \mathbf{r}_2) \\
\hat{\mathcal{O}}^{[3]}(\mathbf{r}_0, \mathbf{r}_1, \mathbf{r}_2) &\cong \hat{\mathcal{O}}_{pN}(\mathbf{r}_1)[\delta(\mathbf{r}_1 - \mathbf{r}_0) + \delta(\mathbf{r}_1 - \mathbf{r}_2)]g(\mathbf{r}_0, \mathbf{r}_2) \\
\hat{\mathcal{O}}^{[3]}(\mathbf{r}_0, \mathbf{r}_1, \mathbf{r}_2) &\cong \hat{\mathcal{O}}_{pN}(\mathbf{r}_2)[\delta(\mathbf{r}_2 - \mathbf{r}_0) + \delta(\mathbf{r}_2 - \mathbf{r}_1)]g(\mathbf{r}_0, \mathbf{r}_1).
\end{aligned} \tag{6.19}$$

The matrix element is now composed of three parts, each part corresponding to one of the three possibilities to fix the incoming proton to one of the coordinates $\mathbf{r}_0, \mathbf{r}_1$ and $\mathbf{r}_2$. As can easily be deduced these three terms yield the same contribution. Integrating the

delta functions give the remaining terms

$$\begin{aligned}\mathcal{M} = \frac{1}{2}\int d\mathbf{r}_1 \int d\mathbf{r}_2 \; & S_{\text{IFSI}}(\mathbf{r}_1,\mathbf{r}_2) g(\mathbf{r}_1,\mathbf{r}_2) \\ & [\quad \varphi^\dagger_{0f}(\mathbf{r}_1)\varphi^\dagger_{1f}(\mathbf{r}_1)\varphi^\dagger_{2f}(\mathbf{r}_2)\hat{\mathcal{O}}_{pN}(\mathbf{r}_1)\varphi_{0i}(\mathbf{r}_1)\varphi_{1i}(\mathbf{r}_1)\phi_{2i}(\mathbf{r}_2) \quad \leftarrow \\ & + \varphi^\dagger_{0f}(\mathbf{r}_2)\varphi^\dagger_{1f}(\mathbf{r}_1)\varphi^\dagger_{2f}(\mathbf{r}_2)\hat{\mathcal{O}}_{pN}(\mathbf{r}_2)\varphi_{0i}(\mathbf{r}_2)\varphi_{1i}(\mathbf{r}_1)\phi_{2i}(\mathbf{r}_2) \\ & - \varphi^\dagger_{0f}(\mathbf{r}_1)\varphi^\dagger_{1f}(\mathbf{r}_1)\varphi^\dagger_{2f}(\mathbf{r}_2)\hat{\mathcal{O}}_{pN}(\mathbf{r}_1)\varphi_{0i}(\mathbf{r}_1)\varphi_{2i}(\mathbf{r}_1)\phi_{1i}(\mathbf{r}_2) \quad \leftarrow \\ & - \varphi^\dagger_{0f}(\mathbf{r}_2)\varphi^\dagger_{1f}(\mathbf{r}_1)\varphi^\dagger_{2f}(\mathbf{r}_2)\hat{\mathcal{O}}_{pN}(\mathbf{r}_2)\varphi_{0i}(\mathbf{r}_2)\varphi_{2i}(\mathbf{r}_1)\phi_{1i}(\mathbf{r}_2) \\ & - \varphi^\dagger_{0f}(\mathbf{r}_1)\varphi^\dagger_{2f}(\mathbf{r}_1)\varphi^\dagger_{1f}(\mathbf{r}_2)\hat{\mathcal{O}}_{pN}(\mathbf{r}_1)\varphi_{0i}(\mathbf{r}_1)\varphi_{1i}(\mathbf{r}_1)\phi_{2i}(\mathbf{r}_2) \\ & - \varphi^\dagger_{0f}(\mathbf{r}_2)\varphi^\dagger_{2f}(\mathbf{r}_1)\varphi^\dagger_{1f}(\mathbf{r}_2)\hat{\mathcal{O}}_{pN}(\mathbf{r}_2)\varphi_{0i}(\mathbf{r}_2)\varphi_{1i}(\mathbf{r}_1)\phi_{2i}(\mathbf{r}_2) \quad \leftarrow \\ & + \varphi^\dagger_{0f}(\mathbf{r}_1)\varphi^\dagger_{2f}(\mathbf{r}_1)\varphi^\dagger_{1f}(\mathbf{r}_2)\hat{\mathcal{O}}_{pN}(\mathbf{r}_1)\varphi_{0i}(\mathbf{r}_1)\varphi_{2i}(\mathbf{r}_1)\phi_{1i}(\mathbf{r}_2) \\ & + \varphi^\dagger_{0f}(\mathbf{r}_2)\varphi^\dagger_{2f}(\mathbf{r}_1)\varphi^\dagger_{1f}(\mathbf{r}_2)\hat{\mathcal{O}}_{pN}(\mathbf{r}_2)\varphi_{0i}(\mathbf{r}_2)\varphi_{2i}(\mathbf{r}_1)\phi_{1i}(\mathbf{r}_2)] \quad \leftarrow \end{aligned} \tag{6.20}$$

And finally, assuming the incoming proton only transfers momentum to one of the nucleons (say φ_{1f}), we can exclude half of the terms by demanding the second nucleon will never be detected as the one getting the momentum transfer in the hard collision. This means only the following terms (indicated by the arrows above) remain and by interchanging the initial nucleons 1 and 2 in the second term we get

$$\begin{aligned}\mathcal{M} = \frac{1}{2}\int d\mathbf{r}_1 \int d\mathbf{r}_2 \; & S_{\text{IFSI}}(\mathbf{r}_1,\mathbf{r}_2) g(\mathbf{r}_1,\mathbf{r}_2) \\ & \times\Big[\quad \varphi^\dagger_{0f}(\mathbf{r}_1)\varphi^\dagger_{1f}(\mathbf{r}_1)\varphi^\dagger_{2f}(\mathbf{r}_2)\hat{\mathcal{O}}_{pN}(\mathbf{r}_1)\varphi_{0i}(\mathbf{r}_1)[\varphi_{1i}(\mathbf{r}_1)\varphi_{2i}(\mathbf{r}_2) - \varphi_{2i}(\mathbf{r}_1)\varphi_{1i}(\mathbf{r}_2)] \\ & \quad -\varphi^\dagger_{0f}(\mathbf{r}_2)\varphi^\dagger_{2f}(\mathbf{r}_1)\varphi^\dagger_{1f}(\mathbf{r}_2)\hat{\mathcal{O}}_{pN}(\mathbf{r}_2)\varphi_{0i}(\mathbf{r}_2)[\varphi_{1i}(\mathbf{r}_1)\varphi_{2i}(\mathbf{r}_2) - \varphi_{2i}(\mathbf{r}_1)\varphi_{1i}(\mathbf{r}_2)]\Big]. \end{aligned} \tag{6.21}$$

Here we assumed that $g(\mathbf{r}_1,\mathbf{r}_2) = g(\mathbf{r}_2,\mathbf{r}_1)$ which is allowed since this is a central function. In the second term we can interchange the coordinates $\mathbf{r}_1$ and $\mathbf{r}_2$ since they are just integration variables. This results in

$$\begin{aligned}\mathcal{M} = \int d\mathbf{r}_1 \int d\mathbf{r}_2 \; & S_{\text{IFSI}}(\mathbf{r}_1,\mathbf{r}_2) g(\mathbf{r}_1,\mathbf{r}_2) \\ & \times\varphi^\dagger_{0f}(\mathbf{r}_1)\varphi^\dagger_{1f}(\mathbf{r}_1)\varphi^\dagger_{2f}(\mathbf{r}_2)\hat{\mathcal{O}}_{pN}(\mathbf{r}_1)\varphi_{0i}(\mathbf{r}_1)[\varphi_{1i}(\mathbf{r}_1)\varphi_{2i}(\mathbf{r}_2) - \varphi_{2i}(\mathbf{r}_1)\varphi_{1i}(\mathbf{r}_2)] \end{aligned} \tag{6.22}$$

As we can see this results in two distinct antisymmetric contributions to the matrix element, a direct term and an exchange term. We now set $\mathbf{r}_1 \to \mathbf{r}_0$ for simplicity, why we do this will become clear below.

6.1.3 Calculating the direct term $\mathcal{M}_{①}$

As discussed we don't have to worry about Lorentz-invariant normalization factors here, only those corresponding to non-relativistic normalization are accounted for here. We can split up Eq. 6.22 in a direct term $\mathcal{M}_{①}$ and an exchange term $\mathcal{M}_{②}$. The direct term

will be calculated here. Using the wave functions definitions from Section 6.1.1 and Eq. (6.22) we get

$$\begin{aligned}\mathcal{M}_{\textcircled{1}} = \frac{1}{(2\pi)^3}\int d\mathbf{r}_0 \int d\mathbf{r}_2\; S_{\text{IFSI}}(\mathbf{r}_0,\mathbf{r}_2)\; e^{-i\mathbf{p}_{N_1}\cdot\mathbf{r}_0}\chi^\dagger_{m_{s,1}}(1)\tau^\dagger_{m_{t,1}}(1)e^{-i\mathbf{p}_{N_2}\cdot\mathbf{r}_2}\chi^\dagger_{m_{s,2}}(2)\tau^\dagger_{m_{t,2}}(2)\\ \times e^{-i\mathbf{p}_f\cdot\mathbf{r}_0}\chi^\dagger_{m_{s,f}}(0)\tau^\dagger_{m_{t,f}}(0)\hat{\mathcal{O}}_{pN}(\mathbf{r}_0)g(\mathbf{r}_0,\mathbf{r}_2)e^{-i\mathbf{p}_i\cdot\mathbf{r}_0}\chi_{m_{s,i}}(0)\tau_{m_{t,i}}(0)\\ \times \psi_{\alpha_1}(\mathbf{r}_0)\psi_{\alpha_2}(\mathbf{r}_2).\end{aligned} \tag{6.23}$$

where we stress the fact that the operator does not affect the isospin of the particles. This means we have no charge exchange effects and we further assume the operator also conserves energy and momentum. The coordinate of the spinor (both spin and isospin) part is denoted between parentheses. A necessary step to eventually achieve factorization is the insertion of the completeness relations associated with the spin and isospin parts of the wave functions. These are two-component spinors obeying the relation [75]

$$\sum_{m_s=-1/2}^{+1/2}\chi_{m_s}(1)\chi^\dagger_{m_s}(1) = \mathbb{1}, \qquad \sum_{m_t=-1/2}^{+1/2}\tau_{m_t}(1)\tau^\dagger_{m_t}(1) = \mathbb{1}. \tag{6.24}$$

We also include a Dirac delta function so (6.23) becomes

$$\begin{aligned}\mathcal{M}_{\textcircled{1}} = \frac{1}{(2\pi)^3}\int d\mathbf{r}_0 \int d\mathbf{r}_2\; e^{-i\mathbf{p}_{N_1}\cdot\mathbf{r}_0}\chi^\dagger_{m_{s,1}}(1)\tau^\dagger_{m_{t,1}}(1)\\ \times e^{-i\mathbf{p}_f\cdot\mathbf{r}_0}\chi^\dagger_{m_{s,f}}(0)\tau^\dagger_{m_{t,f}}(0)\hat{\mathcal{O}}_{pN}(\mathbf{r}_0)e^{-i\mathbf{p}_i\cdot\mathbf{r}_0}\chi_{m_{s,i}}(0)\tau_{m_{t,i}}(0)\\ \times \sum_{m_s=-1/2}^{+1/2}\chi_{m_s}(1)\chi^\dagger_{m_s}(1)\sum_{m_t=-1/2}^{+1/2}\tau_{m_t}(1)\tau^\dagger_{m_t}(1)\\ \times \int d\mathbf{r}_1\delta(\mathbf{r}_0-\mathbf{r}_1)S_{\text{IFSI}}(\mathbf{r}_1,\mathbf{r}_2)e^{-i\mathbf{p}_{N_2}\cdot\mathbf{r}_2}\chi^\dagger_{m_{s,2}}(2)\tau^\dagger_{m_{t,2}}(2)\\ \times g(\mathbf{r}_1,\mathbf{r}_2)\psi_{\alpha_1}(\mathbf{r}_1)\psi_{\alpha_2}(\mathbf{r}_2).\end{aligned} \tag{6.25}$$

We now use the Dirac delta function as

$$\delta(\mathbf{r}_0-\mathbf{r}_1) = \frac{1}{(2\pi)^3}\int d\mathbf{k}\; e^{i\mathbf{k}\cdot(\mathbf{r}_0-\mathbf{r}_1)} \tag{6.26}$$

to isolate the free scattering cross section that includes the initial and final protons, the scattered nucleon and a free nucleon state with momentum $\mathbf{k}$, spin χ_{m_s} and isospin τ_{m_t}:

$$\begin{aligned}\mathcal{M}_{\textcircled{1}} = \frac{1}{(2\pi)^3}\sum_{m_s,m_t}\int d\mathbf{k}\,\langle \mathbf{p}_{N_1}\chi_{m_{s,1}}\tau_{m_{t,1}},\mathbf{p}_f\chi_{m_{s,f}}\tau_{m_{t,f}}|\mathcal{O}_{pN}|\mathbf{p}_i\chi_{m_{s,i}}\tau_{m_{t,i}},\mathbf{k}\chi_{m_s}\tau_{m_t}\rangle\\ \times\int d\mathbf{r}_1\int d\mathbf{r}_2\; S_{\text{IFSI}}(\mathbf{r}_1,\mathbf{r}_2)e^{-i\mathbf{k}\cdot\mathbf{r}_1}\chi^\dagger_{m_s}(1)\tau^\dagger_{m_t}(1)e^{-i\mathbf{p}_{N_2}\cdot\mathbf{r}_2}\chi^\dagger_{m_{s,2}}(2)\tau^\dagger_{m_{t,2}}(2)\\ \times g(\mathbf{r}_1,\mathbf{r}_2)\psi_{\alpha_1}(\mathbf{r}_1)\psi_{\alpha_2}(\mathbf{r}_2).\end{aligned} \tag{6.27}$$

Another critical step is to switch to relative and c.o.m. coordinates, this is particularly simple since the Jacobian J [28] is equal to one

$$\begin{cases} \mathbf{r}_{12} = \mathbf{r}_1 - \mathbf{r}_2, \\ \mathbf{R}_{12} = \frac{1}{2}(\mathbf{r}_1 + \mathbf{r}_2) \end{cases} \quad , \qquad J = \begin{vmatrix} 1 & -1 \\ \frac{1}{2} & \frac{1}{2} \end{vmatrix} = 1. \tag{6.28}$$

This transformation results in

$$\begin{aligned} \mathcal{M}_{①} = \frac{1}{(2\pi)^3} \sum_{m_s,m_t} \int d\mathbf{k} \, \langle \mathbf{p}_{N_1} \chi_{m_{s,1}} \tau_{m_{t,1}}, \mathbf{p}_f \chi_{m_{s,f}} \tau_{m_{t,f}} | \mathcal{O}_{pN} | \mathbf{p}_i \chi_{m_{s,i}} \tau_{m_{t,i}}, \mathbf{k} \chi_{m_s} \tau_{m_t} \rangle \\ \times \int d\mathbf{r}_{12} e^{-i(\mathbf{k}-\mathbf{p}_{N_2})\cdot\frac{\mathbf{r}_{12}}{2}} g(\mathbf{r}_{12}) \\ \times \int d\mathbf{R}_{12} S_{\mathrm{IFSI}} \left(\mathbf{R}_{12} \pm \frac{\mathbf{r}_{12}}{2} \right) e^{-i(\mathbf{k}+\mathbf{p}_{N_2})\cdot\mathbf{R}_{12}} \\ \times \langle \chi_{m_s} \tau_{m_t} | \psi_{\alpha_1}(\mathbf{R}_{12} + \frac{\mathbf{r}_{12}}{2}) \rangle \, \langle \chi_{m_{s,2}} \tau_{m_{t,2}} | \psi_{\alpha_2}(\mathbf{R}_{12} - \frac{\mathbf{r}_{12}}{2}) \rangle \end{aligned} \tag{6.29}$$

Note that we require momentum conservation at the interaction point for the "free" transition, so we can write

$$\mathbf{k} = \mathbf{p}_{N_1} + \mathbf{p}_f - \mathbf{p}_i = \mathbf{p}_{N_1} - \mathbf{q} \qquad \text{with} \qquad \mathbf{q} = \mathbf{p}_i - \mathbf{p}_f \tag{6.30}$$

which cancels the $\mathbf{k}$ integral. Since we assume by selective kinematics the momentum transfer in the collision occurs with only one of the two nucleons (here nucleon 1) we get

$$\mathbf{k}_{N_1} = \mathbf{p}_{N_1} - \mathbf{q} \tag{6.31}$$

This means the relative and c.o.m. momenta become[2]

$$\mathbf{k}_{12} = \frac{\mathbf{k}_{N_1} - \mathbf{k}_{N_2}}{2} = \frac{\mathbf{p}_{N_1} - \mathbf{p}_{N_2}}{2} - \frac{\mathbf{q}}{2} \qquad \text{and} \qquad \mathbf{K}_{12} = \mathbf{k}_{N_1} + \mathbf{k}_{N_2} = \mathbf{p}_{N_1} + \mathbf{p}_{N_2} - \mathbf{q}$$

with $\mathbf{k}_{N_2} = \mathbf{p}_{N_2}$. These definitions are in agreement with what has been stated in Chapter 4 on SRC pair kinematics. Using these definitions, Eq. (6.29) becomes

$$\begin{aligned} \mathcal{M}_{①} = \frac{1}{(2\pi)^3} \sum_{m_s,m_t} \langle \mathbf{p}_{N_1} \chi_{m_{s,1}} \tau_{m_{t,1}}, \mathbf{p}_f \chi_{m_{s,f}} \tau_{m_{t,f}} | \mathcal{O}_{pN} | \mathbf{p}_i \chi_{m_{s,i}} \tau_{m_{t,i}}, \mathbf{k} \chi_{m_s} \tau_{m_t} \rangle \\ \times \int d\mathbf{r}_{12} e^{-i\mathbf{k}_{12}\cdot\mathbf{r}_{12}} g(\mathbf{r}_{12}) \int d\mathbf{R}_{12} \; S_{\mathrm{IFSI}} \left(\mathbf{R}_{12} \pm \frac{\mathbf{r}_{12}}{2} \right) e^{-i\mathbf{K}_{12}\cdot\mathbf{R}_{12}} \\ \times \langle \chi_{m_s} \tau_{m_t} | \psi_{\alpha_1}(\mathbf{R}_{12} + \frac{\mathbf{r}_{12}}{2}) \rangle \, \langle \chi_{m_{s,2}} \tau_{m_{t,2}} | \psi_{\alpha_2}(\mathbf{R}_{12} - \frac{\mathbf{r}_{12}}{2}) \rangle \, . \end{aligned} \tag{6.32}$$

This expression is already split into a part concerning the relative motion of the pair $(\mathbf{k}_{12}, \mathbf{r}_{12})$ and a part concerning the total or c.m. motion of the pair $(\mathbf{K}_{12}, \mathbf{R}_{12})$.

[2]We choose to define the relative and c.o.m. momenta with the factor 1/2 switched w.r.t. the relative and c.o.m. coordinates due to the fact that the commutation relations need to yield the correct results.

6.1.4 The zero-range approximation

Now we have defined the (distorted) c.m. momentum distribution it is time to introduce the most fundamental of approximations to factorize the cross section: the *zero-range approximation* (ZRA). One could almost say the succes of factorization hinges upon this particular approximation [26]. It amounts to stating that the two knocked out nucleons will be brought into the continuum *at the exact same point*. Here, this point is taken to be the c.m. coordinate $\mathbf{R}_{12}$ so the made approximation amounts to setting $\mathbf{r}_{12} \to 0$. This means for the product wave function of the two bound nucleons and the IFSI factor the following:

$$\begin{aligned} \psi_{\alpha_1}(\mathbf{R}_{12} + \frac{\mathbf{r}_{12}}{2})\psi_{\alpha_2}(\mathbf{R}_{12} - \frac{\mathbf{r}_{12}}{2}) \approx \psi_{\alpha_1}(\mathbf{R}_{12})\psi_{\alpha_2}(\mathbf{R}_{12}), \\ S_{\text{IFSI}}(\mathbf{R}_{12} \pm \frac{\mathbf{r}_{12}}{2}) = S_{\text{IFSI}}(\mathbf{R}_{12}) \end{aligned} \tag{6.33}$$

The zero-range approximation stems from the operator product expansion in quantum field theory [76]. Let us consider any two local fields $\mathcal{O}_A(x)$ and $\mathcal{O}_B(y)$ at closely located points x and y. The product of these fields can be expanded as

$$\mathcal{O}_A(x)\mathcal{O}_B(y) \sim \sum_C \mathcal{C}^C_{AB}(x-y)\mathcal{O}_C\left(\frac{x+y}{2}\right) \tag{6.34}$$

and therefore represents the product as a sum over all local fields in a given theory. The coefficients $\mathcal{C}^C$ are called the Wilson[3] coefficients and depend on the distance $x - y$. The ZRA acts as a projection operator on the very short-range relative components of the product wave function [26]. The ZRA makes sure that if we sum and square the direct and exchange transition amplitudes ($\mathcal{M}_{(1)}$ and $\mathcal{M}_{(2)}$), the factorization holds. We restrict the calculations in this work to the direct term $\mathcal{M}_{(1)} = \mathcal{M}$ but remain aware of the fact that including the exchange term, how small the contribution may very well be, yields a more realistic result.

In the ZRA we set $\mathbf{r}_{12} \to 0$. From (6.32), we can define the Fourier transform of the central correlation function $g(\mathbf{r}_{12})$ as

$$\mathcal{G}(\mathbf{k}_{12}) \equiv \frac{1}{(2\pi)^{3/2}} \int d\mathbf{r}_{12} e^{-i\mathbf{k}_{12}\cdot\mathbf{r}_{12}} g(\mathbf{r}_{12}) \tag{6.35}$$

and we can also define a distorted (due to the presence of the factor S_{IFSI}, denoted with letter "D") c.m. momentum distribution as

$$\begin{aligned} F^D(\mathbf{K}_{12}) \equiv \frac{1}{(2\pi)^{3/2}} \int d\mathbf{R}_{12}\ S_{\text{IFSI}}(\mathbf{R}_{12})\, e^{-i\mathbf{K}_{12}\cdot\mathbf{R}_{12}} \\ \times \langle \chi_{m_s}\tau_{m_t}|\psi_{\alpha_1}(\mathbf{R}_{12})\rangle \langle \chi_{m_{s,2}}\tau_{m_{t,2}}|\psi_{\alpha_2}(\mathbf{R}_{12})\rangle . \end{aligned} \tag{6.36}$$

[3]The operator product expansion was first proposed by K. Wilson and W. Zimmermann [77].

The bound nucleon wave functions are approximated by HO states as defined by Eq. (6.7). Using this form we can calculate

$$\chi^{\dagger}_{m_s}(1)\tau^{\dagger}_{m_t}(1)\psi_{\alpha_1}(\mathbf{R}_{12}) = \delta_{m_t,m_{t,\alpha_1}} R_{E_{\alpha_1} l_{\alpha_1}}(R_{12}) \sum_{m'_l} \left\langle l_{\alpha_1}\ m'_l\ \frac{1}{2}\ m_s \right|\ j_{\alpha_1}\ m_{\alpha_1} \Big\rangle Y_{l_{\alpha_1} m'_l}(\Theta_{12}, \Phi_{12}) \tag{6.37}$$

and

$$\chi^{\dagger}_{m_{s,2}}(1)\tau^{\dagger}_{m_{t,2}}(1)\psi_{\alpha_2}(\mathbf{R}_{12}) = \delta_{m_{t,2},m_{t,\alpha_2}} R_{E_{\alpha_2} l_{\alpha_2}}(R_{12}) \sum_{m'_l} \left\langle l_{\alpha_2}\ m'_l\ \frac{1}{2}\ m_{s,2} \right|\ j_{\alpha_2}\ m_{\alpha_2} \Big\rangle Y_{l_{\alpha_2} m'_l}(\Theta_{12}, \Phi_{12}). \tag{6.38}$$

with the spherical harmonics now expressed in terms of the c.m. coordinate of the pair $\mathbf{R}_{12} = (R_{12}, \Theta_{12}, \Phi_{12})$. These expressions will become important in the next section when we sum and square the matrix element.

The product wave function in the distorted c.m. distribution (6.36) can also be expressed in terms of relative and c.m. coordinates. The HO states can readily be expanded in terms of relative and c.m. quantum number by use of Moshinsky brackets [78]. The summation over the quantum numbers of the pair is then likely to be dominated by relative $nl = 00$ components due to the nature of the tensor interaction [11].

6.2 Summing and squaring the matrix element $\mathcal{M}_{fi}$

As dictated by (6.2), the next step should be to sum and square the matrix element or amplitude. This is required since in many experiments, the colliding particles are unpolarized and the polarizations of the particles in the final state are undetected. This means the average over the initial spins and sum over final spins must be taken [79]

$$\overline{\sum_i} \sum_f |\mathcal{M}_{fi}|^2 . \tag{6.39}$$

The average over the initial spins is straightforward and equal to

$$\overline{\sum_i} \equiv \frac{1}{2}\frac{1}{2J_A+1} \sum_{m_{s,i}} \sum_{M_A} \tag{6.40}$$

with M_A the total angular momentum orientation of the nucleus A. We assume the isospin of the proton and the nucleus to be determined from experiment making the summation over these orientations redundant. In the summation over the possible final states the orientation of the residual nucleus, M_{A-2}, should be included. However, assuming the spectator approximation we can limit this to the possible total angular momenta j_{α_i} of the bound nucleons and their respective orientations m_{α_i}. Furthermore we assume the

orbital angular momenta l_{α_i} for the bound nucleons are known and fixed and we assume both possible levels $j_{\alpha_i} = l_{\alpha_i} + 1/2$ and $j_{\alpha_i} = l_{\alpha_i} - 1/2$ are filled for the calculations. If this is not the case, the result is multiplied by a factor $N_{12}/(2j_{\alpha_i}+1)$ with N_{12} the number of nucleons in both levels[4]. This means the summation over the possible final states becomes

$$\sum_f \equiv \sum_{j_{\alpha_1}} \sum_{m_{\alpha_1}} \sum_{j_{\alpha_2}} \sum_{m_{\alpha_2}} \sum_{m_{s,1}} \sum_{m_{s,2}} \sum_{m_{t,\alpha_1}} \sum_{m_{t,\alpha_2}} . \tag{6.41}$$

Using all these definitions and what we have already calculated above we find

$$\begin{aligned}
&\overline{\sum_i} \sum_f \mathcal{M}^\dagger \mathcal{M} \\
&\approx \frac{1}{2(2\pi)^6} \frac{1}{2J_A+1} \frac{E_{p_i} E_A E_{p_f} E_{N_1} E_{N_2} E_{A-2}}{m_{p_i} m_A m_{p_f} m_{N_1} m_{N_2} m_{A-2}} \sum_{m_{s,i}} \sum_{M_A} \sum_{j_{\alpha_1}} \sum_{m_{\alpha_1}} \sum_{j_{\alpha_2}} \sum_{m_{\alpha_2}} \sum_{m_{s,1}} \sum_{m_{s,2}} \sum_{m_{t,\alpha_1}} \sum_{m_{t,\alpha_2}} \\
&\times \sum_{m_s} \langle \mathbf{p}_{N_1} \chi_{m_{s,1}} \tau_{m_{t,1}}, \mathbf{p}_f \chi_{m_{s,f}} \tau_{m_{t,f}} | \mathcal{O}_{pN} | \mathbf{p}_i \chi_{m_{s,i}} \tau_{m_{t,i}}, \mathbf{k} \chi_{m_s} \tau_{m_{t,1}} \rangle^\dagger \int d\mathbf{r}_{12} e^{i\mathbf{k}_{12}\cdot\mathbf{r}_{12}} g(\mathbf{r}_{12}) \\
&\times \sum_{m'_s} \langle \mathbf{p}_{N_1} \chi_{m_{s,1}} \tau_{m_{t,1}}, \mathbf{p}_f \chi_{m_{s,f}} \tau_{m_{t,f}} | \mathcal{O}_{pN} | \mathbf{p}_i \chi_{m_{s,i}} \tau_{m_{t,i}}, \mathbf{k} \chi_{m'_s} \tau_{m_{t,1}} \rangle \int d\mathbf{r}'_{12}\ e^{-i\mathbf{k}_{12}\cdot\mathbf{r}'_{12}} g(\mathbf{r}'_{12}) \\
&\times \sum_{m'_l} \left\langle l_{\alpha_1}\ m'_l\ \frac{1}{2}\ m_s \right| \left. j_{\alpha_1}\ m_{\alpha_2} \right\rangle \sum_{m''_l} \left\langle l_{\alpha_2}\ m''_l\ \frac{1}{2}\ m_{s,2} \right| \left. j_{\alpha_2}\ m_{\alpha_2} \right\rangle \delta_{m_t, m_{t,\alpha_1}} \\
&\times \sum_{\mu'_l} \left\langle l_{\alpha_1}\ \mu'_l\ \frac{1}{2}\ m'_s \right| \left. j_{\alpha_1}\ m_{\alpha_2} \right\rangle \sum_{\mu''_l} \left\langle l_{\alpha_2}\ \mu''_l\ \frac{1}{2}\ m_{s,2} \right| \left. j_{\alpha_2}\ m_{\alpha_2} \right\rangle \delta_{m_{t_2}, m_{t,\alpha_2}} \\
&\times \int d\mathbf{R}_{12}\ S_{\mathrm{IFSI}}(\mathbf{R}_{12})\, e^{i\mathbf{K}_{12}\cdot\mathbf{R}_{12}} R_{E_{\alpha_1} l_{\alpha_1}}(R_{12}) Y^*_{l_{\alpha_1} m'_l}(\Theta_{12}, \Phi_{12}) R_{E_{\alpha_2} l_{\alpha_2}}(R_{12}) Y^*_{l_{\alpha_2} m''_l}(\Theta_{12}, \Phi_{12}) \\
&\times \int d\mathbf{R}'_{12}\ S_{\mathrm{IFSI}}(\mathbf{R}'_{12})\, e^{i\mathbf{K}_{12}\cdot\mathbf{R}'_{12}} R_{E_{\alpha_1} l_{\alpha_1}}(R'_{12}) Y_{l_{\alpha_1} \mu'_l}(\Theta'_{12}, \Phi'_{12}) R_{E_{\alpha_2} l_{\alpha_2}}(R'_{12}) Y_{l_{\alpha_2} \mu''_l}(\Theta'_{12}, \Phi'_{12}).
\end{aligned} \tag{6.42}$$

Now we can use the summation over j_{α_i} and m_{α_i} to apply the orthogonality relation

$$\sum_{j=|j_1-j_2|}^{j_1+j_2} \sum_{m=-j}^{+j} \langle j_1 m_1 j_2 m_2 | j m \rangle \langle j_1 m'_1 j_2 m'_2 \rangle = \delta_{m_1, m'_1} \delta_{m_2, m'_2}. \tag{6.43}$$

Using this and the definitions (6.35) and (6.36) we get

$$\begin{aligned}
&\overline{\sum_i} \sum_f \mathcal{M}^\dagger \mathcal{M} \\
&\approx \frac{E_{p_i} E_A E_{p_f} E_{N_1} E_{N_2} E_{A-2}}{m_{p_i} m_A m_{p_f} m_{N_1} m_{N_2} m_{A-2}} |\mathcal{G}(\mathbf{k}_{12})|^2 \sum_{m_l=-l_{\alpha_1}}^{l_{\alpha_1}} \sum_{m'_l=-l_{\alpha_2}}^{l_{\alpha_2}} \left| F^{D, E_{\alpha_2} l_{\alpha_2} m'_l}_{E_{\alpha_1} l_{\alpha_1} m_l}(\mathbf{K}_{12}) \right|^2 \\
&\quad \times \sum_{m_{s,i}} \sum_{m_{s,1}} \sum_{m_{s,f}} \sum_{m_s} \left| \langle \mathbf{p}_{N_1} \chi_{m_{s,1}} \tau_{m_{t,1}}, \mathbf{p}_f \chi_{m_{s,f}} \tau_{m_{t,f}} | \mathcal{O}_{pN} | \mathbf{p}_i \chi_{m_{s,i}} \tau_{m_{t,i}}, \mathbf{k} \chi_{m_s} \tau_{m_{t,1}} \rangle \right|^2
\end{aligned} \tag{6.44}$$

[4]This can best be understood by working in second quantization and considering occupation numbers by means of a simple example.

with

$$F^{D,E_{\alpha_2}l_{\alpha_2}m_l'}_{E_{\alpha_1}l_{\alpha_1}m_l}(\mathbf{K}_{12}) = \frac{1}{(2\pi)^{3/2}}\int d\mathbf{R}_{12}\; S_{\mathrm{IFSI}}\left(\mathbf{R}_{12}\right)\, e^{i\mathbf{K}_{12}\cdot\mathbf{R}_{12}} R_{E_{\alpha_1}l_{\alpha_1}}(R_{12}) Y^*_{l_{\alpha_1}m_l}(\Theta_{12},\Phi_{12}) \times R_{E_{\alpha_2}l_{\alpha_2}}(R_{12}) Y^*_{l_{\alpha_2}m_l'}(\Theta_{12},\Phi_{12}). \tag{6.45}$$

The fully factorized cross section will also be proportional to this c.m. momentum distribution as we will see later. From the looks of Eq. (6.44) we almost have what we need. Inserting this result into the cross section (6.2) does however not yield the fully factorized cross section yet. To be able to write the free proton-nucleon cross section as a separate factor we first need to develop an adequate expression for it.

6.3 The free proton-nucleon cross section

The free proton-nucleon scattering reaction

$$p_i + N_i \rightarrow p_f + N_f, \tag{6.46}$$

can be represented using four-momenta by

$$k^\mu_{p_i}(E_{p_i},\mathbf{p}_i) + k^\mu_{N_i}(E_{N_i},\mathbf{p}_{N_i}) \rightarrow k^\mu_{p_f}(E_{p_f},\mathbf{p}_f) + k^\mu_{N_f}(E_{N_f},\mathbf{p}_{N_f}) \tag{6.47}$$

To write down the free nucleon-proton cross section we first look at the matrix element for the two-body initial and final states we have in this case, we therefore deal with a two-body operator. In a similar way as described in Section 6.1.2 we can approximate the matrix element by first requiring $\mathcal{O}_{pN}(\mathbf{r}_1,\mathbf{r}_2) = \mathcal{O}_{pN}(\mathbf{r}_2,\mathbf{r}_1)$ and subsequently posing a kinematical restriction on the momenta in (6.47) so the nucleon and the proton can always be correctly distinguished from each other. The matrix element then reduces to

$$\mathcal{M}^{pN}_{fi} = \langle k_{p_f}\chi_{m_{s,f}}\tau_{m_{t,f}}, k_{N_f}\chi_{m_{s,Nf}}\tau_{m_{t,1}}, |\mathcal{O}_{pN}| k_{p_i}\chi_{m_{s,i}}\tau_{m_{t,i}}, k_{N_i}\chi_{m_{s,Ni}}\tau_{m_{t,Ni}}\rangle \tag{6.48}$$

where the Lorentz-invariant normalization has been incorporated in the notation of the matrix element itself, hence the presence of four-momenta of the initial and final particles. The proton-nucleon scattering flux factor as defined by (3.119) can be written as

$$\frac{1}{F} = \frac{m_p m_N}{E_{p_i}E_{N_i}\beta_{p_iN_i}} = \frac{m_p m_N}{\sqrt{(k_i\cdot k_{N_i})^2 - m_p^2 m_N^2}} \tag{6.49}$$

with $\beta_{p_iN_i}$ the relative speed of the proton and the nucleon in the initial state. This expression will be evaluated in the c.m. frame of the two particles since it is the most straightforward frame to do this. The free nucleon-proton scattering is well understood and cross sections in both the c.m. and lab frame can be obtained from experimental data (e.g., from the Nijmegen group [80]). This is an obvious benefit coming from using a factorized expression to analyze quasi-free reactions. The flux factor in the c.m. frame becomes

$$\frac{m_p m_N}{\sqrt{(k_i\cdot k_{N_i})^2 - m_p^2 m_N^2}} = \frac{2m_p m_N}{\sqrt{(s - m_p^2 - m_N^2)^2 - 4m_p^2 m_N^2}} \tag{6.50}$$

using the triangular λ function defined by Eq. (3.126). Averaging over the initial states, summing over the final states, squaring the amplitude and including the appropriate Lorentz-invariant phase space results in the proton-nucleon scattering cross section:

$$\begin{aligned} d\sigma^{pN} =& \frac{m_p^2 m_N^2}{2\sqrt{(s-m_p^2-m_N^2)^2-4m_p^2m_N^2}} \sum_{m_{s,Ni}} \sum_{m_{s,i}} \sum_{m_{s,Nf}} \sum_{m_{s,f}} \\ & \times \left| \langle k_{p_f} \chi_{m_{s,f}} \tau_{m_{t,f}}, k_{N_f} \chi_{m_{s,Nf}} \tau_{m_{t,1}}, |\mathcal{O}_{pN}| k_{p_i} \chi_{m_{s,i}} \tau_{m_{t,i}}, k_{N_i} \chi_{m_{s,Ni}} \tau_{m_{t,Ni}} \rangle \right|^2 \\ & \times (2\pi)^4 \delta^{(4)}(k_{p_i} + k_{N_i} - k_{p_f} - k_{N_f}) \frac{m_p}{E_{p_f}} \frac{d\mathbf{p}_f}{(2\pi)^3} \frac{m_N}{E_{N_f}} \frac{d\mathbf{p}_{N_f}}{(2\pi)^3} \end{aligned} \tag{6.51}$$

To express this in the proton-nucleon c.m. frame, the delta function can be split up according to

$$\delta^{(4)}((k_{p_i} + k_{N_i} - k_{p_f} - k_{N_f}) = \delta^{(3)}(\mathbf{p}_i + \mathbf{p}_{N_i} - \mathbf{p}_f - \mathbf{p}_{N_f}) \delta(E_{p_i} + E_{N_i} - E_{p_f} - E_{N_f}). \tag{6.52}$$

This three-momentum conservation delta function cancels the integral over $\mathbf{p}_f$. Expressing the integration over $\mathbf{p}_{Nf}$ in spherical coordinates and using the fact that $\sqrt{s} = E_{p_i} + E_{N_i}$ in the proton-nucleon c.m. frame, what remains is

$$\frac{\delta(\sqrt{s} - E_{p_f} - E_{N_f})}{E_{p_f} E_{N_f}} p_{N_f}^2 dp_{N_f} d\Omega_{N_f}. \tag{6.53}$$

We now define using the four-momentum relation

$$f(p_{n_f}) \equiv \sqrt{s} - \sqrt{m_p^2 + p_{N_f}^2} - \sqrt{m_N^2 + p_{N_f}^2}, \qquad \text{and} \qquad g(p_{N_f}) \equiv \frac{p_{N_f}^2}{E_{p_f} E_{N_f}}. \tag{6.54}$$

where we have used that in an elastic collision also the final momenta must be equal in size. These expressions can be used in a standard procedure to integrate over the phase space [79] which uses the identity

$$\int g(x) \delta(f(x)) dx = \left[\frac{g(x)}{f'(x)} \right]_{f=0}. \tag{6.55}$$

In case of the definitions (6.54) we made here, we simply get

$$\frac{\delta(\sqrt{s} - E_{p_f} - E_{N_f})}{E_{p_f} E_{N_f}} p_{N_f}^2 dp_{N_f} d\Omega_{N_f} = \frac{p_{N_f}}{\sqrt{s}} d\Omega_{N_f}. \tag{6.56}$$

This means we can eventually write

$$\begin{aligned} \left(\frac{d\sigma^{pN}}{d\Omega_{N_f}} \right)_{\text{c.m.}} =& \frac{1}{(2\pi)^2} \frac{m_p^2 m_N^2}{2\sqrt{(s-m_p^2-m_N^2)^2-4m_p^2m_N^2}} \frac{p_{N_f}}{\sqrt{s}} \sum_{m_{s,Ni}} \sum_{m_{s,i}} \sum_{m_{s,Nf}} \sum_{m_{s,f}} \\ & \times \left| \langle k_{p_f} \chi_{m_{s,f}} \tau_{m_{t,f}}, k_{N_f} \chi_{m_{s,Nf}} \tau_{m_{t,1}}, |\mathcal{O}_{pN}| k_{p_i} \chi_{m_{s,i}} \tau_{m_{t,i}}, k_{N_i} \chi_{m_{s,Ni}} \tau_{m_{t,Ni}} \rangle \right|^2. \end{aligned} \tag{6.57}$$

and the free proton-nucleon scattering cross section will be inserted in the complete two-nucleon knockout cross section accordingly.

6.4 The factorized two-nucleon knockout cross section

Using (6.57) we can insert the free proton-nucleon scattering cross section into the expression for the complete two-nucleon knockout cross section (6.2). Just as for the free proton-nucleon scattering, we include the relativistic factors again in the matrix element itself. This gives

$$\begin{aligned} d\sigma \approx & \frac{2m_A m_{A-2}}{(2\pi)^8} \frac{\sqrt{(s-m_p^2-m_N^2)^2-4m_p^2m_N^2}}{\sqrt{(k_{p_i}\cdot k_A)^2-m_p^2m_A^2}E_{p_f}E_{N_1}E_{N_2}E_{A-2}} \frac{\sqrt{s}}{p_{N_f}} \\ & \times \left(\frac{d\sigma^{pN}}{d\Omega_{N_f}}\right)_{\text{c.m.}} |\mathcal{G}(\mathbf{k}_{12})|^2 \\ & \times \sum_{m_l=-l_{\alpha_1}}^{l_{\alpha_1}} \sum_{m_l'=-l_{\alpha_2}}^{l_{\alpha_2}} \left| F^{D,E_{\alpha_2}l_{\alpha_2}m_l'}_{E_{\alpha_1}l_{\alpha_1}m_l}(\mathbf{K}_{12}) \right|^2 \\ & \times (2\pi)^4\delta^{(4)}(k_{p_i}+k_A-k_{p_f}-k_{N_1}-k_{N_2}-k_{A-2})\; d\mathbf{p}_f d\mathbf{p}_{N_1} d\mathbf{p}_{N_2} d\mathbf{p}_{A-2}. \end{aligned} \tag{6.58}$$

where we rewrote the flux factor for the initial proton and nucleus in the same way as the flux factor for the free proton-nucleon scattering cross section. The total Lorentz-invariant cross section is composed of factors which are Lorentz-invariant themselves, as e.g., the free proton-nucleon cross section. Note that we have also placed the free scattering cross section and the squared Fourier transform of the correlation function together. This is done to stress that in fact the incoming proton scatters off a correlated pair, characterized by its relative momentum $\mathbf{k}_{12}$. The factorization in terms of relative and c.m. motion therefore becomes even more apparent. The previous expression can then be written in a much more convenient way as

$$d^8\sigma \propto K\sigma^{pN}(\mathbf{k}_{12})F^D_{\alpha_1,\alpha_2}(\mathbf{K}_{12})d\Phi \tag{6.59}$$

with K a factor containing all kinematical information, σ^{pN} the free scattering from a correlated pair, F^D the distorted c.m. momentum distribution of the nucleon pair inside the nucleus and $d\Phi$ the factor representing the phase space. The superscript $'8'$ denotes an eight-fold cross section. There are four particles in the final state which means twelve momentum components. This subtracted by the four conservation laws we impose reflects indeed eight degrees of freedom. Note that we have the possibility here to replace the distorted distribution by the undistorted distribution multiplied by a nuclear transparency factor to account for the IFSI.

In a situation where all approximations we have made are valid, the two-nucleon knockout cross section factorizes according to (6.59). A very positive consequence of this expression is that it makes calculations concerning quasi-free two-nucleon knockout reactions a lot easier. The expressions developed here can be used to simulate cross sections in actual experimental situations. It opens the gate to comparative studies where experiments probe the momentum distributions in different nuclei w.r.t. a reference nucleus. This allows us to probe the mass dependence of SRC dynamics [52] *if* the kinematics probed is the same

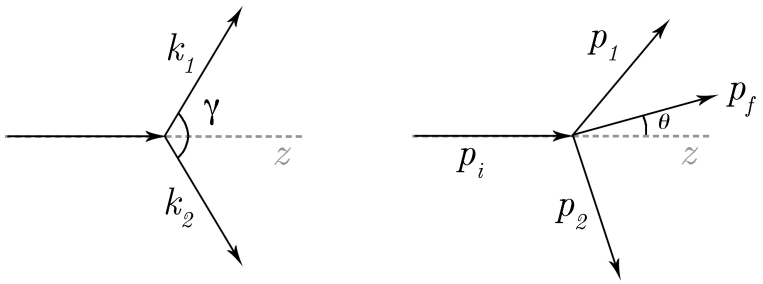

Figure 6.3: The kinematical configurations assumed in the simulation. We assume the initial momenta $\mathbf{k}_1$ and $\mathbf{k}_2$ to be symmetric w.r.t to the z-axis along the direct of incidence (left). The scattered proton with momentum $\mathbf{p}_f$ will always be detected at an angle $\theta = 25°$, p_f will vary as a function of the opening angle γ.

in these experiments. We also stress once more that – next to the zero-range approximation – the kinematic restrictions to eventually allow factorization are severe. In addition to the conditions that need to be fulfilled to only probe SRC pairs, other restrictions on the kinematics are made to assure the factorization scheme. This of course limits the available phase space to probe the nucleon momentum distributions.

6.5 Numerical simulation

As an illustration to what end the expression for the factorized cross section (6.59) can be used, a simulation of the opening angle distribution (Fig. 4.4) for SRC pairs is executed using computer code that was originally developed for $(p, 2p)$ knockout reactions in inverse kinematics. The simulated reaction under study here is the two nucleon knockout from an unstable Carbon isotope: $^{10}C(p, p'pn)^8B$. As to not make things overly complicated in this illustrative numerical calculation, we assume the kinematical conditions depicted in Fig. 6.3. We will assume the individual momenta of the nucleons in the pair $\mathbf{k}_1$ and $\mathbf{k}_2$ to be symmetrical around the z-axis which is fixed along the direction if the incident proton with momentum $\mathbf{p}_i$. After the collision, $\mathbf{p}_f$ will be detected at a fixed angle. However the value of p_f will vary as the opening angle γ between $\mathbf{k}_1$ and $\mathbf{k}_2$ changes. It is assumed that all interactions take place in a single plane, hence the angle ϕ denoting the orientation around the z-axis will be equal to 0 or π. The kinematics will be calculated by determining p_f from using fixed $\mathbf{p}_i$, $\mathbf{p}_2$, $\mathbf{K}_{12}$ and Ω_f. From this $\mathbf{p}_1$ follows by using momentum conservation. A general way to make sure the cross section can be expressed using these fixed values is to rewrite the phase space factor $d\Phi$ in (6.59). The delta function can be rewritten as a product of two: one concerning energy momentum conservation and one concerning momentum conservation. The last one can be used to eliminate a necessary integration over a final momentum needed to calculate the cross section. Converting another integration variable to spherical coordinates and using the same procedure as used to calculate the free proton-nucleon scattering cross section in Section 6.3 eliminates the momentum conserving delta function. This procedure allows the cross section to be written by selecting appropriate kinematical variables. In the specific case of the kinematical situation explained above, what remains from these manipulations

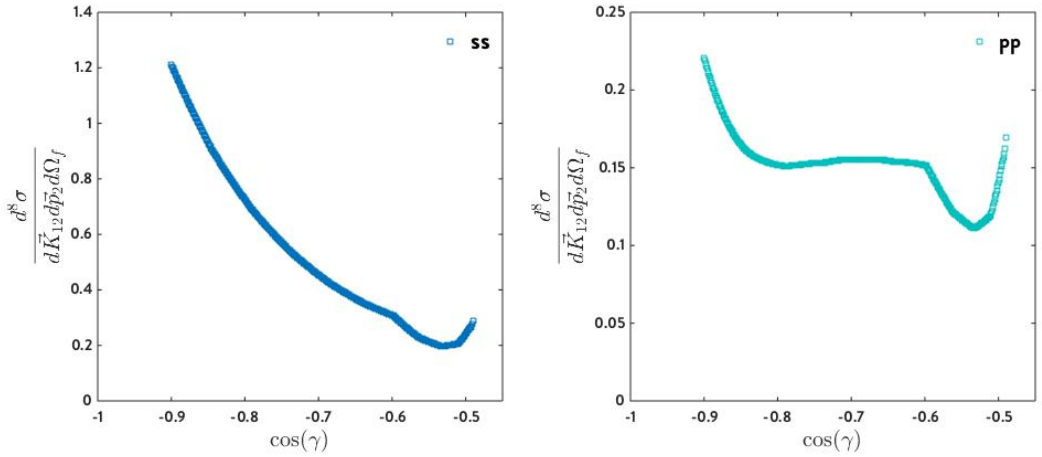

Figure 6.4: The calculated cross sections for the reaction $^{10}C(p,p'pn)^8B$ using the kinematics described in the text as function of the $cos(\gamma)$. The values were calculated for s-shell knockout (left) and p-shell knockout (right). Both simulations show the correct augmented distribution for the back-to-back configuration of $\cos(\gamma) \approx -1$ but the s-shell knockout produces a more realistic global trend. The sizes of the cross sections are given in arbitrary units because no IFSI factors are included.

can be brought to the right hand side of Eq. (6.59) giving

$$\frac{d^8\sigma}{d\mathbf{K}_{12}d\mathbf{p}_2d\Omega_f} \propto K'\sigma^{pN}(\mathbf{k}_{12})F^D_{\alpha_1,\alpha_2}(\mathbf{K}_{12}) \tag{6.60}$$

where we have identified $d\mathbf{K}_{12} = d\mathbf{p}_{A-2}$ according to (4.15). For this simulation of the $^{10}C(p,p'pn)^8B$ reaction, nucleon knockout from the s- and p-shells was considered. In the projectile frame, the incoming proton energy was fixed to 1700 MeV. The initial nucleon momenta were chose as $k_1 = k_2 = 450$ MeV. The angle of detection for the scattered proton $\mathbf{p}_f$ is fixed at $\theta = 25°$. The size of this momentum will change as $\cos(\gamma)$ is varied between ~ -0.5 and -1. The cross sections themselves were calculated using the central correlation function calculated by Dickhoff and Gearheart as described in [11] and plotted in Fig. 4.2, the bound HO-states were parametrized according to [81]. No IFSI effects were included, as noted in Chapter 5 these should have the effect of attenuating the cross sections.

The results of the calculations are shown in Fig. 6.4. Both simulations show that the cross sections tend to be larger when approaching $\cos(\gamma) = 1$ corresponding to a back-to-back configuration of the nucleon momenta. However, the s-shell knockout cross sections do show a more similar global trend in comparison to Fig. 4.4 than for p-shell knockout. The sizes of the cross sections themselves are not important since in this simulation a very particular type of kinematics was chosen and IFSI effects were not included. The correlation function $g(r_{12})$ is not included for simulations of single-nucleon knockout reactions from which the code was developed. When it is included for these crude simulations of two-nucleon knockout reactions, the expected effect of placing SRC pairs in a back-to-back configuration is observed for this particular kinematics. Simulations concerning more realistic experimental conditions require a more profound approach.

Chapter 7

Summary and outlook

In nuclear physics, mean-field theories are adequate to explain the general properties of atomic nuclei. However, experimental tests of mean-field frameworks like the Fermi gas model fall short in explaining certain effects due the assumption that the nucleons can be treated as independent particles. Nucleon-nucleon correlations are needed to account for the universal presence of a high-momentum tail above the Fermi momentum.

A way to study the characteristics of correlations between nucleons is the use of collisions or scattering processes. In particular, a quasi-free reaction type was proposed as an appropriate method to probe the entire nuclear volume. This quasi-free picture allows us to divide the collision in a "hard" and a "soft" interaction. In this work the $A(p, p'NN)A-2$ two-nucleon knockout reaction was studied as a tool to extend the study of short-range correlations to unstable nuclei by use of inverse kinematics. This method however requires relativistic particle energies which implied the necessary theoretical and experimental considerations.

One of these considerations was the definition of a number of relevant reference frames in which the kinematics of the scattering process could be described properly. As for the dynamics of the collisions we relied on quantum collision theory. Using the basic formalism of potential scattering we quoted the Lippmann-Schwinger equation as one of the most used identities to describe scattering in quantum mechanics. In the Plane Wave Impulse Approximation we were able to construct the transition matrices from evolution operators in the interaction picture. Lorentz-invariance conditions were imposed on the particle states as well as the phase space to eventually formulate a general expression for a Lorentz-invariant $A(p, p'NN)A-2$ cross section.

In order to calculate the matrix elements that are included in the cross section, the effects of a NN potential should be included. From observed experimental features of NN correlation effects, a correlation operator was introduced that shifted the complexity from the wave functions to an effective operator. This operator included only the central correlation function which incorporates the strong repulsive nature of the NN potential for short relative distances. Short-range correlated (SRC) pairs experience this repulsive force and are found in "back-to-back" configurations.

Distortion of the wave functions when traveling through the nuclear medium is something which is not to be overlooked. The relativistic energies of the incoming and outgoing particles allowed us to include the effects of initial and final state interactions (IFSI) in a semi-classical way. The eikonal approximation was developed using the Lippmann-Schwinger equation and extended into a relativistic multiple scattering Glauber formalism (RMSGA): incoming and outgoing particles experience attenuation and distortion effects due to the presence of multiple scatterers inside the nucleus. Nuclear transparencies were described as a possible tool to account for RMSGA effects in quasi-free knockout reactions.

The cross section was shown to factorize after making a number of allowed approximations in the quasi-free scattering framework, including the spectator approximation. We assumed a point interaction and imposed a considerable amount of kinematical constraints to make sure we exclusively probe SRC pairs and in addition keep calculations manageable. These cuts narrowed down the available phase space that is needed to study momentum distributions. The succes of the factorization hinges upon the validity of the zero-range approximation. The factorized cross section includes the free proton-nucleon scattering cross section which is well understood, both on a theoretical and an experimental level. The factorized cross section was also shown to be sensitive to the c.m. distribution of the SRC pairs in the nucleus. Simulations of the opening angle of SRC pairs were performed using the factorized expression for the cross section and yielded the expected opening angle distribution profile for SRC pairs.

The use of two-nucleon knockout reactions to study unstable nuclei in inverse kinematics is still in its infancy. This work represents but a first attempt to develop the general theoretical framework for $(p, p'NN)$ reactions, built from methods developed for studying electron induced two-nucleon knockout $(e, e'NN)$ reactions using stable nuclei and (p, pn) reactions in inverse kinematics. A number of improvements can be made to calculate even more realistic cross section. First, we could use a more general three-body operator formalism that reflects the properties of the interaction in a better way. In this sense we could also use a more elaborate form of the effective operator which also accounts for other features of NN correlations than simply the central repulsive nature. A straightforward augmentation could be to include the tensor correlation in calculations as well. This would also allow us to study the effects of short-range correlations on the isospin nature of the pairs. Charge exchange effects can also be included in the IFSI to yield more adequate results.

The theoretical framework presented in this thesis, along with the possible augmentations listed above can give rise to cross section simulations that can be tested against real experimental measurements. This (possible) verification will tell us if the quasi-free two-nucleon knockout formalism described here is appropriate to study short-range phenomena in unstable nuclei.

Appendix A

Complex integrals

A.1 The Lippmann-Schwinger equation

To eventually arrive at the Lippmann-Schwinger equation, we need to integrate the expression

$$G(\mathbf{r},\mathbf{r}') = -\frac{1}{(2\pi)^3}\int \frac{e^{i\mathbf{k}'\cdot(\mathbf{r}-\mathbf{r})}}{k'^2-k^2}d\mathbf{k}' \tag{A.1}$$

in such a way it exhibits the appropriate asymptotic conditions for $r \to \infty$. This means it should behave like an outgoing spherical wave as the stationary scattering wave function (3.22) requires. To achieve this we first set

$$\mathbf{R} = \mathbf{r} - \mathbf{r}' \tag{A.2}$$

and adopt a spherical coordinate system in such a way that the z-axis coincides with $\mathbf{R}$ [27]. Using $d\mathbf{k}' = k'^2 dk' \sin\theta d\theta' d\phi'$, the above equation then becomes

$$G(R) = -\frac{1}{(2\pi)^3}\int_0^{\pi} d\theta' \sin\theta' \int_0^{2\pi} d\phi' \int_0^{\infty} dk'\ k'^2 \frac{e^{ik'R\cos\theta'}}{k'^2-k^2}. \tag{A.3}$$

After performing the angular integrations and using the fact that the integrand is an even function of k' we get

$$G(R) = -\frac{1}{4\pi^2 R}\int_{-\infty}^{+\infty} \frac{k'\sin k'R}{k'^2-k^2}dk'. \tag{A.4}$$

The next step is splitting up the integral using the representation of the sine in the complex plane and the special product in the denominator

$$\begin{aligned} G(R) = -\frac{1}{16\pi^2 iR}\Bigg\{ &\int_{-\infty}^{+\infty} e^{ik'R}\left[\frac{1}{k'-k}+\frac{1}{k'+k}\right]dk' \\ &- \int_{-\infty}^{+\infty} e^{-ik'R}\left[\frac{1}{k'-k}+\frac{1}{k'+k}\right]dk'\Bigg\}. \end{aligned} \tag{A.5}$$

We will evaluate this expression in the complex k'-plane so

$$k' = \mathrm{Re}\ k' + i\mathrm{Im}\ k' \quad \text{and} \quad e^{ik'R} = e^{iR\ \mathrm{Re}\ k'}e^{-R\ \mathrm{Im}\ k'}. \tag{A.6}$$

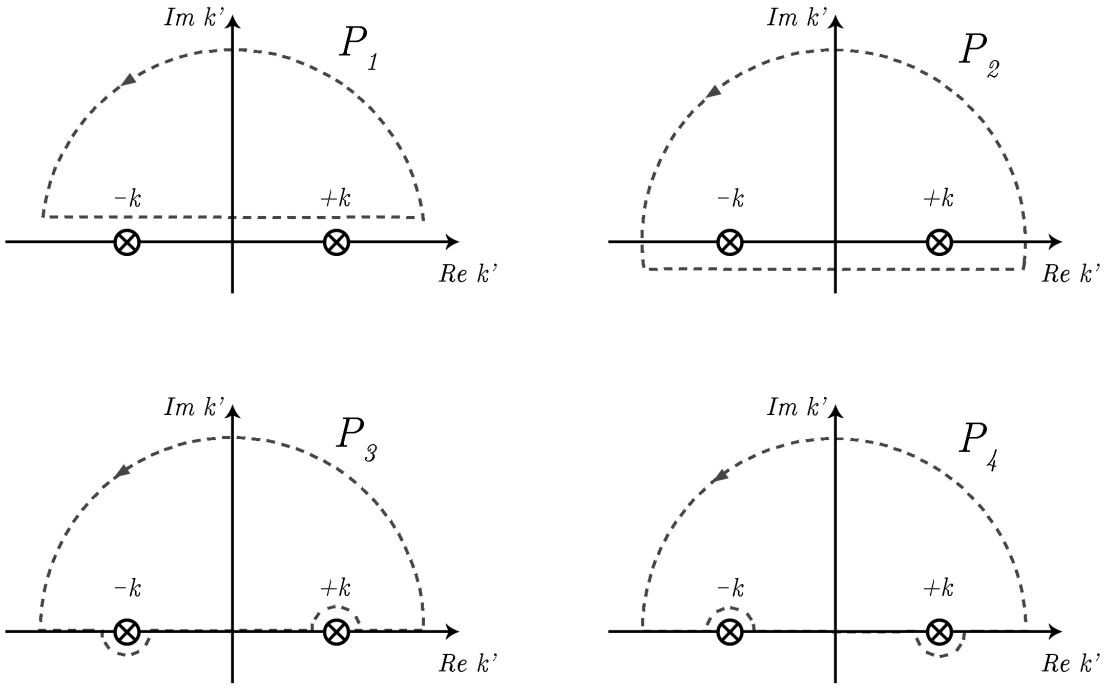

Figure A.1: The four possible contour possibilities to avoid the poles at $k' = k$ for the evaluation of the integral (A.5)

This form suggests to use infinite semi-circle contours along which we integrate: for the first term we close the contour in the upper half plane Im $k' > 0$ and for the second term in the lower half plane Im $k' < 0$. The contributions to the integral from the semi-circles become zero as we let the radius go to infinity, the integral is then equal to the integral along the real axis. Now to avoid the poles at $k' = \pm k$ on this axis we have four possibilities, shown in Fig. A.1 for the contour closed in the upper half plane. We apply Cauchy's residue theorem [82]

$$\oint_C f(z)dz = 2\pi i \sum_{a\in A} \underset{z=a_i}{\text{Res}} f(z) \tag{A.7}$$

with A the set of poles inside the contour C. For the first and second term the outcomes are

$$\begin{cases} P_1 : 0, \\ P_2 : 2\pi i[e^{ikR} + e^{-ikR}], \\ P_3 : 2\pi i e^{-ikR}, \\ P_4 : 2\pi i e^{ikR}, \end{cases} \quad \text{and} \quad \begin{cases} P_1 : -2\pi i[e^{ikR} + e^{-ikR}], \\ P_2 : 0, \\ P_3 : -2\pi i e^{-ikR}, \\ P_4 : -2\pi i e^{ikR}. \end{cases}$$

From these results we can conclude that only performing the integration along P_4 is appropriate so the Green's function behaves as a spherical outgoing wave. Hence

$$G(R) = -\frac{1}{4\pi^2 R} \oint_{P_4} \frac{k' \sin k'R}{k'^2 - k^2} dk' = -\frac{1}{4\pi} \frac{e^{ikR}}{R} \tag{A.8}$$

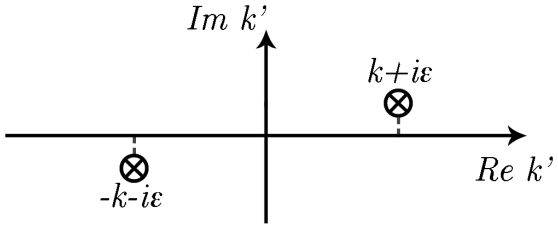

Figure A.2: Displacement of the poles at $k' = \pm k$ by an infinitesimal amount ϵ above and below the real k' axis.

Returning to the original variables $\mathbf{r}$ and $\mathbf{r}'$ we get

$$G(\mathbf{r}, \mathbf{r}') = -\frac{1}{4\pi} \frac{e^{ik|\mathbf{r}-\mathbf{r}'|}}{|\mathbf{r}-\mathbf{r}'|}. \tag{A.9}$$

The can be used to eventually derive the Lippmann-Schwinger equation. Starting again from the top we noted about the Green's function in wave vector space

$$G(\mathbf{r}, \mathbf{r}') = -\frac{1}{(2\pi)^3} \int \frac{e^{i\mathbf{k}'\cdot(\mathbf{r}-\mathbf{r})}}{k'^2 - k^2} d\mathbf{k}' \tag{A.10}$$

that this expression can be reformulated as to avoid the poles at $k' = \pm k$. This is done by displacing the poles slightly by an amount ϵ above and below the real k' axis (Fig. A.2).

The poles are then located at

$$k' = \pm(k + i\epsilon), \qquad \epsilon \to 0^+. \tag{A.11}$$

To first order we then have

$$k'^2 = k^2 + i\epsilon, \qquad \epsilon \to 0^+. \tag{A.12}$$

The integral representation of the Green's function in wave vector space then becomes

$$G(\mathbf{r}, \mathbf{r}') = -\frac{1}{(2\pi)^3} \lim_{\epsilon \to 0+} \int \frac{e^{i\mathbf{k}'\cdot(\mathbf{r}-\mathbf{r}')}}{k'^2 - k^2 - i\epsilon} d\mathbf{k}'. \tag{A.13}$$

This expression will be used when developing the eikonal approximation in Section 5.2.

A.2 Eikonal approximation

In Section 5.2, developing the eikonal approximation, we need to calculate the linearized Green's function

$$G_0^{(1)}(\mathbf{R}) = -\frac{e^{(i\mathbf{k}\cdot\mathbf{R})}}{(2\pi)^3} \int d\mathbf{p} \frac{e^{i\mathbf{p}\cdot\mathbf{R}}}{2kp_z - i\epsilon}. \tag{A.14}$$

Writing out the integrand in Cartesian coordinates gives

$$\begin{aligned} \int d\mathbf{p} \frac{e^{i\mathbf{p}\cdot\mathbf{R}}}{2kp_z - i\epsilon} &= \int_{-\infty}^{+\infty} dp_x \; e^{ip_x X} \int_{-\infty}^{+\infty} dp_y \; e^{ip_y Y} \int_{-\infty}^{+\infty} dp_z \frac{e^{ip_z Z}}{p_z - i\epsilon} \\ &= (2\pi)^2 \delta(X)\delta(Y) \frac{1}{2k} \int_{-\infty}^{+\infty} dp_z \frac{e^{ip_z Z}}{p_z - i\epsilon} \end{aligned} \tag{A.15}$$

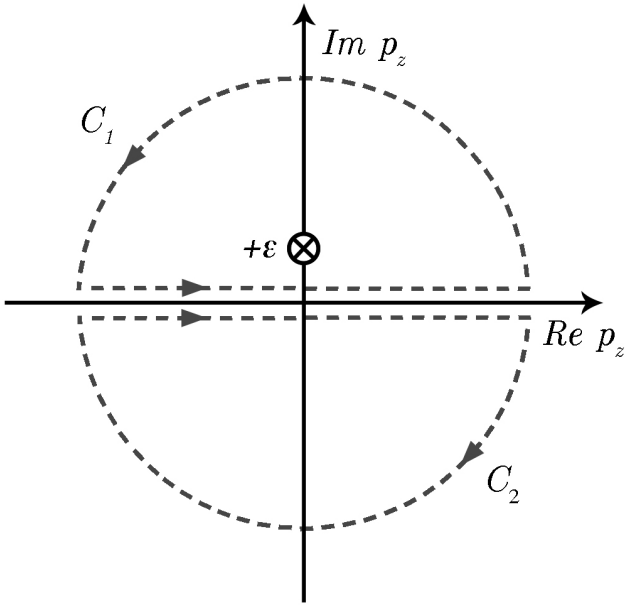

Figure A.3: The contours closed in both hemispheres, only in the upper hemisphere the pole is inside the contour.

The integrals over the x and y coordinates can be calculated easily. For the integral over p_z we will use contour integration where the integrand is evaluated in the complex p_z plane [27]. Since Z can be positive or negative we should close the contours by infinite semi-circles in the upper or lower hemisphere plus the real axis (Fig. A.3). We apply Cauchy's residue theorem as in Appendix A.1. There is only one pole in the contour C_1 enclosing the upper hemisphere, so for $Z > 0$

$$\int_{-\infty}^{+\infty} dp_z \frac{e^{ip_z Z}}{p_z - i\epsilon} = 2\pi i, \qquad (Z > 0). \tag{A.16}$$

In the lower hemisphere there are no poles inside the contour C_2 so

$$\int_{-\infty}^{+\infty} dp_z \frac{e^{ip_z Z}}{p_z - i\epsilon} = 0, \qquad (Z < 0). \tag{A.17}$$

These results give for the linearized Green's function

$$G_0^{(1)}(\mathbf{R}) = \begin{cases} -\frac{ie^{ikZ}}{2k}\delta(X)\delta(Y) & \text{if } Z > 0, \\ 0 & \text{if } Z < 0. \end{cases} \tag{A.18}$$

Bibliography

[1] F. Yang and J. H. Hamilton, *Modern Atomic and Nuclear Physics*. World Scientific Publishing Co., 2010.

[2] S. Sharma, *Atomic and Nuclear Physics*. Dorling Kindersley Pvt. Ltd., 2008.

[3] C. A. Bertulani and P. Danielewicz, *Introduction to Nuclear Reactions*. Institute of Physics Publishing, 2004.

[4] I. Ragnarsson and S. G. Nilsson, *Shapes and Shells in Nuclear Structure*. Cambridge University Press, 1995.

[5] O. Benhar, D. Day, and I. Sick, "Inclusive quasielastic electron-nucleus scattering," *Rev. Mod. Phys.*, vol. 80, pp. 189–224, Jan 2008.

[6] J. Arrington, D. W. Higinbotham, G. Rosner, and M. Sargsian, "Hard probes of short-range nucleon-nucleon correlations," *Prog. Part. Nucl. Phys.*, vol. 67, pp. 898–938, 2012.

[7] M. Alvioli, C. Ciofi Degli Atti, L. P. Kaptari, C. B. Mezzetti, and H. Morita, "Universality of nucleon-nucleon short-range correlations and nucleon momentum distributions," *Int. J. Mod. Phys.*, vol. E22, p. 1330021, 2013.

[8] O. Hen *et al.*, "Momentum sharing in imbalanced fermi systems," *Science 346, 614 (2014)*.

[9] O. Hen, *High-momentum nucleons in nuclei*. PhD thesis, Tel Aviv University, 2015.

[10] I. Korover *et al.*, "Probing the Repulsive Core of the Nucleon-Nucleon Interaction via the $^4He(e, epN)$ Triple-Coincidence Reaction," *Phys. Rev. Lett.*, vol. 113, no. 2, p. 022501, 2014.

[11] M. Vanhalst, *Quantifying short-range correlations in nuclei*. PhD thesis, UGent, 2014.

[12] B. H. Bransden and C. Joachain, *Quantum Mechanics*. Pearson Educationd Ltd., 2 ed., 2000.

[13] G. Neyens, "Nuclear magnetic and quadrupole moments for nuclear structure research on exotic nuclei," *Reports on Progress in Physics*, vol. 66, no. 7, p. 1251, 2003.

[14] P. G. Hansen and J. A. Tostevin, "Direct reactions with exotic nuclei," *Ann. Rev. Nucl. Part. Sci.*, vol. 53, pp. 219–261, 2003.

[15] K. S. Krane, *Introductory Nuclear Physics*. John Wiley & Sons, Inc., 1988.

[16] G. R. Satchler, *Introduction to Nuclear Reactions*. Macmillan Press Ltd., 1980.

[17] M. Holl, L. Atar, and V. Panin, "Quasi-Free Scattering from Relativistic Carbon and Oxygen Isotopes," *PoS*, vol. Bormio2015, p. 043, 2015.

[18] S. Boffi, C. Giusti, F. D. Pacati, and M. Radici, *Electromagnetic Response of Atomic Nuclei*. Oxford University Press Inc.

[19] C. Sheidenberger and M. Pfutzner, *The Euroschool on Exotic Beams, Vol. IV*. Springer-Verlag, 2014.

[20] A. Gade *et al.*, "Reduction of spectroscopic strength: Weakly-bound and strongly-bound single-particle states studied using one-nucleon knockout reactions," *Phys. Rev. C*, vol. 77, p. 044306, Apr 2008.

[21] R. A. Niyazov *et al.*, "Two nucleon momentum distributions measured in ^{3}He(e,e' pp)n," *Phys. Rev. Lett.*, vol. 92, p. 052303, 2004. [Erratum: Phys. Rev. Lett.92,099903(2004)].

[22] R. Shneor *et al.*, "Investigation of proton-proton short-range correlations via the ^{12}C(e, e' pp) reaction," *Phys. Rev. Lett.*, vol. 99, p. 072501, 2007.

[23] F. Wamers, "Quasifree scattering with relativistic ^{17}Ne beams in inverse kinematics," *Verhandlungen der Deutschen Physikalischen Gesellschaft*.

[24] K. S. Egiyan *et al.*, "Observation of nuclear scaling in the A(e, e') reaction at x(B) greater than 1," *Phys. Rev.*, vol. C68, p. 014313, 2003.

[25] Q. Ho-Kim and X.-Y. Pham, *Elementary Particles and Their Interactions*. Springer-Verlag, 1998.

[26] C. Colle, W. Cosyn, and J. Ryckebusch, "Final-state interactions in two-nucleon knockout reactions," *Phys. Rev.*, vol. C93, no. 3, p. 034608, 2016.

[27] C. J. Joachain, *Quantum Collision Theory*. North-Holland Publishing Co., 1979.

[28] R. Adams and C. Essex, *Calculus: A complete course*. Pearson, 2013.

[29] D. Belkic, *Quantum Theory of High-Energy Ion-Atom Collisions*. Taylor & Francis, 2009.

[30] H. J. Weber and G. B. Arfken, *Essential Mathematical Methods for Physicists*. Academic Press, 2003.

[31] J. Rammer, *Quantum Transport Theory*. Westview Press, 2004.

[32] I. R. Afnan, *Quantum Mechanics with Applications*. Bentham Science Publishers, 2011.

[33] J. Sakurai and J. Napolitano, *Modern Quantum Mechanics*. Pearson Education Inc., 2011.

[34] T. Aumann, C. A. Bertulani, and J. Ryckebusch, "Quasifree (p,$2p$) and (p,pn) reactions with unstable nuclei," *Phys. Rev. C*, vol. 88, p. 064610, Dec 2013.

[35] L. F. Canto and M. S. Hussein, *Scattering Theory of Molecules, Atoms and Nuclei*. World Scientific Publishing Co., 2013.

[36] M. Thomson, *Modern Particle Physics*. Cambridge University Press, 2013.

[37] D. M. Gingrich, *Practical Quantum Electrodynamics*. Taylor & Francis, 2006.

[38] H. Garcilazo, "The one-pion-exchange potential in the three-body model of nucleon-nucleon scattering," *Physics Letters B*, vol. 99, no. 3, pp. 195 – 199, 1981.

[39] R. Roth, T. Neff, and H. Feldmeier, "Nuclear Structure in the Framework of the Unitary Correlation Operator Method," *Prog. Part. Nucl. Phys.*, vol. 65, 2010.

[40] C. E. Carlson, "The Proton Radius Puzzle," *Prog. Part. Nucl. Phys.*, vol. 82, 2015.

[41] M. Alvioli, C. Ciofi degli Atti, L. P. Kaptari, C. B. Mezzetti, and H. Morita, "Nucleon momentum distributions, their spin-isospin dependence, and short-range correlations," *Phys. Rev. C*, vol. 87, p. 034603, Mar 2013.

[42] W. Dickhoff and D. Van Neck, *Many-body Theory Exposed!: Propagator Description of Quantum Mechanics in Many-body Systems*. World Scientific, 2008.

[43] R. B. Wiringa, V. G. J. Stoks, and R. Schiavilla, "Accurate nucleon-nucleon potential with charge-independence breaking," *Phys. Rev. C*, vol. 51, pp. 38–51, Jan 1995.

[44] B. Mihaila, "Matrix elements of the Argonne v18 potential," 2011.

[45] O. Benhar, V. R. Pandharipande, and S. C. Pieper, "Electron-scattering studies of correlations in nuclei," *Rev. Mod. Phys.*, vol. 65, pp. 817–828, Jul 1993.

[46] H. Feldmeier, W. Horiuchi, T. Neff, and Y. Suzuki, "Universality of short-range nucleon-nucleon correlations," *Phys. Rev. C*, vol. 84, p. 054003, Nov 2011.

[47] M. Vanhalst, W. Cosyn, and J. Ryckebusch, "Counting the number of correlated pairs in a nucleus," *Phys. Rev. C*, vol. 84, 2011.

[48] H. Muther and A. Polls, "Correlations derived from modern nucleon-nucleon potentials," *Phys. Rev.*, vol. C61, p. 014304, 2000.

[49] P. Ring and P. Schuck, *The Nuclear Many-Body Problem*. Springer-Verlag, 2004.

[50] K. Blomqvist *et al.*, "Investigation of short-range nucleon-nucleon correlations using the reaction ^{12}C(e,e'pp) in close to 4π geometry.," *Physics Letters B*, vol. 421, no. 1-4, pp. 71–78, 1998.

[51] R. Starink *et al.*, "Evidence for short-range correlations in ^{16}o.," *Physics Letters B*, vol. 474, no. 1-2, pp. 33–40, 2000.

[52] C. Colle, O. Hen, W. Cosyn, I. Korover, E. Piasetzky, J. Ryckebusch, and L. B. Weinstein, "Extracting the mass dependence and quantum numbers of short-range correlated pairs from $A(e, e'p)$ and $A(e, e'pp)$ scattering," *Phys. Rev. C*, vol. 92, p. 024604, Aug 2015.

[53] C. B. Mezzetti, *Theoretical investigation of two- and three-body short range correlations in inclusive electron scattering off nuclei at high momentum transfer.* PhD thesis, Universita degli Studi di Perugia, 2009.

[54] A. Tang *et al.*, "*n-p* short-range correlations from $(p, 2p + n)$ measurements," *Phys. Rev. Lett.*, vol. 90, p. 042301, Jan 2003.

[55] B. V. Overmeire, W. Cosyn, P. Lava, and J. Ryckebusch, "Relativistic eikonal description of A(p,pn) reactions," *Phys. Rev.*, vol. C73, p. 064603, 2006.

[56] K. G. Fissum *et al.*, "Dynamics of the quasielastic $^{16}\mathrm{O}(e, e'p)$ reaction at $Q^2 \approx 0.8$ $(\mathrm{GeV}c)^2$," *Phys. Rev. C*, vol. 70, p. 034606, Sep 2004.

[57] P. Lava, M. Martnez, J. Ryckebusch, J. Caballero, and J. Udías, "Nuclear transparencies in relativistic A(e,ep) models," *Physics Letters B*, vol. 595, no. 14, pp. 177 – 186, 2004.

[58] J. Ryckebusch, W. Cosyn, and M. Vanhalst, "Density dependence of quasifree single-nucleon knockout reactions," *Phys. Rev. C*, vol. 83, p. 054601, May 2011.

[59] F. W. Byron, C. J. Joachain, and E. H. Mund, "Potential scattering in the eikonal approximation," *Phys. Rev. D*, vol. 8, pp. 2622–2639, Oct 1973.

[60] Y. Suzuki, K. Yabana, R. G. Lovas, and K. Varga, *Structure and Reactions of Light Exotic Nuclei.* Taylor & Francis, Inc., 2003.

[61] E. Henley and A. Garcia, *Subatomic Physics.* World Scientific Publishing Co., 2006.

[62] J. Ryckebusch, D. Debruyne, P. Lava, S. Janssen, B. Van Overmeire, and T. Van Cauteren, "Relativistic formulation of Glauber theory for $A(e, e'p)$ reactions," *Nucl. Phys.*, vol. A728, pp. 226–250, 2003.

[63] R. Glauber and G. Matthiae, "High-energy scattering of protons by nuclei," *Nuclear Physics B*, vol. 21, no. 2, pp. 135 – 157, 1970.

[64] D. Debruyne, *The Eikonal Approximation in Dirac-Based Models for $A(e, ep)$ Reactions.* PhD thesis, UGent, 2001.

[65] B. V. Overmeire, *A relativistic eikonal description of nucleon propagation through nuclei.* PhD thesis, UGent, 2007.

[66] *Particle Data Group.* `http://pdg.lbl.gov/`.

[67] D. Debruyne, J. Ryckebusch, S. Janssen, and T. Van Cauteren, "Bridging two ways of describing final state interactions in A(e,e' p) reactions," *Phys. Lett.*, vol. B527, pp. 62–68, 2002.

[68] G. Alkhazov, S. Belostotsky, and A. Vorobyov, "Scattering of 1 gev protons on nuclei," *Physics Reports*, vol. 42, no. 2, pp. 89 – 144, 1978.

[69] O. Benhar, S. Fantoni, N. N. Nikolaev, J. Speth, A. A. Usmani, and B. G. Zakharov, "Glauber theory of initial and final state interactions in (p, 2 p) scattering," *Z. Phys.*, vol. A355, p. 267, 1996.

[70] C. Colle, W. Cosyn, J. Ryckebusch, and M. Vanhalst, "Factorization of exclusive electron-induced two-nucleon knockout," *Phys. Rev.*, vol. C89, no. 2, p. 024603, 2014.

[71] S. Boffi, C. Giusti, F. Pacati, and S. Frullani, "Validity of the factorized dwia in (e, ep) reactions," *Nuclear Physics A*, vol. 319, no. 3, pp. 461 – 476, 1979.

[72] D. L. Groep *et al.*, "Investigation of the exclusive ^{3}He (e, e'pp p) n reaction," *Phys. Rev.*, vol. C63, p. 014005, 2001.

[73] D. A. Varshalovich, A. N. Moskalev, and V. K. Khersonskii, *Quantum Theory of Angular Momentum*. World Scientific Publishing Co., 1988.

[74] P. Van Isacker and I. Talmi, "Effective three-body interactions in nuclei," *Europhys. Lett.*, vol. 90, p. 32001, 2010.

[75] M. D. Scadron, *Advanced Quantum Theory and Its Applications Through Feynman Diagrams*. Springer Science + Business Media, LLC, 1979.

[76] R. Balian and J. Zinn-Justin, *Methods in Field Theory*. North Holland/World Scientific, 1981.

[77] K. G. Wilson and W. Zimmermann, "Operator product expansions and composite field operators in the general framework of quantum field theory," *Comm. Math. Phys.*, vol. 24, no. 2, pp. 87–106, 1972.

[78] M. Moshinsky, *The Harmonic Oscillator in Modern Physics: From Atoms to Quarks*. Gordon & Breach Science Publishers, 1969.

[79] F. Mandl and G. Shaw, *Quantum Field Theory*. John Wiley & Sons, 2010.

[80] *Nijmegen NN-online baryon-baryon interaction database*. `http://nn-online.org/`.

[81] "Inpc 2007 (p,2p) reactions on 916c at 250 mev/a," *Nuclear Physics A*, vol. 805, no. 1, pp. 431c – 438c, 2008.

[82] H. Cohen, *Complex Analysis with Applications in Science and Engineering*. Springer, 2007.

DEPARTEMENT NATUURKUNDE EN STERRENKUNDE
Celestijnenlaan 200d bus 2412
3001 HEVERLEE, BELGIË
tel. + 32 16 32 71 24
fys.kuleuven.be